Integrated Traffic Flow Control in a Connected Network

December 2018

A Research Report from the Pacific Southwest Region University Transportation Center

Petros Ioannou, University of Southern California
Yihang Zhang, University of Southern California

[page intentionally left blank]

Contents

About the Pacific Southwest Region University Transportation Center

The Pacific Southwest Region University Transportation Center (UTC) is the Region 9 University Transportation Center funded under the US Department of Transportations University Transportation Centers Program. Established in 2016, the Pacific Southwest Region UTC (PSR) is led by the University of Southern California and includes seven partners: Long Beach State University; University of California, Davis; University of California, Irvine; University of California, Los Angeles; University of Hawaii; Northern Arizona University; Pima Community College. The Pacific Southwest Region UTC conducts an integrated, multidisciplinary program of research, education and technology transfer aimed at improving the mobility of people and goods throughout the region. Our program is organized around four themes: 1) technology to address transportation problems and improve mobility; 2) improving mobility for vulnerable populations; 3) Improving resilience and protecting the environment; and 4) managing mobility in high growth areas.

U.S. Department of Transportation (USDOT) Disclaimer

The contents of this report reflect the views of the authors, who are responsible for the facts and the accuracy of the information presented herein. This document is disseminated in the interest of information exchange. The report is funded, partially or entirely, by a grant from the U.S. Department of Transportations University Transportation Centers Program. However, the U.S. Government assumes no liability for the contents or use thereof.

Disclosure

Principal Investigator, Co-Principal Investigators, others, conducted this research titled, Integrated Traffic Flow Control in a Connected Network at Ming Hsieh Department of Electrical Engineering, Viterbi School of Engineering, University of Southern California. The research took place from 1/1/2018 to 12/31/2018 and was funded by a grant from the USDOT in the amount of $100,000. The research was conducted as part of the Pacific Southwest Region University Transportation Center research program.

Abstract

In this report, a combined variable speed limit and lane change traffic flow controller is developed using the cell transmission traffic flow model, which can provide consistent improvement in traffic mobility, safety and the environmental impact. The controller is then extended to coordinate with the ramp metering controller which maintains the flow rates on both mainline and on-ramps of highway. Furthermore, we investigate the stability properties of the cell transmission model under all possible traffic flow scenarios, with consideration of the capacity drop phenomenon. The analysis is used to motivate the design of variable speed limit control to overcome capacity without lane change control and achieve the maximum possible flow under all feasible traffic situations. We also consider the case where the system disturbance is included and extend the VSL controller by adding the integral action in order to reject the disturbance while avoiding the capacity drop.

Integrated Traffic Flow Control in a Connected Network

Executive Summary

Highway congestion is detrimental to traffic mobility, safety and the environment. Numbers of studies have been conducted to avoid or relieve highway congestion with different traffic flow control strategies such as Variable Speed Limit (VSL), Ramp Metering (RM) and Lane Change (LC) recommendation and their combinations. While consistent improvement on traffic safety is reported under existing traffic flow control strategies in macroscopic and microscopic simulations, the results are rather controversial when it goes to the improvement on traffic mobility and the environmental impact, especially in microscopic simulations. Some researchers attribute the inconsistencies to the complexity of underlying reasons of the congestion and highly disordered and stochastic behavior at the bottleneck. Therefore, it is necessary to investigate the dynamical behavior of the open-loop traffic flow systems under all possible demand levels as well as initial densities in order to find out the reasons of the chaotic behavior at the bottleneck, and based on which find an integrated traffic flow controller which is able to provide consistent improvement in traffic mobility, safety and the environmental impact under different traffic scenarios.
In this report, we discover that one of the major reasons of the disordered behavior is the forced lane changes at vicinity of the bottleneck. A lane change controller is proposed which provides lane change recommendations to upstream vehicles in order to avoid the capacity drop. A feedback linearization variable speed limit controller is designed based on the first order cell transmission traffic flow model in order to improve the flow rate at highway bottleneck together with the lane change controller. The combined lane change and variable speed limit controller can analytically guarantee the global exponential convergence to the desired equilibrium point at which maximum possible flow rate is achieved. Then the combined LC and VSL controller is extended to coordinate with ramp metering controllers. The coordinated VSL, RM and LC controller is able to improve system performance, maintain the queue length on ramps and keep the fairness between mainline and on-ramp flows. Microscopic simulations show consistent improvement under different traffic demand and scenarios. Furthermore, we modify the cell transmission model to include the effect of capacity drop and the decreasing discharging flow of the road section and rigorously investigate its stability properties under all possible traffic flow scenarios. The analysis is used to motivate the design of variable speed limit control to overcome capacity drop without lane change control and achieve the maximum possible flow under all feasible traffic situations. We also consider the case where the system disturbance is included and extend the VSL controller by adding the integral action in order to reject the disturbance while avoiding the capacity drop.

1 Introduction

Due to the rapidly increasing demand for transportation, congestion has become a significant problem all around the world. Congestion has negative impact on traffic mobility, safety and the environment. In the United States, the yearly delay time per auto commuter due to congestion was 42 hours in 2014, which is increased by 13.5% compared to 37 hours in 2000. The fuel wasted in congestion is 19 gallons per commuter per year in 2014, which increased by 26.7% when compared to 15 gallons per commuter per year in 2000 [1]. Unstable traffic flow conditions on highway segments are known to increase the possibility of crash [2].
In highway traffic, bottlenecks often arise due to incidents, construction, merge or diverge points and other road conditions. When traffic demand is higher than the capacity of the bottleneck, congestion occurs. One possible way to solve highway congestion problem is to expand highway networks, which is usually constrained by long building period and limited capital investment. Hence, increasing the utility of existing road infrastructure with advanced traffic control strategies is a more attractive solution. To prevent or relieve highway congestion, different Intelligent Transportation Systems (ITS) techniques, e.g. dynamic routing, driver information systems, variable speed limit (VSL), and ramp metering (RM) etc., are widely studied and applied to improve the efficiency of existing road networks [3–7].

Figure 1: Traffic Flow Control Signs on Highway

(a) Variable Speed Limit

(b) Ramp Metering

(c) Lane Change Control

There are various factors that may lead to highway congestion. For example, capacity drop at highway bottlenecks which deteriorates the maximum possible throughput of a highway, overloaded mainline traffic which creates shockwave propagating upstream and excessive on-ramp flow which disturbs the mainline traffic. Due to the variety and complexity of underlying reasons of highway congestion, it has never been an easy task to find a control strategy which is able to efficiently regulate the traffic flow and improve traffic mobility, safety and the environment impact when congestion occurs on highway.
Numbers of previous studies have been conducted to relieve or postpone highway congestion with different control strategies. Variable speed limit (VSL), ramp metering (RM) and lane change (LC) control are among the most intensively studied and applied highway traffic flow control

strategies. Variable speed limit dynamically changes the speed limits along a highway segment thus regulates the traffic flow and improve traffic condition at the bottleneck. Ramp metering limits the number of vehicles entering the highway in unit time from on-ramps in order to maintain an appropriate demand on highway and attenuate the disturbance of ramp flows to the mainline. Lane change control provides lane change instructions to vehicle drivers therefore help them avoid closed lanes and efficiently move to the open lanes.
Existing works on the development and evaluation of VSL, RM and LC control have reported consistent improvements in traffic safety in theories, macroscopic simulations, microscopic simulations and field tests [8–10], while the impact on traffic mobility and environment is rather controversial. Although most of previous studies are able to show improvements of traffic mobility in macroscopic simulations with different traffic flow control strategies, when it comes to microscopic simulations and field tests, these improvements are not consistent under different traffic conditions or incident scenarios. In some cases, the travel time is improved and in others deteriorated due to the deployment of traffic flow controllers which raises questions as to the ability of VSL, RM and LC to improve traffic mobility [11–16]. Most researchers attribute the inconsistencies in travel time improvement to the highly disordered and stochastic traffic conditions at congested bottlenecks, which are difficult to predicts and regulate [8, 13, 16, 17]. While these arguments have an element of truth, some questions we need to ask here is as follows:

1. What is the behavior of the traffic flow in a road network? Under what condition the road network will get congested and what are the reasons of the disordered behavior of the traffic flow at the bottleneck?

2. Is it possible to reduce the level of disorder at the bottleneck, therefore the consistency between macroscopic and microscopic simulations can be achieved?

3. Is it possible to find efficient VSL, RM and LC control strategies which are able to improve the traffic mobility at highway bottlenecks and robust to different incident scenarios?

4. Given the complexity of underlying reasons of highway congestion, is it possible to apply multiple traffic flow control strategies simultaneously in an integrated and systematic manner, such that different control strategies can work along with each other coordinately without deteriorate the benefit introduced by other control strategies.

5. Is it possible to find a traffic control strategy that can improve the traffic mobility under all possible traffic scenarios and capacity constraints as well as initial conditions?

In this study, to answer the above questions, the problem of analysis of traffic flow systems and the design, analysis and evaluation of integrated VSL, RM and LC controller for highway traffic is addressed. The goal of the integrated controller is to stabilize and homogenize the traffic flow upstream a highway bottleneck, therefore improve the traffic mobility, safety and the environmental impact. We also evaluate the robustness of the integrated controller with respect to different levels of traffic demand, model parameters and measurement noise in both macroscopic and microscopic simulations. Furthermore, the open-loop stability properties of the modified cell

transmission traffic flow model (CTM) which takes the capacity drop phenomenon into consideration under all possible traffic flow scenarios are investigated, which motivates the design of a VSL controller which is able to avoid the capacity drop, stabilize the system and maximize the flow rate at the bottleneck. The VSL controller is extended with integral action in order to reject system disturbance.

2 Literature Review

In the past several decades, numerous studies have been conducted to explore the effect of VSL, RM and LC control on traffic mobility, safety and the environmental impact.
VSL control has been one of the widely studied highway traffic control technologies since the 1990s [18]. Papageorgiou et al. studied the effect of VSL on the fundamental diagram in [19]. It is shown that VSL control decreases the slope of the fundamental diagram when the vehicle density is lower than the critical value and increases the critical density. The flow at the same density would be higher with VSL in over critical conditions.
Muralidharan et al. proposed a MPC VSL controller based on the LN-CTM model that is able to recover the bottleneck from capacity drop and obtain an optimal trajectory in the absence of capacity drop [20]. In 2014, Frejo et al. proposed a hybrid MPC controller which combines VSL with ramp metering. The proposed method reduced the computation load of the receding horizon optimization by using genetic and exhaustive algorithms while achieving a good performance in simulation [21].
In [22], Khondaker and Kattan designed a MPC VSL controller based on a microscopic car following model with the assumption of a connected vehicle environment. The proposed method predicts traffic conditions on the microscopic level and optimizes a cost function which is the weighted sum of TTT and time to collision (TTC), therefore improves both traffic mobility and safety. The method was evaluated using a microscopic simulation model based on the commercial software, VISSIM. Significant improvement on travel time is demonstrated. However, the authors assumed that all vehicle information is available in real time and the vehicle states can be accurately predicted, which is very difficult, if at all possible.
In 2013, Carlson et al. [23] proposed two local feedback VSL controllers. The local feedback controllers were compared to a nonlinear optimal controller via macroscopic simulations. Results showed that the simple feedback controllers can provide similar improvement with respect to the total time spent (TTS) as the optimal controller by using much lower computational effort. The method is extended to multiple bottlenecks in [24] and evaluated to be also effective in microscopic simulations in [25]. In [26], Jin and Jin proposed a proportional-integral (PI) VSL controller to maximize the bottleneck throughput with only one VSL sign by locally stabilizing the vehicle density at a critical value. Since the analysis is local there is no guarantee that a traffic disturbance would not lead to a capacity drop and unstable situation. In addition it is not clear how the design for one section can be extended to multiple sections upstream the bottleneck.
In [27], Hegyi et al. proposed the SPECIALIST VSL controller strategy based on shockwave theory. The SPECIALIST method detects the shockwave upstream the bottleneck and uses VSL to

make the shockwave accumulate slower and dissipate faster thus dampen the shockwave and improve traffic mobility. In [28], a local feedback VSL control strategy integrated with ramp metering is proposed based on the fundamental diagram. An extended version of this control strategy is evaluated in [29] with microscopic simulations. The method is shown to be able to improve freeway efficiency as well as be robust with respect to modeling error and measurement noise. The effects of VSL on traffic safety and the environment is also assessed. In [30], Abdel-Aty et al. showed that well-configured VSL strategies can decease the crash likelihood but large gaps of speed limit in time and space may increase it. No improvement in travel time is observed in this study. In [31], a genetic algorithm was used to choose the control parameters in order to minimize the rear-end collision risks near freeway recurrent bottlenecks. With the proposed control strategy, the VSL control reduced the rear-end crash potential by 69.84% for the high demand scenario and by 81.81% for the moderate demand scenario. [32] evaluated the environmental impact of the VSL and LC control method proposed in [33] with a microscopic emission model CMEM and a macroscopic one MOVES. It is shown that the environmental benefits are evaluated to be qualitatively similar with both models while the microscopic CMEM is more sensitive to transient process.

In [34], a MPC VSL strategy was proposed using a car-following model to reduce both total time spent (TTS) and total emissions. It is shown that a reduction of TTS alone may not reduce the total emissions. [22] showed that in case of 100% penetration rates of connected vehicles, optimizing for safety alone is enough to achieve simultaneous and optimum improvements in all measures. However, in case of lower penetration rate, a higher collision risk was observed when optimizing for only mobility or fuel consumption.

The aim of RM is to adjust the on-ramp flow into the mainline in order to improve the overall traffic condition. RM has been widely used in United States and the Europe [35, 36]. ALINEA, one of the most popular RM strategies, is a heuristic local feedback control method with integral action [6].

In [37], ALINEA is expanded to MALINEA, which includes the mainline occupancy upstream the on-ramp in the feedback loop. MALINEA addresses two main disadvantages to ALINEA. The first is that although ALINEA optimizes the occupancy downstream of the entrance ramp, congestion can still occur upstream of the ramp. The second is that the optimal detector location can be difficult to determine.

[38] proposed FL-ALINEA which includes feedback downstream flow rate instead of occupancy and ALINEA/Q algorithm which combines queue control with ALINEA. MALINEA addresses two main disadvantages to ALINEA. The first is that although ALINEA optimizes the occupancy downstream of the entrance ramp, congestion can still occur upstream of the ramp. The second is that the optimal detector location can be difficult to determine. Its formula is identical to the formula used for traditional occupancy-based ALINEA, except that it measures flow, and tries to reach a set point flow rather than a set point occupancy. However, when the occupancy is over the critical occupancy, the metering rate is set to the minimum rate, since the freeway is already over capacity. ALINEA/Q algorithm calculates two metering rates. The first rate is calculated exactly the same as in the traditional ALINEA algorithm. The second rate that is calculated is the minimum rate needed to keep the ramp queue at or below the maximum allowable queue length.

The final calculated rate is the greater of either the ALINEA rate or the queue control rate.
Some model-based RM algorithms are also developed. Coordinated ramp metering is based on a second order traffic flow model and an optimal control approach that decides the metering rates of multiple ramps in a coordinated manner [39]. Coordinated ramp metering is basically a vectorization of the ALINEA equation, which uses vectors of occupancy, and 2 control gain matrices to return a vector of metering rates.
SWARM is a data-based ramp metering strategy which uses linear regression of measured data to predict the density [40]. Despite the intensive application of RM, it is recognized that ramp metering can only control the vehicle density immediately downstream the on-ramp therefore barely improves the overall traffic condition in practice, especially when the mainstream demand is high [41, 42]. The above limitations of RM motivates the investigation of combining ramp metering with mainline traffic control strategies such as VSL.
Previous efforts to study the effect of lane changes at bottlenecks and develop traffic flow control strategies with consideration of lane management include the following:
In 1986, Rathi et al. [43] developed a microscopic simulation model to evaluate the effect of LC control in a freeway work zone at different driver compliance rate. In 1988, Mahmassani et al. [44] applied a macroscopic simulation model to evaluate lane closure strategy for planned work zone. The work in [43, 44] is focused on long-term lane closure strategies rather than temporary lane closures.
In 1998, Schaefer et al. [45] assessed the effectiveness of overhead lane control signals. The signals are placed at 1/2 mile intervals ahead of the highway incident area and indicate lane closure with red "x" symbols. A microscopic simulation using SLAM was used to evaluate the performance of the lane change signal on time delay. In 1999, Jha et al. [46] evaluated three different lane control signal settings for the tunnel of I-93 South. Yellow and red overhead signals were applied ahead of incident location and evaluated with microscopic simulator MITSIM. The study showed that under incident condition, TTT is sensitive to upstream road geometry and driver compliance rate. Carelessly configured LC signal settings may result in increase of TTT.
In [47], Jin stated that systematic lane changes can seriously deteriorate traffic safety and efficiency during lane drop, merge, and other types of bottleneck. The author introduced an entropy condition for the multi-commodity LWR model and solve the Riemann problem inside a homogeneous lane-changing area. In [48], Laval and Daganzo also confirmed that lane changes at the bottleneck reduce the flow rate and result in capacity drop at the bottleneck.
In recently years, researchers start to examine the combination and integration of different traffic flow control schemes. In [49], Baskar et al. proposed a MPC approach to find optimal speed limits and lane allocations for platoons. The method is simulated on a 2-lane highway segment and reported to improve travel time by 5% - 10%. It is assumed that all vehicles are controlled by road-side controllers. In 2014, Roncoli et al. [50] proposed a MPC-based traffic control strategy for multi-lane motorways, which integrates VSL, ramp metering and lane allocation. The authors adopted the first order flow model and treated each lane as different cells. MPC is designed based on a cost function which penalizes TTS, queue length on the ramps and amplitude of oscillations. Simulation results show that VSL performs much better when combined with ramp metering and lane allocation.

The coordination of RM and VSL involves consideration of network mobility, on-ramp queues and fairness between the mainline and the ramps. The objective is to keep a balanced delay time between vehicles on the mainline and the ramps and avoid long queues on the ramps from spilling back to the urban road network. Past efforts to integrate ramp metering with variable speed limit control include the following: [51, 52] chose the optimal VSL and RM commands based on a second order model in an open-loop manner. [53] developed a combined VSL and RM controller by using model predictive control (MPC) based on the METANET model. [54] combined VSL and coordinated RM using an optimal control approach. [41] used a MPC approach to generate the VSL commands which coordinate with pre-existing RM controllers. [7] designed a MPC-based RM controller with a linearized first-order model which is equipped with a heuristic VSL controller.

The design of the coordinated VSL, RM and LC controller is based on the first-order cell transmission traffic flow model, which during the recent years was used to develop variable speed limit (VSL) control strategies. In [55], Hadiuzzaman et al. proposed a model predictive control (MPC)-based VSL control strategy to relieve congestion caused by active bottleneck which introduces capacity drop. No significant improvement was shown in bottleneck throughput. The reason given by the authors of [55] for the lack of improvements by the proposed VSL was that the model and data used were not accurate enough. In [20], an MPC-based coordinated VSL and ramp metering (RM) controller is proposed based on the link-node CTM. The VSL and RM control commands are computed by relaxing the receding-horizon optimization problem into linear programming. In [56], the CTM model is expressed in a piecewise affine switching-mode form, based on which an MPC-based VSL controller is developed to attenuate shockwave.

In [57], Gomes et al. performed a thorough analysis of the equilibrium points and their stability properties of the CTM model. However, the authors did not take the capacity drop phenomenon into consideration. In addition, the convergence rate at which the system states converge to the equilibrium points is not specified. Reference [58] developed sufficient conditions for the stability of the equilibrium points of CTM in terms of connectivity of a graph associated with the traffic network. The results of [57] and [58] are established based on the monotonicity of CTM. However, if the CTM is modified to account for capacity drop and the fact that the discharging flow rate of a congested road section decreases with density [5, 26, 59, 60], then the CTM is no longer monotone. A finite horizon optimal routing and flow control strategy is proposed in [58]. The stability and convergence of the closed-loop system to a desired equilibrium however has not been established. In [61], the authors analyzed the equilibrium points and their stability properties under feasible and infeasible demand, however the capacity drop phenomenon and traffic flow control is not considered. In [62], sufficient conditions for global asymptotic stability and global exponential stability of the equilibrium points of discrete-time CTM model are developed using vector Lyapunov functions. In [63], the authors proposed a feedback control law that guarantees the global exponential stability of the desired equilibrium point of the CTM model. The control input in this case is the flow rate itself. It is not clear, however, how to implement the flow controller with VSL control.

3 Combined Variable Speed Limit and Lane Change Control

As introduced in section 1, inconsistent performance of variable speed limit and ramp metering controllers have been reported in existing studies. Some researchers attribute the inconsistencies to the highly disordered and stochastic behavior at highway bottlenecks. One of the main factors of the disordered behavior at highway bottlenecks is the capacity drop phenomenon, where the maximum achievable traffic flow rate decreases when queues form [64, 65]. Under certain speed limit, when the density at the vicinity of the bottleneck increases to be higher than some critical value, a queue forms upstream of the bottleneck which decreases the capacity of the bottleneck. Capacity drop makes the dynamics of the traffic flow at bottleneck highly unstable, which is difficult for VSL control to maintain a high flow rate. [23] claims that one of the main factors that introduce capacity drop is the inefficient acceleration of vehicles at the bottleneck, thus by providing an acceleration section with reasonable length and regulating the density with VSL, capacity drop can be avoided. Such an approach however has the following drawbacks. First it is difficult to establish in cases of incidents and second enforcing an acceleration section may require reducing the flow upstream considerably. The method in [20] is developed under the assumption that the bottleneck never returns to capacity drop mode from free flow mode, i.e., once the VSL controller recovers the bottleneck from capacity drop, the capacity drop never occurs again. While there is no reason to doubt the reported results, our studies and observations of traffic show clearly that forced lane changes in close proximity to the incident or bottleneck is the major cause of capacity drop and once it takes place VSL control will have limited or no effect in improving travel time. Most likely in the reported results which show significant benefits the scenarios did not involve significant forced lane changes or as in the case of [23] it was prevented by creating an acceleration area before the bottleneck. It should be intuitively clear that once the forced lane changes bring down the speed of vehicles in neighboring lanes there is no way for an VSL control technique to eliminate the capacity drop.

In this section, we first proposed a lane change (LC) controller which can avoid or relieve the capacity drop at the bottleneck. Two types of VSL controller are designed to combine with the LC controller. The first one is an heuristic local feedback controller with integral action. The second one is a feedback linearization controller which is designed based on the first order cell transmission model. Together with a lane change controller, the feedback linearization VSL controller guarantees stability of the traffic flow and convergence of traffic densities to an equilibrium density with an exponential rate of convergence. In contrast to previous studies which relied on linearized models, our approach is based on feedback linearization and the results obtained are global. Therefore from the macroscopic point of view the proposed VSL and lane change control guarantees no capacity drop and maximum flow at the bottleneck. The lane change controller is based on a space model as in this case the control variable is the location of the lane change control commands. This location is found to depend on demand and number of lanes closed. The proposed combined lane change and VSL control design is evaluated using microscopic Monte Carlo simulations under different scenarios. The microscopic results generated are very consistent with the macroscopic ones and demonstrate consistent improvements to traffic mobility and impact on the environment for all the simulated scenarios.

Figure 2: Highway Bottleneck

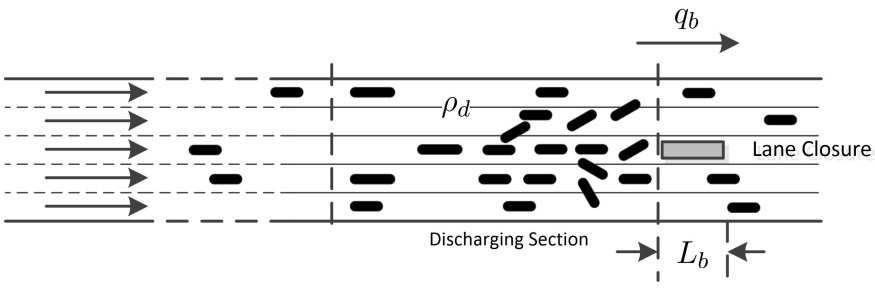

3.1. System Modeling

3.1.1. Model of highway bottleneck

Consider a highway segment without on-ramps and off-ramps. A bottleneck is the point with lowest flow capacity. Due to the bottleneck a queue of vehicles forms as traffic demand increases. The flow rate of the bottleneck determines the throughput of the entire highway segment. Therefore, the modeling of the bottleneck traffic flow is crucial to the design of an efficient traffic control strategy. A bottleneck can be introduced by lane drop, incident lane blockage, merge point or other road conditions.

Fig. 2 shows a highway segment with 5 lanes. A bottleneck is introduced by an incident which blocks one lane. The length of the bottleneck is denoted by L_b. We assume that the capacity of the highway segment before the incident is C. Then the ideal capacity of the bottleneck after the incident should be $C_\mathrm{b} = \frac{4}{5}C$. As we can see in Fig. 2, if L_b is small, the effect of the density within L_b is negligible and will not affect the bottleneck flow. The flow rate q_b at the bottleneck is determined by ρ_d, the vehicle density of the immediate upstream section of the bottleneck, which is referred to as the discharging section in Fig. 2. We adopt the assumption of triangular fundamental diagram, that is, when the value of ρ_d is low, $q_\mathrm{b} = v_\mathrm{f}\rho_\mathrm{d}$, where v_f is the free flow speed. However, when ρ_d is higher than some critical value $\rho_{\mathrm{d,c}}$, i.e. the demand of the bottleneck is higher than its capacity C_b, a queue forms at the discharging section which propagates upstream. Forced lane changes performed by the vehicles in the queue reduce the speed of flow in the open lanes. Therefore, the capacity would drop to $C'_\mathrm{b} = (1-\epsilon)C_\mathrm{b}$ once the queue forms [20, 26, 60]. The relationship between ρ_d and q_b is shown as solid line in Fig. 3 and is described by the equation

$$q_\mathrm{b} = \begin{cases} v_\mathrm{f}\rho_\mathrm{d}, & \rho_\mathrm{d} \le \rho_{\mathrm{d,c}} \\ (1-\epsilon)C_\mathrm{b}, & \rho_\mathrm{d} > \rho_{\mathrm{d,c}} \end{cases} \tag{1}$$

where $C_\mathrm{b} = v_\mathrm{f}\rho_{\mathrm{d,c}},\ \epsilon \in (0,1)$.

Figure 3: Fundamental Diagram

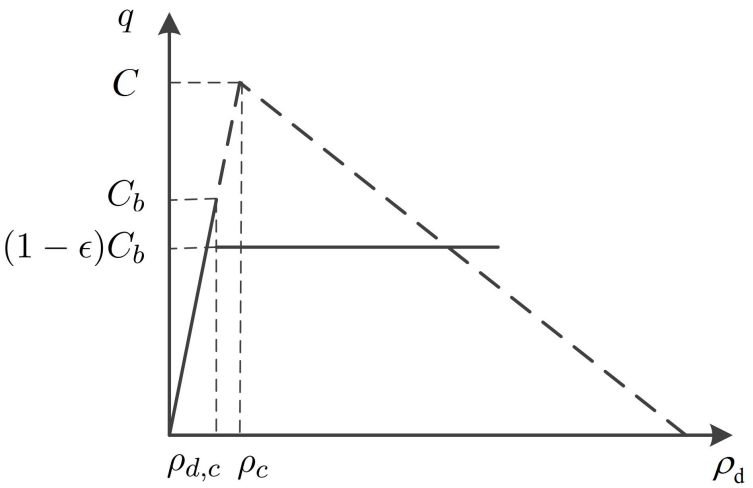

Figure 4: Configuration of VSL Control System

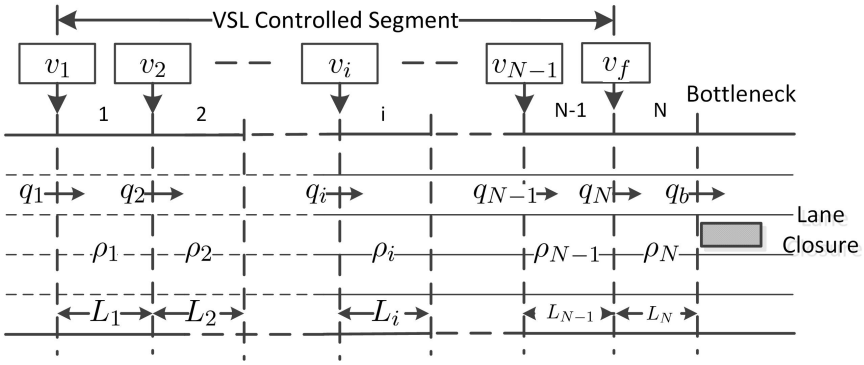

3.2. VSL configuration and cell transmission model

As shown in Fig. 4, the upstream highway segment of bottleneck is divided into N sections. The lengths of different sections are expected to be similar but not necessarily identical. VSL signs are installed at the beginning of section 1 through section $N-1$. The speed limit in section N, which functions as the discharging section in Fig. 2, is constant and equals v_{f}, the maximum possible speed given by the fundamental diagram, which would let vehicles in open lanes get through the bottleneck as fast as possible, under the assumption of triangular fundamental diagram.

For $i = 1, 2, \ldots, N$, we denote the length, vehicle density and the inflow rate of section i with L_i, ρ_i and q_i respectively. For $i = 1, \ldots, N-1$, we denote the variable speed limit in section i with v_i. The variables $\rho_i,\ q_i,\ v_i$ are all functions of time t. By conservation law, the dynamics of

densities ρ_i are described by the differential equations

$$\begin{aligned} \dot{\rho}_i &= (q_i - q_{i+1})/L_i,\ i = 1, 2, \ldots, N-1 \\ \dot{\rho}_N &= (q_N - q_{\mathrm{b}})/L_N \end{aligned} \tag{2}$$

Under the assumption of triangular fundamental diagram, the flow rate q_i can be found as follows:

$$\begin{aligned} q_1 &= \min\{d, C_1, w_1(\rho_{\mathrm{j},1} - \rho_1)\} \\ q_i &= \min\{v_{i-1}\rho_{i-1}, C_i, w_i(\rho_{\mathrm{j},i} - \rho_i)\},\ i = 2, 3, \ldots, N \end{aligned} \tag{3}$$

where d is the demand flow of this highway segment assumed to be constant relative to the other variables. $\rho_{\mathrm{j},i}$ is the jam density of section i, at which q_i would be 0. w_i is the backward propagating wave speed in section i, C_i the capacity, i.e. the maximum possible flow rate in section i, given by $C_i = v_i w_i \rho_{\mathrm{j},i}/(v_i + w_i)$. We should note that for $i = N$, C_N and $\rho_{N,\mathrm{c}}$ are not the same as C_{b} and $\rho_{\mathrm{d,c}}$. When ρ_N reaches $\rho_{\mathrm{d,c}}$, q_{b} decreases but section N still has enough space for vehicles in section $N-1$ to flow in. Therefore, $\rho_{N,\mathrm{c}} > \rho_{\mathrm{d,c}}$, $C_N > C_{\mathrm{b}}$. The goal of the VSL controller is to stabilize the system described in (1) - (3) and maximize the flow rate q_{b}. According to (1), maximum q_{b} is obtained at $\rho_N = \rho_{\mathrm{b}}$, which is a discontinuity point of the fundamental diagram. From the macroscopic point of view, it is possible to find a VSL controller to maintain that $\rho_N = \rho_{\mathrm{d,c}}$ [26]. However, microscopic simulations in [33] demonstrate that when congestion occurs at the bottleneck, the queue accumulates so fast that VSL control can hardly reduce the density back to $\rho_{\mathrm{d,c}}$, therefore it fails to maintain maximum flow. The reason is explained in the following subsection.

3.3. Effects of Lane Change Control

In order to study the effect of lane change control, we build a hypothetical highway segment as shown in Fig. 2, which is straight, 8 km long and with 5 lanes, with the microscopic traffic flow simulated using the commercial software VISSIM [66]. The VISSIM model is calibrated with typical freeway road geometry and driving behavior. The bottleneck is formed by an incident which blocks the middle lane. We investigate the relationship between the flow of the bottleneck q_{b} and the density ρ_{d} in the 500 m long discharging section immediately upstream the bottleneck under different levels of traffic demand. Fig. 5 shows the relationship between q_{b} and ρ_{d} without any VSL control. The small blue circles describe the fundamental diagram in the case of lane change control. The red asterisks show the corresponding fundamental diagram in the absence of lane change control. The design procedure of LC controller is described in Section 3.4. Observing Fig. 5, we can see that when LC control is applied, the capacity of the bottleneck is around 7600 veh/h, which is achieved at $\rho_{\mathrm{d}} \approx 135$ veh/mi. However, when there is no LC control, q_{b} stops increasing even before ρ_{d} reaches 135 veh/mi (around ρ_{d} = 100 veh/mi). The highest flow rate is around 6300 veh/h. The reason why the flow rate in the no control case fails to reach higher level is demonstrated in Fig. 2. When vehicles approach the incident spot without being aware that their lane is blocked they are forced to slow down considerably and change lanes.

Figure 5: Fundamental Diagram with and without LC Control

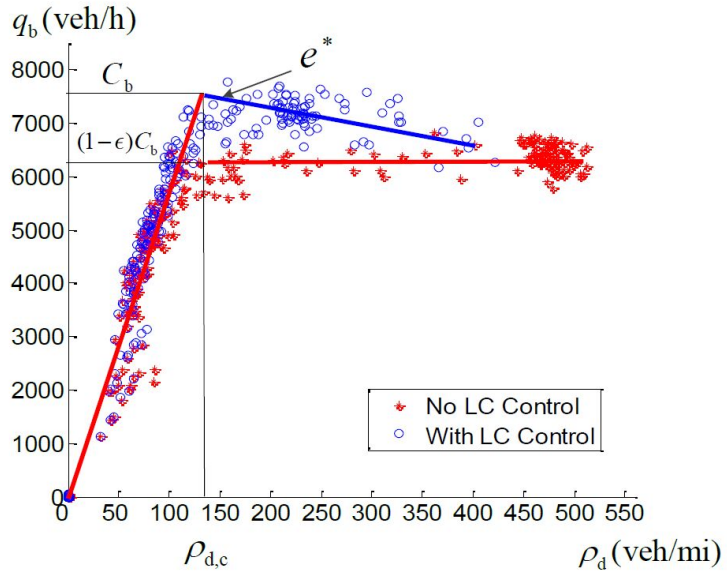

These forced lane changes at low speed cause the traffic to slow down in the open lanes before and after the incident leading to lower volume, while the average density of the discharging section, ρ_d, is still low. Other parts of the fundamental diagram in the no control case fit equation (1) very well. Compared to the fundamental diagram with LC control, we can calibrate the parameters as, $\rho_{d,c} = 135$ veh/mi, $C_b = 7600$ veh/h and $\epsilon = 0.16$. The above stated behavior of the bottleneck makes it difficult for VSL control to increase q_b at the bottleneck, as VSL is only able to regulate the average density ρ_d in the discharging section, but cannot eliminate the forced lane changes at the vicinity of the bottleneck.
On the other hand, with the LC control, we can see that

1. no obvious capacity drop is observed at $\rho_d = \rho_{d,c}$;
2. q_b at $\rho_d > \rho_{d,c}$ is approximately linear with a negative slope w_b, which represents the wave propagation rate;
3. most data points scatter close to $\rho_d = \rho_{d,c}$. The points of high density are rare.

These observations show that the LC controller is able to reduce the number of vehicle stops in the queue at bottleneck and decrease the vehicle density, which makes the system continuous and easier for the VSL controller to stabilize. As a consequence of the LC control action, in the cell transmission model the relationship between ρ_N and q_b can be modeled as:

$$q_b = \begin{cases} v_f \rho_N, & \rho_N \leq \rho_{d,c} \\ w_b(\rho_{j,d} - \rho_N), & \rho_N > \rho_{d,c} \end{cases} \tag{4}$$

where $\rho_{j,d} = v_f \rho_{d,c}/w_b + \rho_{d,c}$.

Although the lane change control is able to recover the triangular shape of the fundamental diagram, when the demand is higher than the capacity C_{b}, a congestion will still occur at the bottleneck. Now the goal is to design a VSL controller to stabilize system (2) - (4) by homogenizing the densities in all sections and have them converge to an equilibrium which corresponds to the maximum possible flow as shown in the following section.

3.4. Design of the Lane Change Controller

The design of LC controller includes the pattern of the LC recommendation messages and the length of LC controlled segment. As we will explain below the control variable for LC control is the location of the LC recommendation which depends on a nonlinear spatial model that we developed.

3.4.1. Lane Change Recommendation Messages

Suppose a general highway segment has m lanes, with Lane 1 (Lane m) being the right (left) most lane in the direction of flow. We select the LC recommendation message R_i for lane $i, i = 1, 2, \ldots, m$ using the following rules:

1. For $1 \leq i \leq m$, if lane i is open, $R_i =$ "Straight Ahead";
2. For $i = 1 (i = m)$, if lane i is closed, $R_i =$ "Change to Left (Right)";
3. For $1 < i < m$, if lane i is closed, lane $i-1$ and lane $i+1$ are both open, $R_i =$ "Change to Either Side";
4. For $1 < i < m$, if lane i is closed, lane $i-1$ (lane $i+1$) is closed but lane $i+1$ (lane $i-1$) is open, $R_i =$ "Change to Left (Right)";
5. For $1 < i < m$, if lane i is closed, lane $i-1$ and lane $i+1$ are both closed, then we check R_{i-1} and R_{i+1}. If $R_{i-1} = R_{i+1}$, then $R_i = R_{i-1} = R_{i+1}$, else if $R_{i-1} \neq R_{i+1}$, $R_i =$ "Change to Either Side".

Rules (1)-(5) determine the LC recommendation messages depending on the incident location. The 5 rules covers all incident cases and are also mutually disjoint. Therefore they are well-defined and self-consistent.

3.4.2. Length of LC Control Segment

The control variables in the LC control case are the length of the LC control segment and the location of the LC recommendation. Within that segment, a LC recommendation is given at each section within the segment. The length of the LC controlled segment need to be long enough in order to provide adequate space and time for upstream vehicles to change lanes. Intuitively, if more lanes are closed at the bottleneck, a longer LC control distance is required. In addition, the capacity of the bottleneck and demand will also affect the LC control distance. On the other hand

Figure 6: ξ under different traffic demands

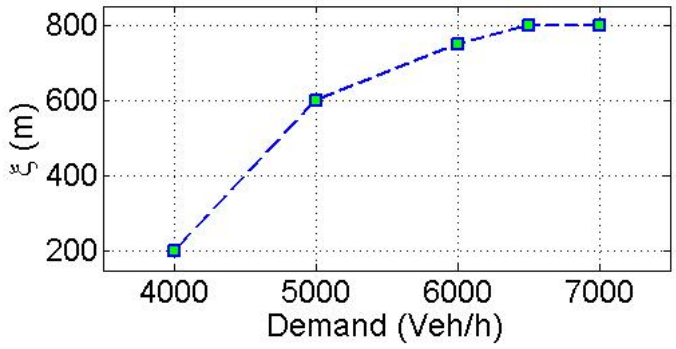

if the length of LC control segment is too long it may cause other problems as the blocked lane will appear empty to drivers inviting more lane changes in and out of the blocked lane which is going to deteriorate performance in terms of unnecessary maneuvers. We used extensive microscopic simulation studies to develop the following empirical model that allows us to generate the control variable d_{LC} which is the length of the LC controlled section given by the following equation:

$$d_{\text{LC}} = \xi \cdot n, \tag{5}$$

where n is the number of lanes closed at the bottleneck, ξ a design parameter related to the capacity of bottleneck and the traffic demand which in our case is found to have the relationship shown in Figure 6. For a specific highway segment, the minimum value of ξ required under different traffic demands can be found by simulation. Since LC signs are only deployed at the beginning of sections, we choose the number of LC controlled sections M, as $M = \text{argmin} \ \sum_{i=N-M+1}^{N} l_i - d_{\text{LC}}$, where l_i represents the length of section i. More details can be found in [33]. Here we assume that the LC controlled segment has no on-ramp or off-ramps. The model (5) is empirical and more spacial than temporal despite the dependence of ξ on demand which may be time varying. The purpose of the LC control is to ask drivers to start changing lanes before the incident. It is an off and on controller i.e change lanes or not required to change lanes. It is different than the VSL controller which is purely dynamic.

3.5. Feedback Linearization Variable Speed Limit Controller

In this section, we designed a feedback linearization VSL controller based on the cell transmission model (2)-(4).

3.5.1. Desired Equilibrium Point

The fundamental diagram under LC control is shown in Fig. 7. We consider the demand $d > C_{\text{b}}$, which may introduce congestion at the bottleneck. From the nonlinear system (2) - (4), we calcu-

Figure 7: Desired Equilibrium Point

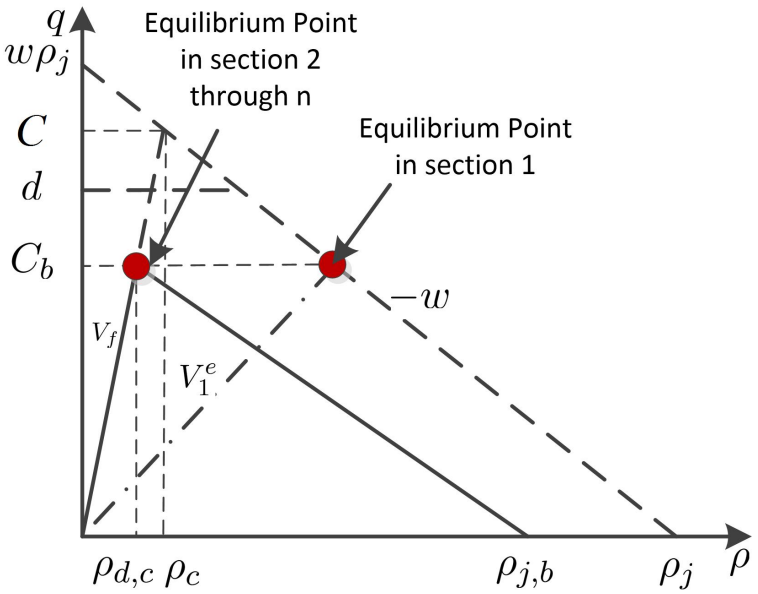

late the equilibrium point by setting the derivatives in (2)-(4) to be zero. Let $\rho^{\mathrm{e}} = [\rho_1^{\mathrm{e}}, \rho_2^{\mathrm{e}}, \ldots, \rho_N^{\mathrm{e}}]^T$ and $v^{\mathrm{e}} = [v_1^{\mathrm{e}}, v_2^{\mathrm{e}}, \ldots, v_{N-1}^{\mathrm{e}}]^T$ denote the vector of equilibrium density and the corresponding equilibrium speed limits in each section respectively. The desired equilibrium point should be the one at which maximum possible flow rate C_{b} is achieved and the upstream traffic flow is homogenized. According to the triangular fundamental diagram (4), since the speed limit is constant and equals v_{f} in section N, therefore the optimum equilibrium density for maximum flow is $\rho_N^{\mathrm{e}} = C_{\mathrm{b}}/v_{\mathrm{f}}$. For section 2 through $N-1$, we set

$$\rho_2^{\mathrm{e}} = \cdots = \rho_N^{\mathrm{e}} = C_{\mathrm{b}}/v_{\mathrm{f}},\ v_2^{\mathrm{e}} = \cdots = v_{N-1}^{\mathrm{e}} = v_{\mathrm{f}}. \tag{6}$$

hence at the desired equilibrium point, the densities and speed limits in section 2 through N would be the same and the upstream traffic flow of the bottleneck is homogenized.
Since $d > C_{\mathrm{b}}$, we need to lower the speed limit in section 1 in order to suppress the traffic flow entering the controlled segment. According to (3), the equilibrium point satisfies:

$$v_1^{\mathrm{e}}\rho_1^{\mathrm{e}} = w_1(\rho_{\mathrm{j},1} - \rho_1^{\mathrm{e}}) = C_{\mathrm{b}}.$$

which gives

$$\rho_1^{\mathrm{e}} = \rho_{\mathrm{j},1} - C_{\mathrm{b}}/w_1,\ v_1^{\mathrm{e}} = C_{\mathrm{b}}w_1/(\rho_{\mathrm{j},1}w_1 - C_{\mathrm{b}}) \tag{7}$$

The equilibrium point described in (6) - (7) is the desired equilibrium point which maximizes the flow at the bottleneck and homogenizes the upstream traffic. In addition, it minimizes the average travel time according to the fundamental diagram. Without loss of generality, we assume the length of all sections are the same and equal to unit length. The system (2) - (4) can be expressed

as follows:

$$\begin{aligned}
\dot{\rho}_1 &= w_1(\rho_{\mathrm{j},1} - \rho_1) - v_1\rho_1 \\
\dot{\rho}_i &= v_{i-1}\rho_{i-1} - v_i\rho_i, \text{ for } i = 2, \ldots, N-1 \\
\dot{\rho}_N &= \begin{cases} v_{N-1}\rho_{N-1} - v_{\mathrm{f}}\rho_N, & \rho_N \leq \rho_{\mathrm{d,c}} \\ v_{N-1}\rho_{N-1} - w_{\mathrm{b}}(\rho_{\mathrm{j,b}} - \rho_N), & \rho_N > \rho_{\mathrm{d,c}} \end{cases}
\end{aligned} \tag{8}$$

In (8), the only switching point is $\rho_N = \rho_{\mathrm{d,c}}$. This is consistent with real-world, since the capacities of upstream sections are much larger than C_{b}. As long as system (8) converges to the desired equilibrium point, the steady-state bottleneck flow is maximized and upstream traffic is homogenized.

3.5.2. Feedback Linearization VSL Controller

For the design and analysis of the VSL controller we define the deviations of the state of (8) from the desired equilibrium (6) - (7) by defining the error system as: $e_i = \rho_i - \rho_i^{\mathrm{e}}$ for $i = 1, 2, , \ldots, N$ and $u_i = v_i - v_i^{\mathrm{e}}$ for $i = 1, 2, \ldots, N-1$. Substitute into (8), we have

$$\begin{aligned}
\dot{e}_1 &= -w_1 e_1 - v_1^{\mathrm{e}} e_1 - u_1\rho_1 \\
\dot{e}_i &= v_{i-1}^{\mathrm{e}} e_{i-1} + u_{i-1}\rho_{i-1} - v_i^{\mathrm{e}} e_i - u_i\rho_i \\
&\qquad \text{for } i = 2, \ldots, N-1 \\
\dot{e}_N &= \begin{cases} v_{N-1}^{\mathrm{e}} e_{N-1} + u_{N-1}\rho_{N-1} - v_{\mathrm{f}} e_N, & e_N \leq 0 \\ v_{N-1}^{\mathrm{e}} e_{N-1} + u_{N-1}\rho_{N-1} + w_{\mathrm{b}} e_N, & e_N > 0 \end{cases}
\end{aligned} \tag{9}$$

The transformation of (8) to (9) shifts the non zero equilibrium state of (8) to the zero equilibrium point of (9). The nonlinear terms in (9) are $u_i\rho_i$ for $i = 1, 2, ..., N-1$. Now the problem is to select u_1 through u_{N-1} in order to stabilize system (9) and force all the errors or deviations from the equilibrium state to converge to zero.
We introduce the following feedback controller which 'kills' all nonlinearities and forces the closed loop system to be linear, an approach known as feedback linearization [67]. We choose

$$\begin{aligned}
u_i &= (-v_i^{\mathrm{e}} e_i - \lambda_i e_{i+1})/\rho_i, \text{for } i = 1, \ldots, N-2 \\
u_{N-1} &= \begin{cases} \dfrac{-\lambda_{N-1} e_N - v_{N-1}^{\mathrm{e}} e_{N-1} + v_{\mathrm{f}} e_N}{\rho_{N-1}}, e_N \leq 0 \\ \dfrac{-\lambda_{N-1} e_N - v_{N-1}^{\mathrm{e}} e_{N-1} - w_{\mathrm{b}} e_N}{\rho_{N-1}}, e_N > 0 \end{cases}
\end{aligned} \tag{10}$$

where $\lambda_i > 0$ for $i = 1, \ldots, N-1$ are design parameters. This is a switching controller, whose switching logic is based on the value of e_N. Since we avoid the capacity drop by applying the LC control, the controller is continuous at the switching point. With the feedback linearization

controller (10), the closed loop system becomes:

$$\begin{aligned}
\dot{e}_1 &= -w_1 e_1 + \lambda_1 e_2 \\
\dot{e}_i &= -\lambda_{i-1} e_i + \lambda_i e_{i+1}, \text{for } i = 2 \ldots, N-2 \\
\dot{e}_{N-1} &= \begin{cases} -\lambda_{N-2} e_{N-1} - \lambda_{N-1} e_N + v_{\mathrm{f}} e_N, & e_N \leq 0 \\ -\lambda_{N-2} e_{N-1} - \lambda_{N-1} e_N - w_{\mathrm{b}} e_N, & e_N > 0 \end{cases} \\
\dot{e}_N &= -\lambda_{N-1} e_N
\end{aligned} \tag{11}$$

The stability properties of the closed loop system (11) are described by the following Theorem.

Theorem 3.1. *The equilibrium point $e_i = 0$, $i = 1, 2, \ldots, N$ of the system (11) is isolated and exponentially stable. The rate of exponential convergence depends on the control design parameters λ_i, $i = 1, 2, \ldots, N-1$.*

Proof For $i = 1, 2, \ldots, N$, setting $\dot{e}_i = 0$ in (11), the only equilibrium point is $e_i = 0$. From (11), we can see that the state e_N is decoupled from other states, i.e. $\dot{e}_N = -\lambda_{N-1} e_N.$, whose solution is

$$e_N(t) = e_N(0) \exp(-\lambda_{N-1} t), \ \forall t > 0. \tag{12}$$

Since $\exp(-\lambda_{N-1} t) > 0$ for all t, $e_N(t)$ and $e_N(0)$ have the same sign for all $t > 0$, i.e. if $e_N(0) \leq 0$, then $e_N(t) \leq 0$, if $e_N(0) > 0$, then $e_N(t) > 0$ for all $t > 0$. In other words e_N is either non increasing or non decreasing which means that the state e_N will not switch between $e_N \leq 0$ and $e_N > 0$. Therefore, the dynamics of state e_{N-1} can be written as

$$\dot{e}_{N-1} = \begin{cases} -\lambda_{N-2} e_{N-1} - \lambda_{N-1} e_N + v_{\mathrm{f}} e_N, & e_N(0) \leq 0 \\ -\lambda_{N-2} e_{N-1} - \lambda_{N-1} e_N - w_{\mathrm{b}} e_N, & e_N(0) > 0 \end{cases}$$

Let us define $e = [e_1, e_2, \ldots, e_N]^T$, then the system (11) can be written in the compact form

$$\dot{e} = \begin{cases} A_1 e, & e_N(0) \leq 0 \\ A_2 e, & e_N(0) > 0 \end{cases} \tag{13}$$

where

$$A_i = \begin{bmatrix} -w_1 & \lambda_1 & & & \\ & -\lambda_1 & \lambda_2 & & \\ & & \ddots & \ddots & \\ & & & -\lambda_{N-2} & -\lambda_{N-1} + \beta_i \\ & & & & -\lambda_{N-1} \end{bmatrix}, \ i = 1, 2$$

and $\beta_1 = -w_{\mathrm{b}}, \beta_2 = v_{\mathrm{f}}$. A_1 and A_2 are both upper triangular matrices with all diagonal entries being negative real numbers, i.e. A_1, A_2 are both Hurwitz. Hence, system (13) is exponentially stable. Therefore (11) is also exponentially stable. In addition, for a given sign of $e_N(0)$ there is no switching taking place in (13).
The rate of convergence to the equilibrium depends on the design parameters $\lambda_i, i = 1, 2, ...N - 1$ which can be tuned to achieve a desirable convergence rate. It would also depend on the sign

of the initial condition $e_N(0)$ as the dynamics that drive the error system depend on whether the initial condition $e_N(0)$ is negative or positive. Q.E.D.

The feedback linearization controller (10) is continuous in time. To apply it on real highway, we discretize the controller and apply the following constraints.

1. *Discretization in time.* We discretized the continuous time VSL control commands using the sampling period T_c so that the VSL command is kept constant to its value at $t = kT_c$ till $t = (k+1)T_c$ where $k = 0, 1, 2, ...$

2. *Finite command space.* We use a quantization of 5 mi/h to truncate the generated VLS commands which is easy to follow.

3. *Saturation of Speed Limit Variations.* It is dangerous to decrease the speed limit too fast in both time and space. The decrease should be within some threshold $C_v > 0$ between successive control periods and highway sections. We don't bound the speed limit variation if the speed limit increases. In addition the VSL commands never exceed the legal speed limit.

Using the above constraints we modify the VSL control commands as follows:
Let $u_i(k)$ denotes u_i computed by equation (10) at $t = kT_c$. We have,

$$\bar{v}_i(k) = [v_i^e + u_i(k)]_5 \tag{14}$$

$$\tilde{v}_i(k) = \max\{\bar{v}_i(k), v_i(k-1) - C_v, v_{i-1}(k) - C_v\} \tag{15}$$

$$v_i(k) = \begin{cases} v_{\max}, & \text{if } \tilde{v}_i(k) > v_{\max} \\ v_{\min}, & \text{if } \tilde{v}_i(k) < v_{\min} \\ \tilde{v}_i(k), & \text{otherwise} \end{cases} \tag{16}$$

for $i = 1, 2, \ldots, N-1, k = 0, 1, 2, \ldots$.
In (14), $[\cdot]_5$ is the operator which rounds a real number to its closest whole 5 number. Equation (15) describes the saturation limits on the amount of decrease of VSL commands between successive control steps and highway sections. In (16), $v_{\max}$ and $v_{\min}$ are the upper and lower bounds of VSL commands respectively.
The above modifications will influence the ideal performance of the VSL controller described by Theorem 1. Such modifications are necessary in every control application [17,68,69] and the way to deal with possible deterioration from the ideal performance is to use the design parameters $\lambda_1, \lambda_2, \ldots, \lambda_{N-1}$ to tune the system using intuition and practical considerations. The selection of the feedback gains $\lambda_1, \lambda_2, \ldots, \lambda_{N-1}$ has to consider the trade off between stability and robustness with respect to modeling errors.
We should note that the design and analysis of the feedback linearization VSL controller are based on model (8), which is a simplified version of model (2)-(3) that assumes that section 1 is congested and section 2 through $N-1$ is free flow according to the location of the equilibrium (6). This assumption is valid under our control scheme. That is when the speed limit in section decreases, the outflow of section 1 will be suppressed, which makes section 1 congested and all downstream sections free flow.

3.5.3. Robustness with respect to varying demands

In the analysis above, we assume that the demand d is a constant and $d > C_{\text{b}}$. As explained below, the proposed VSL controller is robust with respect to different demands.
If $d < C_{\text{b}}$, vehicles in the controlled segment would discharge and the densities in each section would be lower than the desired density. The VSLs in each section would increase, but saturated at v_{f}. This situation is easy as due to the low demand congestion can be avoided or managed very well.
When $d > C_{\text{b}}$ and keeps increasing, according to Theorem 3.1, the controller lowers the speed limit in section 1 and limits the number of vehicles that enter the downstream network. Therefore, a queue would be created whose size will be increasing upstream the flow. It appears, at first glance, as if we are moving congestion from the sections under VSL and LC control to upstream sections. The important question we need to answer is how many vehicles there are in this queue and how fast it grows with and without VSL and LC control in the sections under consideration.
In order to analyze the queue size upstream of section 1, we modify the system (2) - (4) by introducing a new state Q, which represents the number of vehicles in the queue upstream section 1. We assume that $Q = 0$ at steady state flow before the incident. Using the flow conservation equation, we have

$$\dot{Q} = d - q_1 \tag{17}$$

where d is the traffic demand. The inflow rate of section 1, q_1 then becomes

$$q_1 = \begin{cases} \min\{d, C_1, w_1(\rho_{\text{j},1} - \rho_1)\}, & Q \leq 0 \\ \min\{C_1, w_1(\rho_{\text{j},1} - \rho_1)\}, & Q > 0 \end{cases} \tag{18}$$

Equation (18) assumes that as long as the queue upstream section 1 is not fully discharged, the inflow rate of section 1 will be as high as the maximum flow rate that section 1 can receive under current ρ_1. Note that the introduction of Q does not make any difference to system (2) - (4) before and during the incident. It only tracks the growth and discharge of the queue upstream section 1. Therefore the stability of the closed-loop system (11) is not affected.
Hence, with the combined VSL and LC controller, the queue size is measured with Q. In the no control case, a queue forms at section N, whose size is denoted by $\hat{Q}$. The following Lemma holds.

Lemma 3.1. *If the demand $d > C_b$, $\hat{Q}$ grows faster than Q at steady state. In particular,*

$$\dot{Q} - \dot{\hat{Q}} = -\epsilon C_b < 0 \tag{19}$$

Proof Similar to Equation (17), we can estimate $\hat{Q}$ with the following equation $\dot{\hat{Q}} = d - \hat{q}_{\text{b}}$, where $\dot{\hat{Q}}$ is the growth rate of $\hat{Q}$, $\hat{q}_{\text{b}}$ is the outflow rate of section N without control. Since $d > C_{\text{b}}$, q_1 converges according to Theorem 3.1 to the desired flow rate C_{b} exponentially with the combined VSL and LC controller. $\hat{q}_{\text{b}}$ would decrease to $\hat{q}_{\text{b}} = (1-\epsilon)C_{\text{b}}$ due to capacity drop. Substituting the steady state values of q_1 and $\hat{q}_{\text{b}}$ in the above equations we obtain (19). i.e. at steady

Figure 8: Steady State q_b under Different Demands — With Control, - - -Without Control

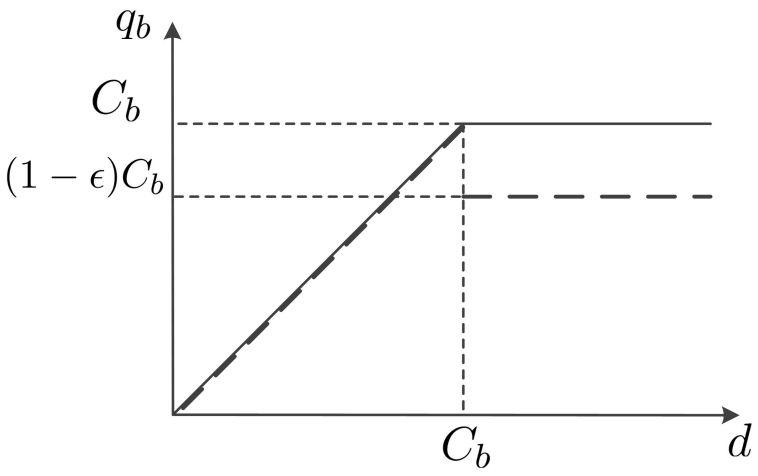

state, the growth rate of Q is less than that of $\hat{Q}$. Q.E.D.

From the analysis above, it is clear that if the demand d increases from below the bottleneck capacity C_b to greater than C_b and keeps increasing, the combined VSL and LC controller is able to protect the bottleneck from getting congested by suppressing the speed limit in section 1 therefore ρ_N can be stabilized at the desired value. On the other hand, in the no control case, the bottleneck is directly exposed to the excessive demand, therefore ρ_N increases and leads to capacity drop. Fig. 8 plots the steady state bottleneck flow q_b with respect to demand d. When $d < C_b$, the bottleneck would not be congested. When $d > C_b$, the bottleneck flow would be stabilized at the maximum value C_b by the combined controller in the controlled case. In the no control case, the flow rate would decrease to $(1-\epsilon)C_b$ due to capacity drop.

Therefore, the combined VSL and LC controller is robust with respect to different levels of traffic demand. The queue of vehicles grows slower in the controlled case than in the case with no control.

3.6. Numerical Results

3.6.1. Simulation Network

We evaluate the combined VSL & LC control method using a microscopic and macroscopic model of the traffic flow on a 10 mile (16 km)-long southbound segment of I-710 freeway in California, United States (between I-105 junction and Long Beach Port), which has a static speed limit of 65 mi/h (105 km/h). We build this freeway network in VISSIM and calibrate the microscopic model using historical data provided by [70]. The car following and lane change behavior of the VISSIM model is calibrated and validated using real measurements under static speed limit of 65 mi/h.

The studied highway segment has 3-5 lanes at different locations. As shown in Fig. 9, we assume the bottleneck is introduced by an incident which blocked one lane. The upstream segment of the

Figure 9: Simulation Network

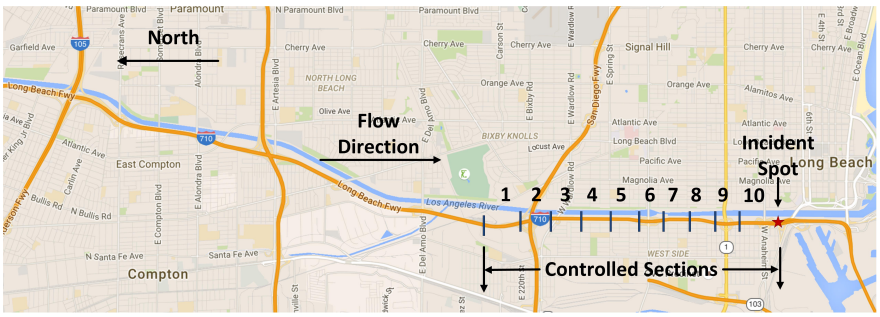

bottleneck is divided to 10 500m-600m sections. The bars across the highway in Fig. 9 are where VSL signs and LC signs deployed. In VISSIM, incidents are simulated by placing stopped bus in certain lane.

3.6.2. Evaluation of the Feedback Linearization VSL Controller

In this section, we design and evaluate a combined VSL and LC controller for the simulation of a real world highway segment. We use both macroscopic and microscopic traffic flow models and carry out Monte Carlo simulations for different incident scenarios in order to evaluate consistency with respect to performance improvements.
We use the same network in Fig. 9 to evaluate the performance of the feedback linearization VSL controller. To demonstrate the performance, robustness and consistency of the proposed controller under different incident conditions, we consider 3 different scenarios with different incident durations. We simulate each scenario under different demand flows. In each scenario, the incident occurs 5 minutes after simulation begins and lasts for **30 min** in scenario 1, which simulates the case of an incident of moderate duration which may be due to an accident; for **10 min** in scenario 2 which simulates the case of a short incident due to a vehicle breakdown or minor accident. The incident is **not removed** after occurrence in scenario 3, which simulates a long time lane closure or a construction site or a physical bottleneck. We evaluate the combined VSL and LC control performance for each scenario with constant demand flows of 6000 veh/h and 6500 veh/h which is higher than the capacity of the bottleneck. 5% of the demand are trucks.
We use a macroscopic model to evaluate the performance of the proposed VSL controller. Since the macroscopic model used does not take into account lane changes and their effect close to the incident, we apply the LC controller to the corresponding microscopic model and use the microscopic model data to validate the macroscopic cell transmission model. The desired equilibrium point of the I-710 highway segment is calculated to be

$$\rho_1^{\mathrm{e}} = 174.6 \text{ veh/mi}, \ \rho_2^{\mathrm{e}} = \rho_3^{\mathrm{e}} = \cdots = \rho_{10}^{\mathrm{e}} = 90 \text{ veh/mi}$$
$$v_1^{\mathrm{e}} = 33.5 \text{ mi/h}, \ v_2^{\mathrm{e}} = v_3^{\mathrm{e}} = \cdots = v_9^{\mathrm{e}} = 65 \text{ mi/h}$$

The LC recommendation sign is deployed at the beginning of section 9 and section 10 in Fig. 9,

Figure 10: Controller Performance without Constraints

(a) Vehicle Density

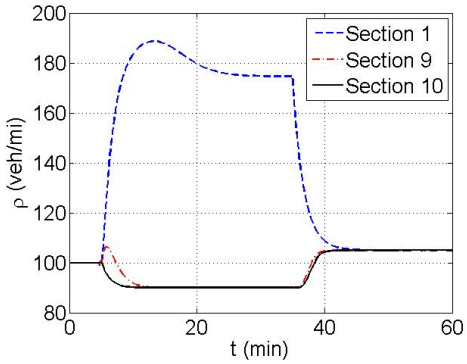

(b) VSL Command

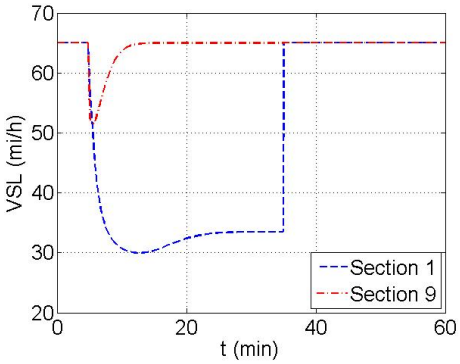

and recommends vehicles to change lanes by moving to the open lanes on either side. For the VSL controller, the following parameters are used: $C_{\mathrm{v}} = 10$ mi/h, $v_{\max} = 65$ mi/h, $v_{\min} = 10$ mi/h, $T_{\mathrm{c}} = 30$ s. We choose $\lambda_1 = \lambda_2 = \cdots = \lambda_9 = 20$. We should note that as mentioned in Section 3.6.1, the capacity of the bottleneck with incident is 4500 veh/h. However, in the macroscopic model, we are assuming a strict triangular fundamental diagram and the capacity C_{b} is calibrated to be $v_{\mathrm{f}} \times \rho_{10}^{\mathrm{e}}$ = 5850 veh/h. The reasons for this difference are explained in the following section. Since the logic of our VSL controller is to stabilize the density at the critical value, the accurate value of equilibrium density is more important than the value of flow rate. The densities and variable speed limits for the case of scenario 1 with demand $d = 6500$ veh/h are plotted in Fig. 10. For clarity of presentation, we only plot the densities in section 1, 9 and 10 and VSL commands in section 1 and 9.

Fig. 10 demonstrates what is predicted by theory. That is the density in section 1 converges to the desired density of 174.6 veh/mi and the densities in sections 9, 10 to the desired density of 90 veh/mi till the incident is removed at $t = 35$ min, in which case the densities converge to 105 veh/h, which is higher than the pre-incident value. This is because the queue formed at section 1 during the incident needs to discharge, therefore the temporary demand of the bottleneck after the incident is higher than the demand of the overall network.

We then apply the constraints (14) - (16) to the VSL controller. The densities and VSL commands with constraints are shown in Fig. 11. Fig. 11a demonstrates that the density in the discharging section converges to $\rho_{10} = 85$ veh/mi, which is lower than $\rho_{10}^{\mathrm{e}} = 90$ veh/mi. According to the fundamental diagram in Fig. 7, the steady state flow would be a bit lower than the desired flow rate. However, the difference is negligible. The VSL command in section 1 converges to $v_1 = 30$ mi/h and the VSL command in section 9 converges to $v_9 = 55$ mi/h, which are not exactly the same as the desired values due to the application of the constraints.

In Fig. 10, ρ_9 and ρ_{10} converge to the corresponding equilibrium point in less than 10 min while ρ_1 converges to ρ_1^{e} much slower (in about 20 min). The reason of this phenomenon is the different values of ρ_1^{e} and ρ_9^{e}. As discussed in [69], a low value of speed limit would suppress the capac-

Figure 11: Controller Performance with Constraints

(a) Vehicle Densities

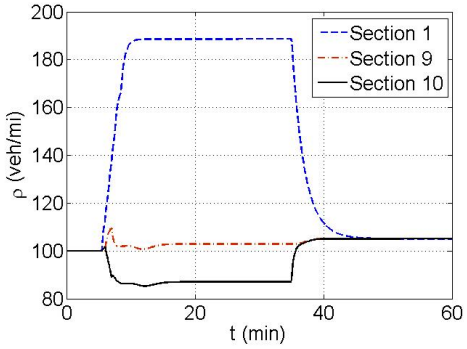

(b) VSL Commands

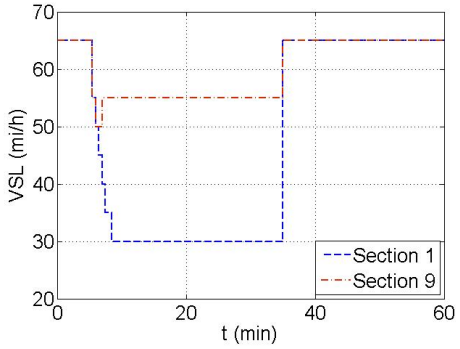

Figure 12: System Behavior without Control

(a) Vehicle Densities without Control

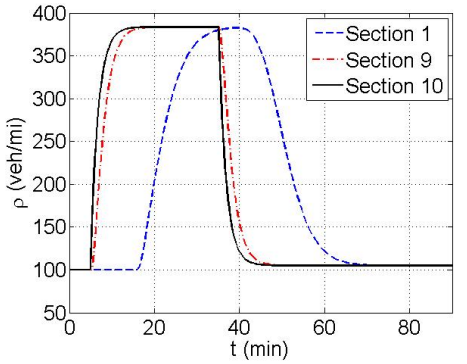

(b) Bottleneck Flow with and without Control

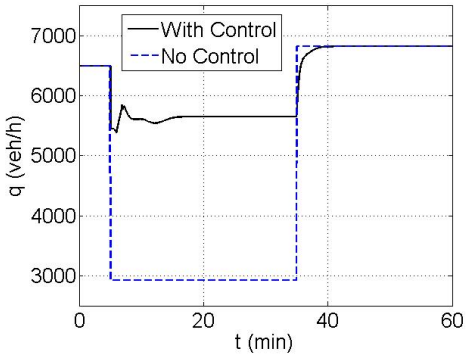

ity of the section. After the incident occurs, v_1 decreases to a low value and ρ_1 increases rapidly, since because of the outflow of section 1, q_2 is suppressed by v_1. Then the process of adjusting ρ_1 from the overshoot to ρ_1^e takes long time due to the low level of q_2.

On the other hand, from Fig. 11, we can see that with the constrained VSL, ρ_1 converges fast and no overshoot is observed. This is because v_1 is constrained by (14) - (16) thus fails to adjust ρ_1 back to ρ_1^e after overshooting, however, as stated before, the difference is negligible. Similarly, in Fig. 11b, the VSL command v_1 converges to 30 mi/h in less than 10 min and stays at that value. Since the VSL commands only take whole 5 mi/h values due to (14), small variation of v_1 in the continuous case are all rounded up. Therefore, in the constrained case, there are no variations of v_1 around 30 mi/h.

Fig. 12a demonstrates how vehicle densities evolve in scenario 1 without any control. The density increases dramatically in the discharging section to 370 veh/h and propagates upstream. Even after the incident is removed at $t = 35$ min, the shockwave continues propagating backwards and takes longer time to discharge. Fig. 12b shows the flow rate at the bottleneck with and without

Figure 13: Growth and Discharge of the Queue

(a)

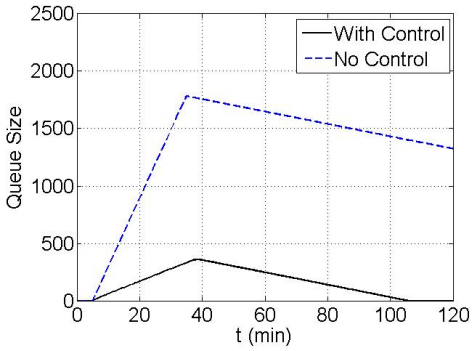

(b)

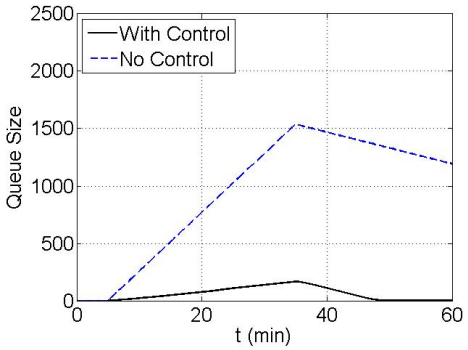

control. During the incident, the flow rate decreases to less than 3000 veh/h due to capacity drop in the case of no control, while the bottleneck flow converges to 5600 veh/h with the combined VSL and LC controller. Again, the flow rate under control is higher than the real capacity of the bottleneck due to the assumption of triangular fundamental diagram.

We use scenario 1 to examine the growth of the queue at the entrance to the controlled network. The numbers of vehicles in the queues are plotted in Fig. 13 with respect to the time t. When the demand $d = 6500$ veh/h, the maximum number of vehicles in the queue is 1700 in the case of no control, while the number is less than 500 in the control case, which demonstrates that the combined VSL and LC controller reduces the queue size significantly. The queues grow slower and discharge faster with lower demand, as less vehicles arrive at the tail of the queue.

We also use a microscopic traffic model that is closer to the real environment in order to confirm the improvements predicted by theory and demonstrated by the macroscopic model. In addition, the microscopic model allows us to evaluate additional performance criteria such as number of stops and lane changes that affect safety as well as the environmental impact of VSL and LC controllers. We simulate the I-710 traffic flow network shown in Fig. 9 for the above mentioned 3 traffic scenarios. The simulated demand consists of 85% light duty passenger vehicles and 15% trucks. This ratio represents the highest truck ratio at peak hours on I-710, therefore shows the worst traffic condition [70]. To show consistency of the results, we conducted 10 sets of Monte-Carlo simulations with different random seeds for each scenario. The curves in Fig. 14 are generated from a single simulation. The evaluation results in Table 1 - 3 are the average of 10 simulations.

Fig. 14 shows the density and flow rate of the discharging section in both microscopic and macroscopic simulations. We can see that the density curve in macroscopic and microscopic simulations match each other. The microscopic flow rates in the no control cases are very similar and consistent with those in macroscopic simulations. However, when the combined VSL and LC controller is applied, the flow rates in microscopic simulations are lower than those in macroscopic simulations, which means that the flow speed in the discharging section in microscopic simulations is lower than what we get from the macroscopic model.

Figure 14: Comparison of Macroscopic and Microscopic Models
— Microscopic without Control, - - - Macroscopic without Control
— Microscopic with Control, - - - Macroscopic with Control

(a)

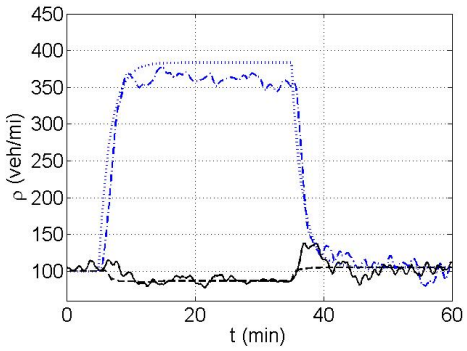

(b)

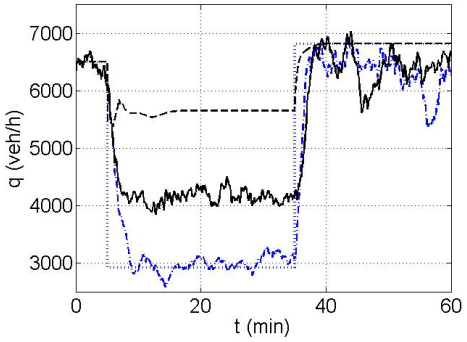

(c)

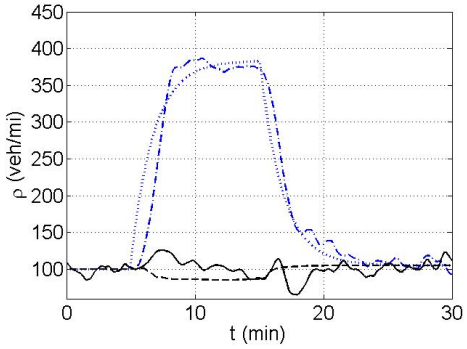

(d)

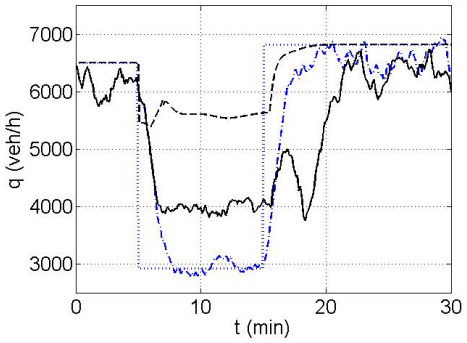

(e)

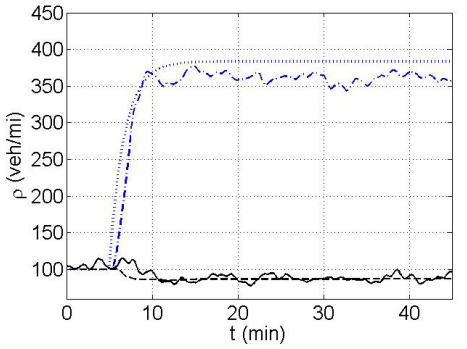

(f)

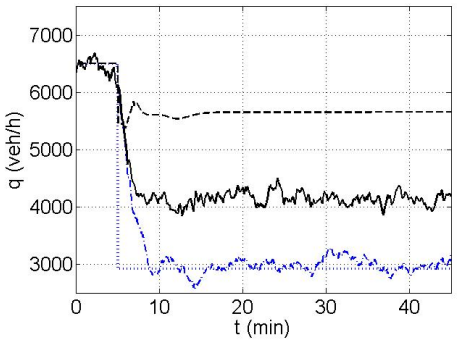

The deviation in speed is due to the following factors:

1. *Modeling error.* In the macroscopic model, we use a simplified triangular fundamental diagram to model the discharging section, which implies that the flow speed at the desired

Figure 15: Fundamental Diagram with Combined Controller

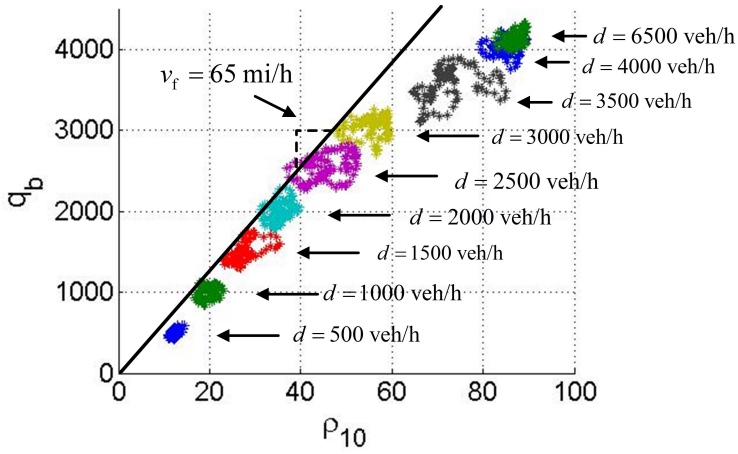

density is v_f. However, the actual speed would be lower than v_f. Especially when the LC controller is applied, drivers are usually conservative when merging to the open lanes.

2. *Speed limit following delay*. In the macroscopic model, we assume that the flow speed follows the speed limit exactly with no delay. However, in the microscopic model, the traffic flow needs time and space to accelerate to the desired speed limit. When vehicles change lanes, they do not adjust to new speeds instantaneously.

3. *Friction effect*. The friction effect reflects the empirically observed drivers' fear of moving fast in the open lanes when an incident or slowly moving vehicles exist in neighboring lanes [71]. In microscopic simulation, this phenomenon is captured and has an effect when compared with the macroscopic simulations.

Fig. 15 demonstrates the relationship between ρ_{10} and q_b at the equilibrium state under the combined VSL and LC controller in microscopic simulations. In Fig. 15, the negative slope part, i.e. the congested part of the fundamental diagram is not observed even when the demand d is higher than the capacity, since the controller protects the bottleneck from getting congested. For different levels of demand, the data points concentrate in different clusters which shows that the controller homogenizes the traffic flow. Furthermore, when $d \leq 3000$ veh/h, the data points stay close to the line with the slope $v_f = 65$ mi/h. When d keeps increasing, the data points move to the right side of the line due to the factors we explained above.
We use the following measurements to evaluate the performance of the proposed controller. To be precise, in scenario 1 and 2, the measurements start at the time instant that the incident begins ($t = 5$ min) and terminate at the time instant 10 minutes after the incident ends ($t = 45$ min in scenario 1 and $t = 25$ min in scenario 2), so that the traffic states can achieve steady state. In scenario 3, where the incident is not removed, the measurements start at the time instant that the incident begins ($t = 5$ min) and terminate at $t = 45$ min. In each scenario, we collect the

Table 1: Evaluation Results of Scenario 1

Demand	6000 veh/h					6500 veh/h				
Control	No Control	LC Only	VSL Only	Control	Improvement	No Control	LC Only	VSL Only	Control	Improvement
T_t	18.85	17.12	18.95	16.85	-10.59%	20.72	17.67	21.21	16.83	-18.76%
$\bar{s}$	11.16	2.45	3.61	1.90	-83.00%	12.10	2.55	3.78	1.91	-84.21%
$\bar{c}$	4.00	4.75	4.74	3.78	-5.60%	4.67	5.54	5.88	4.31	-7.71%
NOx	1.56	1.49	1.61	1.49	-4.43%	1.64	1.58	1.60	1.53	-6.71%
CO2	558.56	543.22	577.59	536.01	-4.04%	589.46	556.47	605.59	537.21	-8.86%
Energy	178.65	173.67	184.76	171.40	-4.06%	186.78	177.93	193.73	170.31	-8.82%
PM25	0.049	0.048	0.047	0.050	0.66%	0.054	0.054	0.053	0.050	-7.73%

data of all vehicles that pass through the bottleneck during the above defined measuring periods and calculate the following values: (a)Average travel time $\bar{T}_t$. (b)Average number of stops $\bar{s}$. (c)Average number of lane changes $\bar{c}$. (d)Average fuel consumption rate. (e)Average CO2 emission rate. (f)Average NOx emission rate. (g)Average PM25 emission rate. Control effects on traffic mobility are evaluated using the average travel time. Let N_v denote the number of vehicles pass through the bottleneck during the measuring period. Average travel time $\bar{T}_t$ is defined as

$$\bar{T}_t = \sum_{i=1}^{N_v} (t_{i,\text{out}} - t_{i,\text{in}})/N_v$$

where $t_{i,\text{in}}$ and $t_{i,\text{out}}$ denote the time instant vehicle i enters and exits the network respectively. Note that our simulation network has enough space upstream of the controlled segment, therefore the time waiting in the queue is also counted.

Control effects on traffic safety are evaluated by the average number of stops and average number of lane changes. Less stops and lane changes indicate smoother traffic flow and lower probability of crash [16]. $\bar{s}$ and $\bar{c}$ are defined as

$$\bar{s} = \sum_{i=1}^{N_v} s_i/N_v, \ \bar{c} = \sum_{i=1}^{N_v} c_i/N_v$$

where s_i, c_i are number of stops and lane changes performed by vehicle i respectively. For environmental impact, we measure the average fuel consumption rate and the average emission rates of CO2, NOx, and PM25. These rates are uniformly defined as:

$$R = \sum_{i=1}^{N_v} E_i / \sum_{i=1}^{N_v} d_i$$

where E_i denotes the fuel consumed or a certain type of emission generated by vehicle i in the highway network, d_i represents the distance traveled by vehicle i in the network, and R denotes the fuel consumption rate or the tailpipe emission rate of CO2, NOx, or PM25. The fuel consumption rate and emission rates are calculated using the MOVES model of the Environment Protection Agency (EPA) based on the speed and acceleration profile of each vehicle [72].

Table 2: Evaluation Results of Scenario 2

Demand	6000 veh/h					6500 veh/h				
Control	No Control	LC Only	VSL Only	Control	Improvement	No Control	LC Only	VSL Only	Control	Improvement
T_t	12.41	11.87	13.46	11.63	-6.25%	13.58	12.62	15.02	12.42	-8.54%
$\bar{s}$	5.16	0.75	2.16	0.65	-87.37%	5.72	1.58	2.33	0.91	-84.09%
$\bar{c}$	3.68	3.80	3.90	3.52	-4.31%	4.27	4.81	5.01	3.91	-8.33%
NOx	1.42	1.41	1.44	1.39	-2.48%	1.48	1.49	1.51	1.42	-4.05%
CO2	483.37	479.17	497.81	470.16	-2.73%	508.13	504.16	524.36	487.18	-4.12%
Energy	154.53	151.65	159.18	150.36	-2.70%	161.04	161.15	167.66	154.18	-4.26%
PM25	0.041	0.041	0.041	0.041	-0.77%	0.046	0.047	0.047	0.045	-2.17%

Table 3: Evaluation Results of Scenario 3

Demand	6000 veh/h					6500 veh/h				
Control	No Control	LC Only	VSL Only	Control	Improvement	No Control	LC Only	VSL Only	Control	Improvement
T_t	19.84	17.25	18.16	16.69	-15.89%	21.25	16.75	20.45	16.55	-22.13%
$\bar{s}$	15.46	2.13	4.00	1.74	-88.75%	16.12	2.54	3.72	1.83	-88.65%
$\bar{c}$	4.61	4.55	5.11	4.21	-8.60%	4.58	5.36	6.36	4.10	-10.48%
NOx	1.58	1.51	1.58	1.50	-4.95%	1.58	1.55	1.66	1.50	-4.95%
CO2	570.72	538.41	564.54	529.76	-7.18%	568.96	550.32	597.94	523.25	-8.04%
Energy	182.55	172.17	180.58	169.39	-7.21%	182.85	175.99	191.26	168.11	-8.06%
PM25	0.052	0.047	0.047	0.050	-3.74%	0.052	0.053	0.053	0.050	-3.74%

Table 1, 2 and 3 demonstrate the results of microscopic evaluation of all 3 scenarios under different traffic demands. From the results, we can see that the combined VSL & LC controller is able to provide significant improvements in traffic mobility, safety and environment. For traffic mobility, the proposed controller reduces the average travel time of each vehicle by 6.25% - 22.13%. For traffic safety, the combined VSL and LC controller dramatically decreases the average number of stops by 83% - 88.75% in different scenarios, therefore drastically reduces the instances of the stop-and-go traffic, smooths the traffic flow and damps the shockwave. Average number of lane changes is also decreased by 5.6% - 10.48%. The combined VSL and LC controller homogenizes the density and speed in each section. Drivers tend to not change lane if densities and speeds are similar in all lanes, therefore the VSL control reduces the number of lane changes in the network under consideration. This is highly important for traffic safety in highway segments with high truck ratio. Trucks not only take long time and large space to change lane, their large size also blocks the eye sight of drivers, which makes lane changes of trucks much more dangerous than other vehicles.

The proposed controller reduces the fuel consumption rate and tailpipe emission rate from two perspectives. First, it reduces the travel time of vehicles, therefore decreases the emission levels of vehicles waiting in the queue. Second, it smooths the traffic flow and suppresses the acceleration and deceleration, therefore decreases the emission in these transient states. In the simulation, fuel consumption rate is decreased by 4.26% - 8.82%. The improvement in CO_2 emission rate is approximately proportional to the improvement of fuel consumption rate, since CO_2 is the main product of fuel burnt. The proposed controller reduces NO_x emission rate by about 3.54% - 6.71%. The emission rate of PM25 is also decreased by 3.74% - 7.73%. Therefore, the combined VSL and LC controller is able to bring environmental benefits.

The question how much of these improvements is due to VSL and LC controller alone is also answered using these simulation studies. From Table 1 - Table 3, we can see that when the LC controller is applied alone, all evaluation criteria improve except for the average number of lane changes. The improvements on T_{t} and $\bar{s}$ are significant, while other criteria are only improved slightly. As discussed in Section 3.3, the LC controller is able to recommend upstream vehicles to make lane changes before stopping at the queue and avoid the capacity drop therefore reduce the average travel time and average number of stops. Improvements on environmental criteria are results of improvements of traffic mobility. However, for the average number of lane changes, the LC controller only makes the lane changes take place in advance, instead of avoiding them, thus fails to reduce $\bar{c}$. Furthermore, when the VSL controller is applied alone, only the average number of stops is reduced. Other criteria are not improved and in some cases are even deteriorated by the VSL controller. This is because the VSL controller (10) is designed based on the assumption that the capacity drop has already been removed by the LC controller. When the LC controller is absent, VSL is not able to improve the bottleneck flow and reduce the vehicle density. But when the VSL controller is applied together with the LC controller, all criteria are further improved since the VSL stabilizes the vehicle densities at the desired equilibrium point and homogenizes the traffic flow. When the traffic flow is homogenized in each section and lane, the drivers do not tend to change lanes frequently, hence the average numbers of lane changes are also reduced.
Comparing the three scenarios, the improvement on each measurement criteria in scenario 2 appears to be less significant than the other 2 scenarios. The reason is that the incident duration in scenario 2 is very short.

4 Coordinated Variable Speed Limit, Ramp Metering and Lane Change Controller

The coordination of RM and VSL considers network mobility, on-ramp queues and fairness between the mainline and the ramps. The objective is to keep a balanced delay time between vehicles on the mainline and the ramps and avoid queues on the ramps from spilling back to the urban roads. In this section, we use an analytical method to design a coordinated VSL and RM controller based on a cell transmission macroscopic model with triangular fundamental diagram which together with a lane change controller guarantees stability of the traffic flow and convergence of traffic density to the desired equilibrium point exponentially fast. Considering the fact that RM controllers have been widely deployed in the United States, we assume that the RM control command is determined before the VSL and design the VSL controller to coordinate with the RM and stabilize the traffic flow. The coordinated VSL and RM controller with lane change is evaluated using Monte Carlo microscopic simulations and shows significant improvement in traffic mobility, safety and the environment impact.

Figure 16: Effects of LC and VSL on Fundamental Diagrams

(a) w/ and w/o LC

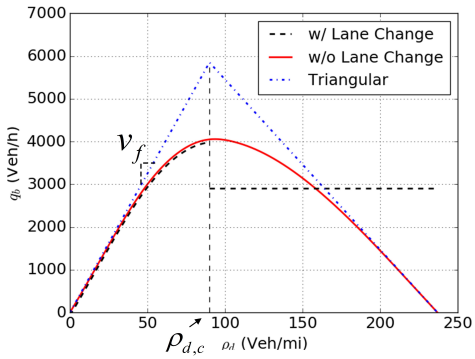

(b) w/ and w/o VSL

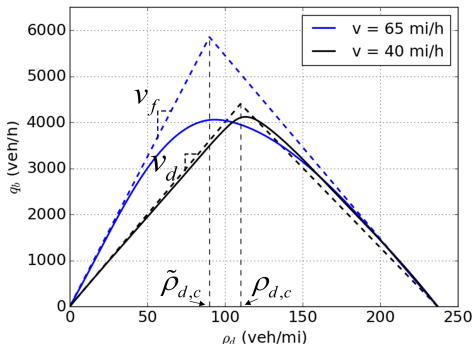

4.1. System Modeling

4.1.1. Effect of VSL on the Fundamental Diagram

Consider the highway bottleneck shown in Fig. 9. A bottleneck is introduced by an incident that blocks one lane. The speed limit upstream the bottleneck is the free flow speed $v_f = 65$ mi/h. As discussed in Section 3.3, the lane change controller can avoid the capacity drop. However, as shown in Fig.16a, in the fundamental diagram with lane change control, the low ρ_d part is very close to its triangular approximation, which means that the flow speed is close to v_f, while the flow speed decreases as ρ_d approaches $\rho_{d,c}$. In the previous section we attribute the reduction of speed to modeling error, delay of speed limit following and driver's caution when passing the incident site. This deviation of speed will not harm the benefit of VSL with respect to traffic mobility when designing the VSL controller based on the triangular fundamental diagram as long as ρ_d is stabilized at $\rho_{d,c}$. However, if the speed limit upstream the bottleneck is v_f, vehicles need to decelerate when approaching the bottleneck, which leads to shock waves that propagate upstream. If we decrease the speed limit upstream the bottleneck to v_d, such that $0 < v_d < v_f$, according to [19], the critical density in the fundamental diagram will be shifted to higher value and the slope of the under-critical part of the fundamental diagram will be decreased and made closer to a straight line. Our microscopic simulations confirm this statement. The black solid line in Fig. 16b shows the fundamental diagram under a speed limit of 40 mi/h. Compared to the one under 65 mi/h, which is shown as the blue solid line in Fig. 16b, the capacity of the bottleneck is not decreased despite under a lower speed limit as the critical density is increased from $\tilde{\rho}_{d,c}$ to $\rho_{d,c}$. As we can see in the figure, this fundamental diagram is very close to its triangular approximation, that is, the speed deviation at $\rho_{d,c}$ is very small. If we design the coordinated VSL and RM controller based on this fundamental diagram and let the VSL command converge to v_d at the equilibrium state, the shockwave upstream the bottleneck will be attenuated. We demonstrate this with microscopic simulations in Section 4.4. To conclude, under speed limit of v_d, the highway

Figure 17: Configuration of the Highway Segment

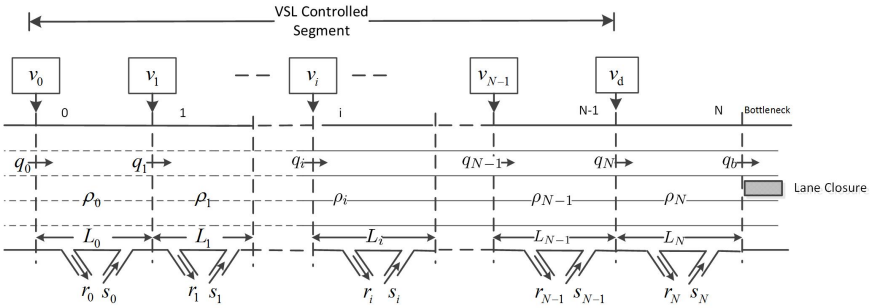

bottleneck can be modeled with high accuracy as equation 4

4.2. Cell Transmission Model with Ramp Flows

The highway segment to be controlled by the coordinated VSL and RM controller is shown in Fig. 17. The bottleneck is introduced by a lane closure. The highway segment upstream the bottleneck is divided into $N+1$ sections, which are indexed as section 0 through section N. For $i = 0, 1, ..., N$, ρ_i, q_i, r_i, s_i represent the vehicle density, mainline in-flow rate, on-ramp flow rate and off-ramp flow rate in section i respectively, where ρ_i, s_i are measurable, r_i are determined by the RM controller, therefore also measurable. For $i = 0, 1, ..., N-1$, v_i denote the variable speed limit in section i. In section N, the speed limit is a constant denoted by v_d. q_b denotes the flow rate through the bottleneck. Let $R_i = r_i - s_i$ be the net ramp flow and L_i the length of section i, for $i = 0, 1, ..., N$. According to the flow conservation law, we have

$$\begin{aligned} \dot{\rho_i} &= \frac{1}{L_i}(q_i - q_{i+1} + R_i), \quad \text{for } i = 0, 1, ..., N-1 \\ \dot{\rho_N} &= \frac{1}{L_N}(q_N - q_b + R_N) \end{aligned} \tag{20}$$

The flow rate and bottleneck model is the same as (3) and (4). For the sake of completeness, we write the equations here.

$$\begin{aligned} q_0 &= \min\{d, C_0, w_0(\rho_{\mathrm{j},0} - \rho_0)\} \\ q_i &= \min\{v_{i-1}\rho_{i-1}, C_i, w_i(\rho_{\mathrm{j},i} - \rho_i)\}, \ i = 1, \ldots, N \end{aligned} \tag{21}$$

$$q_{\mathrm{b}} = \begin{cases} v_{\mathrm{d}}\rho_N, & \rho_N \le \rho_{\mathrm{d,c}} \\ w_{\mathrm{b}}(\rho_{\mathrm{j,d}} - \rho_N), & \rho_N > \rho_{\mathrm{d,c}} \end{cases} \tag{22}$$

4.3. Controller Design

In this section, the coordinated VSL and RM controller is designed. We first design the VSL controller by assuming that the RM control command is given. Then we choose the ramp metering strategy, ALINEA/Q, to manage the ramp flows and the queue lengths on ramps.

4.3.1. Design of VSL

The goals of designing the VSL controller include: (1) Given any type of RM controller, the VSL controller should be able to coordinate with it and stabilize the density ρ_N in the discharging section at the critical value $\rho_{d,c}$, in order to keep q_b at the highest level. (2) Homogenize the traffic flow upstream the bottleneck in order to improve the traffic safety and bring environmental benefits. Consider the subsystem which includes section 1 through section N. Define the error states

$$e_i = \rho_i - \rho_{d,c}, \text{for } i = 1, 2, ..., N$$

We have

$$\begin{aligned} \dot{e}_i &= \frac{1}{L_i}(v_{i-1}\rho_{i-1} - v_i\rho_i + R_i), \text{ for } i = 1, 2, ..., N-1 \\ \dot{e}_N &= \begin{cases} \frac{v_{N-1}\rho_{N-1} - v_d\rho_N + R_N}{L_N}, & \rho_N \le 0 \\ \frac{v_{N-1}\rho_{N-1} - w_b(\rho_{j,b} - \rho_N) + R_N}{L_N}, & \rho_N > 0 \end{cases} \end{aligned} \tag{23}$$

Let

$$\begin{aligned} v_i &= \frac{-\lambda_i L_{i+1} e_{i+1} + v_d\rho_{d,c} - \sum_{j=i+1}^{N} R_j}{\rho_i}, \text{ for } i = 0, 1, ..., N-2 \\ v_{N-1} &= \begin{cases} \frac{-\lambda_{N-1} L_N e_N + v_d\rho_N - R_N}{\rho_N - 1}, & \rho_N \le \rho_{d,c} \\ \frac{-\lambda_{N-1} L_N e_N + w_b(\rho_{j,b} - \rho_N) - R_N}{\rho_N - 1}, & \rho_N \le \rho_{d,c} \end{cases} \end{aligned} \tag{24}$$

Substitute the controller (24) into the open-loop system (23), we have the following closed-loop system:

$$\begin{aligned} \dot{e}_i &= -\lambda_{i-1} e_i + \frac{L_{i+1}}{L_i}\lambda_i e_{i+1}, \text{ for } i = 1, 2, ..., N-2 \\ \dot{e}_{N-1} &= \begin{cases} -\lambda_{N-2} e_{N-1} + \frac{L_N}{L_{N-1}}(\lambda_{N-1} - v_d)e_N, & \rho_N \le 0 \\ -\lambda_{N-2} e_{N-1} + \frac{L_N}{L_{N-1}}(\lambda_{N-1} + w_b)e_N, & \rho_N > 0 \end{cases} \\ \dot{e}_N &= -\lambda_{N-1} e_N \end{aligned} \tag{25}$$

Theorem 4.1. *$e_i = 0$, for $i = 1, 2, ..., N$ is the unique and isolated equilibrium point of the closed-loop system (25) and is guaranteed to be globally exponentially stable. The rate of exponential convergence depends on the control design parameters λ_i, $i = 0, 1, ..., N-1$.*

The proof of Theorem 4.1 is similar to the proof of Theorem 3.1. According to Theorem 4.1, the steady state value of ρ_i is $\rho_{i,ss} = \rho_{d,c}, i = 1, ..., N$. The steady state value of v_i is $v_{i,ss} = v_d - \sum_{j=i+1}^{N} R_i/\rho_{d,c}, i = 1, ..., N-1$. Therefore, by applying the coordinated VSL and RM

controller, ρ_1 through ρ_N are stabilized and homogenized. The effect of a ramp flow is compensated by its upstream VSL and does not affect downstream traffic. If $R_i = 0$, then $v_{i,ss} = v_d$, for $i = 1, ..., N-1$. That is the upstream speed limit converges to v_d. By adjusting the value of v_d, we can guarantee that the shockwave resulted by speed deviation between actual traffic flow and the triangular fundamental diagram is eliminated.
Now let us consider the dynamics of ρ_0 and v_0. Since q_1 converges to $v_d\rho_{d,c}$, if the demand $d > v_d\rho_{d,c}$, ρ_0 will increase. Once $\rho_0 > \rho_{j,0} - d/w_0$, we have

$$\dot{\rho}_0 = \frac{1}{L_0}(w_0(\rho_{j,0} - \rho_0) - v_0\rho_0 + R_0) \tag{26}$$

Substitute (24) into (26), we have

$$\dot{\rho}_0 = \frac{1}{L_0}(w_0(\rho_{j,0} - \rho_0) - v_d\rho_{d,c} + \sum_{j=0}^{N} R_j)$$

Assume that $\sum_{j=0}^{N} R_j$ is constant, then

$$\rho_0 = \rho_{j,0} + \frac{\sum_{j=0}^{N} R_j - v_d\rho_{d,c}}{w_0}$$

is a stable equilibrium point. As long as $\sum_{j=0}^{N} R_j < v_d\rho_{d,c}$, ρ_0 will not exceed the jam density $\rho_{j,0}$ and v_0 will not go negative, thus the VSL controller is feasible.
For driver's acceptance and safety, we as well apply the constraints (14) - (16) to the VSL controller (24).

4.3.2. Design of the RM Controller

According to Theorem 4.1, the VSL controller (24) can stabilize the system and improve the mobility as long as the net ramp flow is lower than the bottleneck capacity. It seems that RM control is unnecessary. However, if no RM is applied and large ramp flows flush into the mainline, the merging of ramp flows will severely disturb the mainline flow. Furthermore, when the net ramp flow is high, the VSL controller (24) will suppress the mainline flow in order to spare the capacity for the ramp flows. That is, without RM control, the ramp flow will always have priority which may harm the fairness between the ramp flows and the mainline flow, or even make the VSL controller infeasible. Furthermore, the RM controller should be able to manage the queue on the ramps so that the queues do not spill backwards to the urban road network. We adopt the ALINEA/Q, which modifies the classic ALINEA ramp metering strategy with queue adjustment. The original ALINEA/Q method proposed in [38] includes the downstream occupancy and the queue length in the feedback loop. In this paper, to be consistent with the VSL controller, we use the downstream density instead of occupancy.
For an on-ramp i, two RM rates, $r_i^d(k)$ and $r_i^q(k)$, are decided respectively based on the down-

stream density and the queue length on the ramp at each time step $t = kT_c$. The final RM rate $r_i(k)$ is the maximum of the two. i.e.

$$\begin{aligned} r_i^d(k) &= r(k-1) + \beta_d[(\rho_{d,c} - \rho_i(k))] \\ r_i^q(k) &= \beta_q(w_i^r - w_i(k)) + d_i(k-1) \\ r_i(k) &= \max\{r_i^d(k), r_i^q(k)\} \end{aligned} \tag{27}$$

where $\rho_i(k)$ is the density in the highway section that connects to ramp i, $w_i(k)$ is the queue length on ramp i at time step k, $d_i(k-1)$ is the demand from ramp i within time step $k-1$, w_i^r is the reference queue length of ramp i. $r_i^d(k)$ is an integral feedback controller that regulates $\rho_i(k)$ to be close to $\rho_{d,c}$, which helps maintain the vehicle density on mainline at the desired equilibrium value. $r_i^q(k)$ adjusts the RM rate in order to prevent the queue length from being too large, i.e. if $w_i(k)$ is larger than w_i^r, the RM rate will increase to discharge excessive vehicles in the queue and newly arrived vehicles. Since the final RM rate is the maximum of the two, the ramp flow will get the priority to pass the bottleneck if the ramp queue is large, while the mainline flow will get the priority if the vehicle density on the mainline is high. In this way, the ALINEA/Q strategy maintains the fairness between the ramp flows and the mainline flow and avoids the ramp queues from piling up towards the urban road.

4.4. Numerical Simulations

In this section , we use the microscopic simulator VISSIM to carry out Monte Carlo simulations to evaluate the performance of the coordinated VSL, RM and lane change control on traffic mobility, safety and the environment.

4.4.1. Scenario Setup

We evaluate the proposed controller on the highway segment in Fig. 9. To coordinate with the ramps, we divide the highway segment in to 8 sections, the VSL signs are deployed at the beginning of section 0 through 6. An incident blocks the middle lane at the end of section 7 and creates a bottleneck. 4 on-ramps, which are equipped with RM, and 5 off-ramps are connected to the highway segment. The lane change control is deployed at the beginning of section 7. The incident occurs at 5 minutes after simulation starts, and lasts for 30 min. The capacity of the highway segment is 6800 veh/h without incident. During the incident, the ideal bottleneck capacity is about 4500 veh/h. We load the network with the real demand at 5pm on Monday, which is a peak hour. The mainline demand is 4500 veh/h, the on-ramp demand from upstream to downstream are 400 veh/h, 500 veh/h, 300 veh/h, 300 veh/h respectively.

4.4.2. Simulation Results

Fig. 19 shows the curve of ρ_7 and ρ_0, which are the vehicle density of the discharging section and the first VSL controlled section, respectively. When there is no control, ρ_7 starts increasing im-

Figure 18: Geometry of Simulation Network

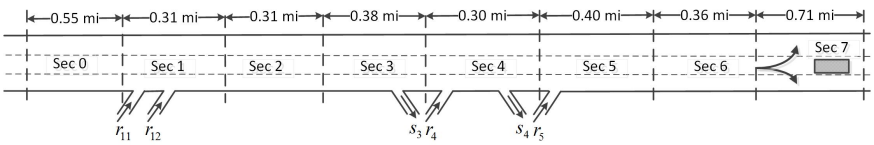

Figure 19: Vehicle Densities w/ and w/o Control
—with control, —no control

(a) Density in section 7

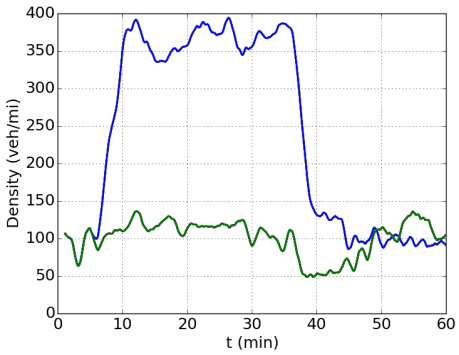

(b) Density in section 0

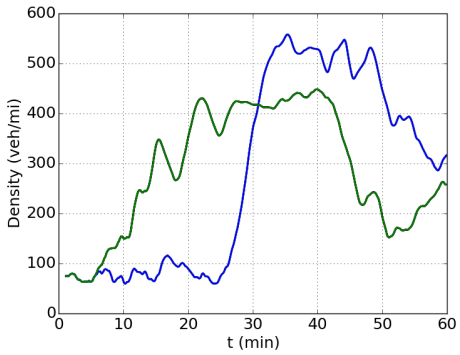

Figure 20: Density Contours

(a) $v_d = 40$ mi/h

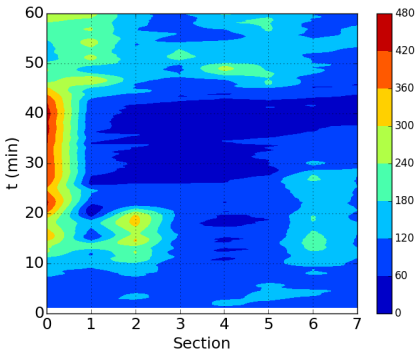

(b) $v_d = 65$ mi/h

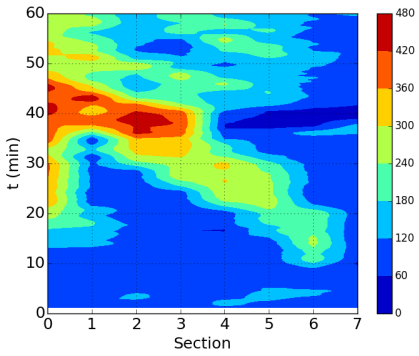

mediately as the incident occurs at $t = 5$ min. In addition the shockwave propagates upstream, which makes ρ_0 starts increasing at $t = 25$ min and reaches 500 veh/mi. The high density in section 0 does not discharge until 15 min after the incident is removed. When the coordinated controller is applied, ρ_7 increases slightly and is stabilized at 110 veh/mi. ρ_0 increases immediately after the incident since v_0 decreases to reduce the flow into downstream sections and is stabilized at around 400 veh/h which is lower than that without control.

Figure 21: Queue Length w/ and w/o Control
—VSL + RM, —RM only

(a) Queue length on r_{11} (b) Queue length on r_4

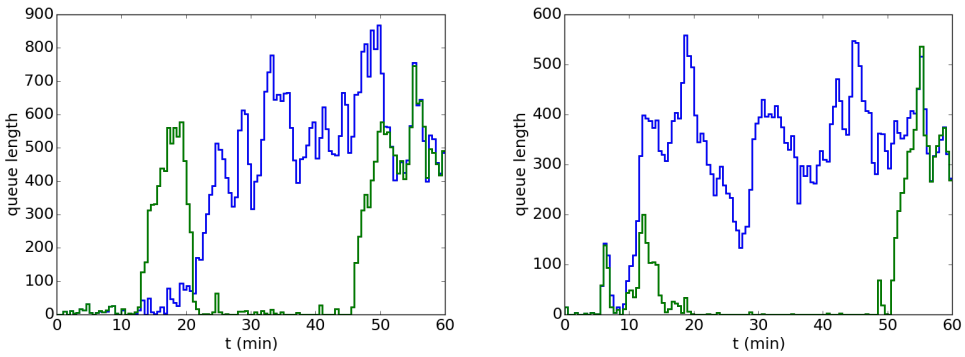

Fig. 20 demonstrates the contour plot of vehicle densities with respect to time and space with different values of v_d. When $v_d = 40$ mi/h, high density is held in section 0 during the incident, while downstream sections are highly homogenized. ρ_2 is higher than $\rho_{d,c}$ at the beginning of the incident as the ramp flows r_{11} and r_{12} flush in but then discharged under control. The density in section 6 is slightly higher than $\rho_{d,c}$ as vehicles receive the lane change recommendations and make lane changes thus slightly disturbs upstream flow. When $v_d = 65$ mi/h, as explained in Section 4.1.1, a shockwave propagates upstream. After the incident is removed, the vehicles in section 0 flush downstream and meet with the shockwave, which leads to a high density area in section 2. However in this case, the discharging section is still well protected. As the shockwave propagates upstream, vehicle densities converge to $\rho_{d,c}$ gradually from downstream section to upstream section. This is because we use the cascade structure of VSL controller in Fig. 4, which attenuates the shockwave section by section. Thus the controller is robust to parameter selection.
Fig. 21 shows the queue length on ramp r_{11} and r_3, with RM control alone and with the coordinated controller. With RM control alone, the queues pile up fast as the densities in mainline increase. Due to the queue adjustment mechanism of ALINEA/Q, the queue lengths are maintained around the reference value. With the coordinated controller, the queue lengths increase in the transient process when the incident begins and the mainline density is being adjusted to the desired level and then discharge fast. After the incident is removed, large flow flushes downstream, the RM controller decrease the rate to give priority to the mainline, therefore the queue lengths increase.
We use the following metrics to evaluate the performance of the coordinated controller. To evaluate traffic mobility, we use: (a) average travel time $\bar{T}_t$; for traffic safety, use (b) average number of stops $\bar{s}$ and (c) average number of lane changes $\bar{c}$; for the environment, we use (d) average emission of CO2 and (e) average fuel consumption. The detailed definition of the above metric can be found in [5].
Table 4 shows the evaluation results. The improvement in traffic mobility, safety and the environ-

Table 4: Evaluation Results

Control Type	No Control	RM + VSL	Improvement
$\bar{T}_t$ (min)	15	11	27%
$\bar{s}$	23	4	82%
$\bar{c}$	5.1	4.6	10%
CO2 (g/veh/mi)	585	538	8%
Fuel (g/veh/mi)	187	172	8%

ment is significant. The average travel time is reduced by about 27% as the bottleneck throughput is increased. For traffic safety, the number of stops dramatically decreased by 81% as the lane change control prevented vehicles from stopping at the bottleneck and waiting for lane changes. The 10% reduction in number of lane changes is contributed by both homogenization of mainline flow and the regulated merging behavior of ramp flows. For the environment metrics, the reductions of CO2 emission and energy consumption are usually proportional to each other, which are both around 8% in this case.

5 Comparison of Feedback Linearization and Model Predictive Strategies in Variable Speed Limit Control

Given the fact that LC control is able to relieve or eliminate the capacity drop, one important question arising at this point is that if other VSL control strategies are combined with the LC control, will the system performance exceed the performance under the FL controller? Intuitively, since MPC control follows an optimization based routine, it should provide the 'optimal' performance to some extent. However, FL controller guarantees exponential stability of the equilibrium point with highest bottleneck flow rate. Therefore, by tuning the feedback gain, the FL controller should be able to force the system to converge as fast as possible, only limited by the saturation of control input.

In this section, we propose FL and MPC schemes for VSL-actuated highway traffic, where we assume that an LC controller is active just upstream of the bottleneck. Both controllers are designed with a CTM-based model representing the ideal system. TTS performance and robustness with respect to perturbations on model parameters and measurement noise of the proposed controllers are evaluated via simulation studies. Results show both VSL controller is able to improve the total time spent under different levels of perturbation and measurement noise. Furthermore, feedback linearization VSL can provide better performance than model predictive VSL with much less computational effort.

5.1. Nonlinear Model Predictive Control

Model predictive control strategy generates the control command at each control step by solving a finite horizon optimal control problem in a receding horizon manner. In this section, we formulate the cost function of the MPC problem as the quadratic error of the states of system (9). To take into consideration the vehicles that are blocked upstream the VSL controlled segment, we augment the system by add a new state Q, that is

$$\dot{Q} = d - q_0, \tag{28}$$

with $Q = 0$ at $t = 0$. Therefore, if the number of vehicles upstream of section 0 is greater than the number at time 0, $Q > 0$, otherwise $Q \leq 0$. We should note here that the introduction of Q is only for the purpose of evaluating the TTS. Both the FL and MPC controllers are implemented based on system (9). The performance metric TTS is defined as follows:

$$\text{TTS} = \int_0^T Q(t) + \sum_{i=0}^{N} \rho_i(t) L_i \, dt \tag{29}$$

The open-loop highway system (9) can be implicitly expressed as

$$\dot{e} = f(e, u) \tag{30}$$

Here we formulate the problem of finding the VSL commands $u(\cdot)$ that try to maintain system (30) at the equilibrium point as the following finite-horizon constrained optimal control problem (OCP):

$$\begin{aligned} \underset{u(\cdot)}{\text{minimize}} \quad & \int_{kT_c}^{kT_c+T_p} e(\tau)^T \tilde{Q} e(\tau) + u(\tau)^T \tilde{R} u(\tau) d\tau \\ \text{subject to} \quad & e(kT_c) = \hat{e}(kT_c) \\ & \dot{e} = f(e, u), \ \forall \tau \in [t, t + T_p] \\ & v_{\min} - v_e \leq u(\tau) \leq v_{\max} - v_e, \end{aligned} \tag{31}$$

where t is the current control sampling instant in time, $\hat{e}(t)$ is the measurement on error states taken at that instant, $\tilde{Q}$ and $\tilde{R}$ are weighting matrices on error and control input, respectively, whereas T_p is the prediction horizon. The optimization problem is solved at the beginning of each control step kT_c, with $\hat{e}(kT_c)$ as the initial condition. Constraint (16) has already been included in the constraints of the optimization problem. (14) and (15) are also applied to the MPC VSL commands before applied to the system.

Due to the continuous-time dynamics, the OCP (31) is an infinite dimensional optimization problem. We resort to approximating it as a finite dimensional nonlinear program (NLP) via the direct multiple shooting method [73]. Details on direct methods from numerical optimal control literature can be found in [74].

Figure 22: Simulation System

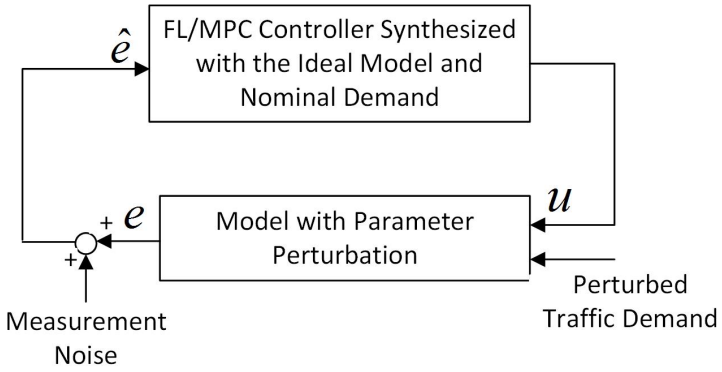

5.2. Numerical Simulation

In this section, macroscopic simulation is used to evaluate the performance and robustness of the FL and NMPC schemes combined with LC.

5.2.1. Scenario setup

The FL and MPC controllers have evaluated on the network shown in Fig. 9 In our simulation, the incident happens 5 minutes after the simulation starts, and it lasts for 30 min. The nominal demand is 6000 veh/h. The desired equilibrium point of this network is calibrated to be:

$$\rho_0^{\mathrm{e}} = 278 \text{ veh/mi}$$
$$\rho_1^{\mathrm{e}} = \rho_2^{\mathrm{e}} = \cdots = \rho_7^{\mathrm{e}} = 110 \text{ veh/mi}$$
$$v_0^{\mathrm{e}} = 15.8 \text{ mi/h}$$
$$v_1^{\mathrm{e}} = v_2^{\mathrm{e}} = \cdots = v_7^{\mathrm{e}} = 40 \text{ mi/h}$$

For the FL controller, we choose $\lambda_i = 50$ for $i = 0, 1, \ldots, 6$. The NMPC controller is implemented using the direct multiple shooting method via the CasADi toolbox [75] in MATLAB 8.5.0 (R2015a), on a 64-bit Windows PC with 3.4-GHz Intel Core i7 processor and 8-GB RAM, where IPOPT [76] is used for solving the NLPs. In our simulation, we choose the prediction horizon $T_p = 10$ min, which is much greater than the control time step $T_c = 30$ s. Weight matrices are chosen as $\tilde{Q} = \mathbf{I}$ and $\tilde{R} = 0.1\mathbf{I}$, with $\mathbf{I}$ denoting the identity matrix of appropriate dimensions. The computation time of NMPC is around 0.35 seconds, whereas it is negligible for FL. The NMPC scheme is still computationally tractable, as its computation time of 0.35 s per step is negligible with respect to the control time step of 30 s.

Figure 23: Simulation System

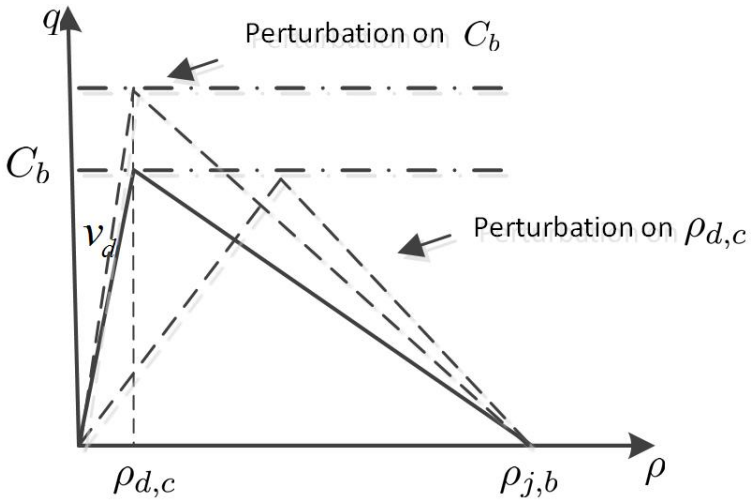

5.2.2. Performance and Robustness Analysis with Macroscopic Simulations

To compare the performance and robustness of the FL and MPC VSL controllers, we evaluate the following criteria for the two controllers: 1) Total time spent (TTS) as defined in (29), and sensitivity of TTS with respect to 2) perturbation on traffic demand, 3) perturbation on model parameters and 4) measurement noise. In the simulation, the FL and MPC controllers are synthesized with the ideal model (30), but the control command are applied on a perturbed model. The structure of the simulation system is shown in Fig. 22. For the traffic demand, we add up to $\pm 20\%$ perturbation on the nominal demand 6000 veh/h. For the model parameters, as shown in Fig. 23, we respectively add up to $\pm 20\%$ perturbation on the nominal value of $\rho_{d,c}$ and C_b, which directly alter the shape of the fundamental diagram of the bottleneck section. For the measurement noise, we use Gaussian white noise with different levels of standard deviation up to $\sigma = 0.1\rho_{d,c}$ to match the scale of the density measurements.

Fig. 24 shows the behavior of the vehicle density in the discharging section under FL and MPC controller. Both controllers are able to maintain the density around the desired value $\rho_7^e = 110$ veh/h after the incident occurs at $t = 5$ min. The oscillation is introduced by the roundup-to-5 constraint. However, the MPC controller introduces higher frequency chattering and a sharp decrease at the beginning of the incident.

A series of simulation experiments are conducted with different levels of perturbation and measurement noise. Figure 25 shows how TTS varies with varying demand levels. The figure showcases that both controllers are able to function properly under various levels of demand, the TTS increases and decreases approximately linear with the demand. This demonstrates that both MPC and FL VSL controllers are robust with respect to the variation of demand, which is due to the selection of the desired equilibrium point (6) - (7). At the equilibrium point, the speed limit in section 0 is decreased to block excessive traffic demand at upstream of the entire control segment, therefore the bottleneck flow is not affected. Furthermore, under different levels of per-

Figure 24: ρ_7 with FL and MPC

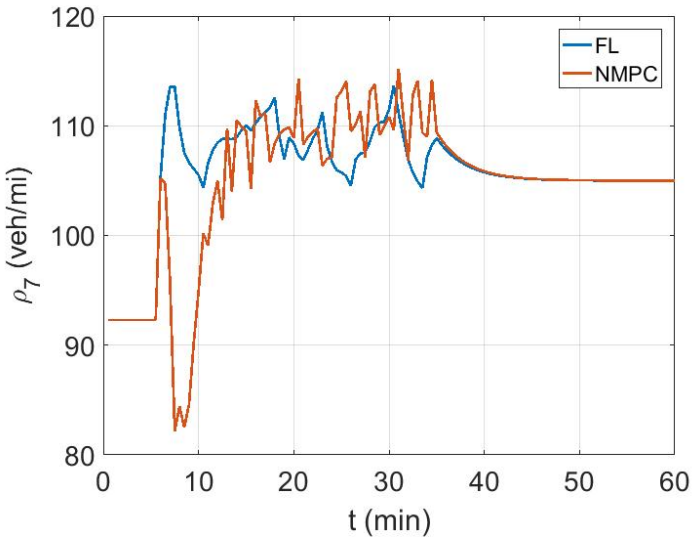

Figure 25: Performance sensitivity of no control (black), FL (blue), and NMPC (red) to perturbations on demand d.

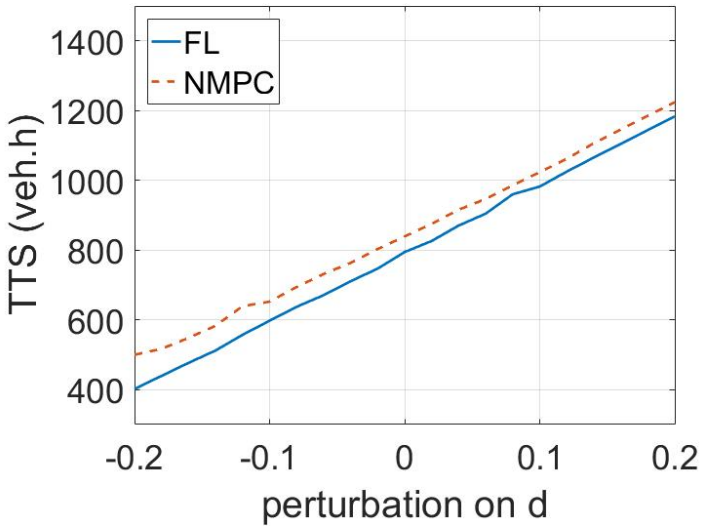

Figure 26: Performance sensitivity of no control (black), FL (blue), and NMPC (red) to perturbations on C_b.

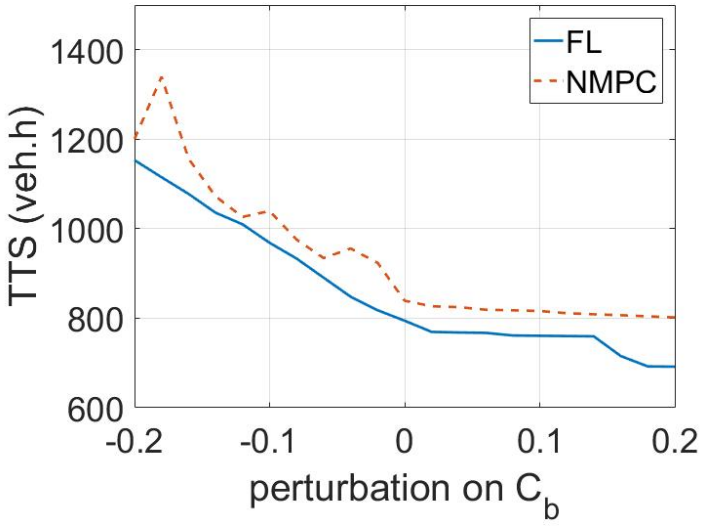

Figure 27: Performance sensitivity of no control (black), FL (blue), and NMPC (red) to perturbations on $\rho_{\mathrm{d,c}}$.

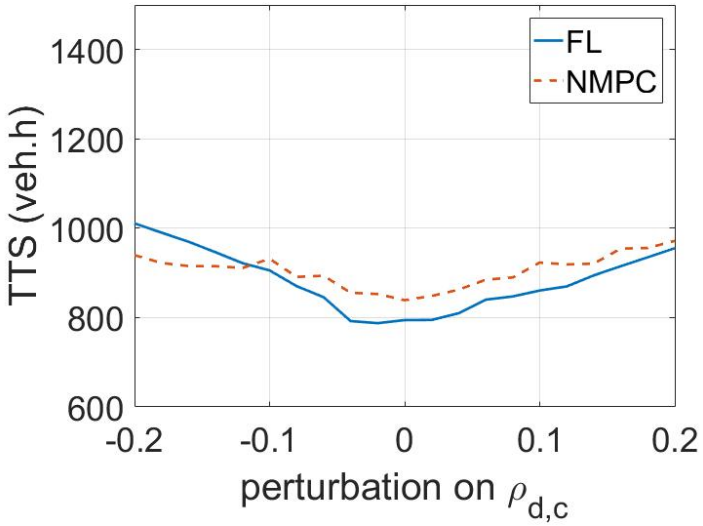

Figure 28: Performance sensitivity of FL (blue) and NMPC (red) to increasing levels of standard deviation in measurement noise.

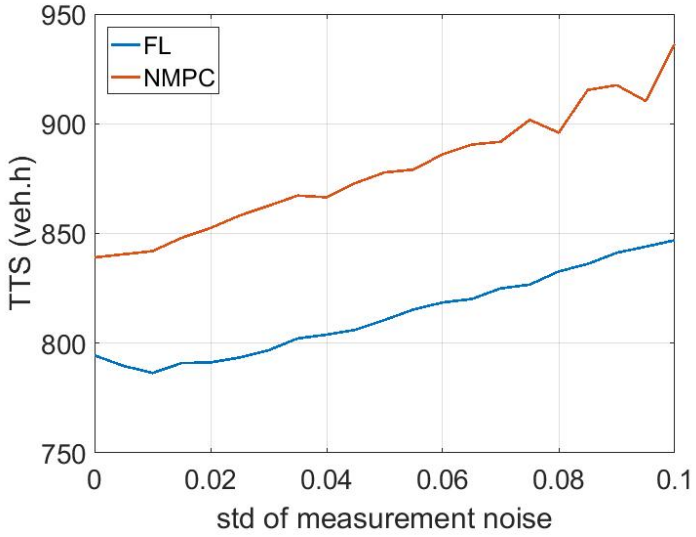

turbation, the performance of FL and MPC controller are similar. But the TTS of FL is always slightly lower than that of MPC, which shows that MPC fails to beat FL in TTS although the control commands are generated by solving the optimization problem in receding horizon fashion.
In figures 26 and 27, the change in TTS is plotted with respect to different values of perturbation on C_b and $\rho_{\mathrm{d,c}}$, respectively. These results show that both controllers achieve significant improvements over the no control case and are able to operate properly even under situations with high amount of uncertainty in these model parameters. With perturbation on C_b, the TTS under FL and MPC are increased by 45% and 43% in the worst case, respectively. Considering the fact that in this case the bottleneck capacity is decreased by 20% as a baseline, the TTS does not increase too much due to the modeling error and is still much lower than that in the no control case. The worst case for the perturbation on $\rho_{\mathrm{d,c}}$ is 27% worse than the non-perturbed value for FL, and 16% for NMPC.
The sensitivity of TTS performance in the case of varying levels of standard deviation in measurement noise is given in figure 28, which shows that the TTS under both controllers increases with the standard deviation of measurement noise. However, the system does not diverge as the no control case. The performance of FL is always better than that of NMPC in this case.

5.2.3. Performance and Robustness Analysis with Microscopic Simulations

Table 5 shows the microscopic simulation results with calibrated model parameter set:

$$w_1 = 14 \text{ mi/h},\ w_b = 40 \text{ mi/h},\ \rho_{d,c} = 110 \text{ veh/mi}$$

The performance of the MPC controller is similar to that of the FL controller.

Table 5: Evaluation Results with Original Parameters

		TTT (hr)	Stops	LC	CO (g/veh/mi)	Nox (g/veh/mi)	CO2 (g/veh/mi)	Energy (g/veh/mi)
No Control	mean ± std	1270 ± 42	23.2 ± 1.3	6.6 ± 0.2	3.4 ± 0.1	1.8 ± 0.1	605 ± 20	194 ± 6
	Improvement	-	-	-	-	-	-	-
LC Only	mean ± std	1075 ± 40	10.5 ± 0.9	5.9 ± 0.3	3.4 ± 0.1	1.7 ± 0.1	552 ± 16	176 ± 5
	Improvement	15%	55%	11%	0%	6%	9%	9%
FL	mean ± std	1036 ± 36	9.9 ± 1.3	5.5 ± 0.2	3.0 ± 0.1	1.6 ± 0.1	529 ± 13	169 ± 4
	Improvement	18%	57%	17%	12%	11%	13%	13%
MPC	mean ± std	1018 ± 41	8.7 ± 1.2	5.5 ± 0.2	3.0 ± 0.1	1.6 ± 0.1	525 ± 15	168 ± 5
	Improvement	20%	63%	17%	12%	11%	13%	13%

Table 6: Evaluation Results under Different w_1

			TTT (hr)	Stops	LC	CO (g/veh/mi)	Nox (g/veh/mi)	CO2 (g/veh/mi)	Energy (g/veh/mi)
FL	w_1=9	mean ± std	1036 ± 36	9.9 ± 1.3	5.5 ± 0.2	3.0 ± 0.1	1.6 ± 0.1	529 ± 13	169 ± 4
		Improvement	18%	57%	17%	12%	11%	13%	13%
	w_1=14	mean ± std	1036 ± 36	9.9 ± 1.3	5.5 ± 0.2	3.0 ± 0.1	1.6 ± 0.1	529 ± 13	169 ± 4
		Improvement	18%	57%	17%	12%	11%	13%	13%
	w_1=6	mean ± std	1036 ± 36	9.9 ± 1.3	5.5 ± 0.2	3.0 ± 0.1	1.6 ± 0.1	529 ± 13	169 ± 4
		Improvement	18%	57%	17%	12%	11%	13%	13%
MPC	w_1=9	mean ± std	1096 ± 55	12.3 ± 2.4	5.5 ± 0.2	3.1 ± 0.1	1.6 ± 0.1	533 ± 16	170 ± 5
		Improvement	14%	47%	17%	9%	11%	12%	12%
	w_1=14	mean ± std	1018 ± 41	8.7 ± 1.2	5.5 ± 0.2	3.0 ± 0.1	1.6 ± 0.1	525 ± 15	168 ± 5
		Improvement	20%	63%	17%	12%	11%	13%	13%
	w_1=6	mean ± std	1226 ± 61	12.1 ± 1.9	5.6 ± 0.3	3.1 ± 0.1	1.6 ± 0.1	546 ± 20	174 ± 6
		Improvement	3%	48%	15%	9%	11%	10%	10%

Table 7: Evaluation Results under Different $\rho_{d,c}$

			TTT (hr)	Stops	LC	CO (g/veh/mi)	NOx (g/veh/mi)	CO2 (g/veh/mi)	Energy (g/veh/mi)
FL	$\rho_{d,c}$ = 100	mean ± std	1024 ± 44	8.8 ± 2	5.5 ± 0.2	3.0 ± 0.1	1.6 ± 0.1	528 ± 14	169 ± 5
		Improvement	19%	62%	17%	12%	11%	13%	13%
	$\rho_{d,c}$ = 110	mean ± std	1036 ± 36	9.9 ± 1.3	5.5 ± 0.2	3.0 ± 0.1	1.6 ± 0.1	529 ± 13	169 ± 4
		Improvement	18%	57%	17%	12%	11%	13%	13%
	$\rho_{d,c}$ = 120	mean ± std	1031 ± 43	9.4 ± 2.2	5.5 ± 0.2	3.0 ± 0.1	1.6 ± 0.1	526± 15	168 ± 4
		Improvement	19%	59%	17%	12%	11%	13%	13%
MPC	$\rho_{d,c}$ = 100	mean ± std	1236 ± 41	11.4 ± 0.3	5.5 ± 0.2	3.1 ± 0.1	1.6 ± 0.1	544 ± 16	174 ± 5
		Improvement	3%	51%	17%	9%	11%	10%	10%
	$\rho_{d,c}$ = 110	mean ± std	1018 ± 41	8.7 ± 1.2	5.5 ± 0.2	3.0 ± 0.1	1.6 ± 0.1	525 ± 15	168 ± 5
		Improvement	20%	63%	17%	12%	11%	13%	13%
	$\rho_{d,c}$ = 120	mean ± std	1242 ± 35	11.6 ± 1.0	5.5 ± 0.2	3.1 ± 0.1	1.6 ± 0.1	542 ± 17	173 ± 6
		Improvement	2%	50%	17%	9%	11%	10%	11%

Table 8: Evaluation Results under Different w_b

			TTT (hr)	Stops	LC	CO (g/veh/mi)	Nox (g/veh/mi)	CO2 (g/veh/mi)	Energy (g/veh/mi)
FL	w_b=20	mean ± std	1025 ± 36	9.6 ± 1.0	5.5 ± 0.2	3.0 ± 0.1	1.6 ± 0.1	527 ± 13	169 ± 4
		Improvement	19%	59%	17%	12%	11%	13%	13%
	w_b=40	mean ± std	1036 ± 36	9.9 ± 1.3	5.5 ± 0.2	3.0 ± 0.1	1.6 ± 0.1	529 ± 13	169 ± 4
		Improvement	18%	57%	17%	12%	11%	13%	13%
	w_b=60	mean ± std	1042 ± 34	10.2 ± 1.8	5.5 ± 0.2	3.0 ± 0.1	1.6 ± 0.1	526 ± 15	168 ± 4
		Improvement	18%	56%	17%	12%	11%	13%	13%
MPC	w_b=20	mean ± std	1098 ± 58	12.4 ± 2.4	5.5 ± 0.2	3.1 ± 0.1	1.6 ± 0.1	533 ± 16	170 ± 5
		Improvement	14%	47%	17%	9%	11%	12%	12%
	w_b=40	mean ± std	1018 ± 41	8.7 ± 1.2	5.5 ± 0.2	3.0 ± 0.1	1.6 ± 0.1	525 ± 15	168 ± 5
		Improvement	20%	63%	17%	12%	11%	13%	13%
	w_b=60	mean ± std	1092 ± 53	12.3 ± 2.2	5.5 ± 0.2	3.1 ± 0.1	1.6 ± 0.1	529 ± 15	169 ± 5
		Improvement	14%	47%	17%	9%	11%	13%	13%

Table 6 - Table 8 demonstrate the simulation results of MPC and FL controller under different values of model parameters. From the result, we can see that the FL controller is robust with respect to the perturbations on w_1, w_b and $\rho_{d,c}$. As to MPC, the mobility performance is significantly adversed by the perturbations on w_1 and $\rho_{d,c}$, which both change the value of the equilibrium point. But MPC is robust with respect to the perturbations on w_b which does not change the equilibrium point and can be compensated by the control input.

6 Stability Analysis of Cell Transmission Model under All Operating Conditions

In Section 3 and Section 4, we designed a coordinated variable speed limit, ramp metering and lane change control based on the first-order cell transmission model. However, the analysis of dynamical behavior and stability properties of the open-loop cell transmission model which takes capacity drop into consideration is missing from the previous work, which makes it difficult for us to perform an analytical comparison of the open-loop and closed-loop performance of the VSL controlled cell transmission model. In addition, the analysis of the closed-loop behavior in Section 3 and Section 4 is performed with a simplified CTM, i.e. consider only the region in the state space near the desired equilibrium point (6) and under the assumption that the demand is higher than the bottleneck capacity. It remains unclear whether the global stability of the desired equilibrium point is still valid with the complete CTM and in other operating scenarios.
In [57], Gomes et al. performed a thorough analysis of the equilibrium points and their stability properties of the CTM model. However, the authors did not take the capacity drop phenomenon into consideration. Reference [58] developed sufficient conditions for the stability of the equilibrium points of CTM in terms of connectivity of a graph associated with the traffic network. The results of [57] and [58] are established based on the monotonicity of CTM. However, if the CTM is modified to account for capacity drop and the fact that the discharging flow rate of a congested road section decreases with density [5, 26, 59, 60], then the CTM is no longer monotone.
Therefore, in this section, We use the CTM which take into consideration the effect of capacity drop which is due to microscopic phenomena such as forced lane changes at a bottleneck [5] and the decreasing discharging flow of the road section, then consider all possible traffic flow scenarios, identify all equilibrium points and analyze their stability properties for a single road section, then extend the results to arbitrary number of sections under different traffic demand levels and capacity constraints as well as under all initial density conditions, based on which the design of the VSL controller which guarantees global stability of the closed-loop system with complete CTM and under all possible operating scenarios is perform in the next section.

6.1. Stability of Traffic Flow in a Single-Section Road Segment

Consider a single road section of unit length with an inflow q_1 and outflow q_2, expected to meet a demand of flow d as shown in Fig. 29. We assume that the vehicle density ρ is uniform along the

Figure 29: Single Road Section

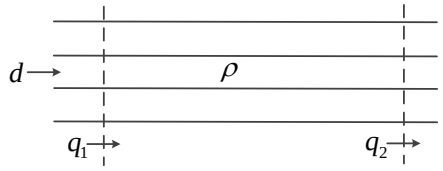

section, i.e. it is independent of distance from the entrance to the exit of the section and does not vary across the lanes in the vertical direction. Under these assumptions, the evolution of ρ with respect to time is given by the following differential equation:

$$\dot{\rho} = q_1 - q_2, 0 \leq \rho(0) \leq \rho^j, \tag{32}$$

where

$$\begin{aligned} q_1 &= \min\{d, C, w(\rho^j - \rho)\}, \\ q_2 &= \begin{cases} \min\{v_f\rho, \tilde{w}(\tilde{\rho}^j - \rho), (1-\epsilon(\rho))C_d\} & \text{if } C_d < C \\ \min\{v_f\rho, \tilde{w}(\tilde{\rho}^j - \rho), C_d\} & \text{otherwise} \end{cases}, \\ v_f\rho_c &= w(\rho^j - \rho_c) = \tilde{w}(\tilde{\rho}^j - \rho_c) = C, \\ 0 &< \rho_c < \rho^j, 0 < \tilde{w} < w, v_f > 0, \\ \epsilon(\rho) &= \begin{cases} 0 & \text{if } 0 \leq \rho \leq \dfrac{C_d}{v_f} \\ \epsilon_0 & \text{otherwise} \end{cases}, \end{aligned} \tag{33}$$

and the constants in equation (32),(33) are defined as follows:

- C: the capacity of the road section.
- w: the back propagation speed.
- ρ^j: jam density, the highest density possible, at which $q_1 = 0$.
- v_f: free flow speed of the road section.
- $\tilde{w}$: the rate that the outflow q_2 decreases with ρ, when $\rho \geq \rho_c$.
- $\tilde{\rho}^j$: the jam density associated with outflow q_2.

- ρ_c: the critical density of the road section, at which $v_f\rho_c = w(\rho^j - \rho_c) = \tilde{w}(\tilde{\rho}^j - \rho_c) = C$.
- C_d: the downstream capacity.

In equation (33), the inflow q_1 is dictated by the upstream demand d as well as the potential ability of the section to absorb traffic flow, which is the value $\min\{C, w(\rho^j - \rho)\}$. If $\rho \leq \rho_c$, the section can absorb as much flow as the capacity C, however if $\rho > \rho_c$, the section's ability to absorb upstream flow decreases with ρ at a rate w. When $\rho = \rho^j$, $q_1 = 0$ as the section is completely congested. The outflow q_2 is dictated by the ability of the section to send traffic flow to downstream and the downstream capacity. When $\rho \leq \rho_c$, the section's ability to send traffic flow increases with ρ, but when $\rho > \rho_c$, this ability decreases with ρ at a rate $\tilde{w}$ [59, 77–79]. Since $w > \tilde{w}$, we have $\tilde{w}(\tilde{\rho}^j - \rho) > w(\rho^j - \rho)$ for all $\rho > \rho_c$, which captures the phenomenon that if the downstream segment has enough capacity, the density in a congested road section upstream will eventually decrease to a value less than or equal to ρ_c. The capacity of the downstream segment is C_d. If $C_d < C$ and $\rho \leq \frac{C_d}{v_f}$, then the outflow $q_2 = v_f\rho$ can increase up to C_d. However, when $\rho > \frac{C_d}{v_f}$, the section generates more flow than C_d, a queue will form at the outlet, which may cause forced lane changes which in turn reduce the flow speed leading to the reduction of flow to lower than the capacity C_d i.e. to $(1 - \epsilon_0)C_d$ [5, 26]. This phenomenon is known as capacity drop. The original CTM is modified to include the capacity drop effect as shown in equation (33). The model (32) - (33) with $\epsilon_0 = 0$ is the CTM of [80]. The $\epsilon_0 > 0$ denotes the level of capacity drop, in which case, despite the availability of flow, q_2 is restricted from reaching the capacity C_d. Note that capacity drop can only occur when the downstream capacity C_d is lower than the capacity of the section C. In system (32)-(33), we model the capacity drop using a reduction in the downstream capacity C_d which has been verified by microscopic simulations using VISSIM in [5]. The modeling of capacity drop has been discussed in [60] more extensively where different models are considered. These models do not change the methodology and results of this section, which can be easily extended to different capacity drop models.
The purpose of this section is to analyze the stability properties of the model (32)-(33). Since these properties will depend on the characteristics of the road section defined by the constants C, C_d, the demand d which could vary and the magnitude of capacity drop ϵ_0 which may depend on microscopic effects [5, 60], the following five possible operating scenarios are identified and represented by the sets Ω_i, $i = 1, 2, ..., 5$. The union of these sets $\bigcup_{i=1}^{5} \Omega_i$, as shown in Fig. 30, covers all possible situations. Let $I = (C_d, C, d, \epsilon_0)$ be the state of the road section. We analyze the stability properties of the dynamical model (32)-(33) when $I \in \Omega_i$, $i = 1, 2, ..., 5$. Theorem 6.1 presents the results of the analysis.

Theorem 6.1. *For constant but otherwise arbitrary demand d, we have the following results:*

a) Let $I \in \Omega_1$. Then $\forall \rho(0) \in [0, \rho^j]$, $\rho(t)$ converges exponentially fast to $\frac{d}{v_f}$.

b) Let $I \in \Omega_2$. Then

- *$\forall \rho(0) \in [0, \frac{C_d}{v_f}]$, $\rho(t)$ converges exponentially fast to $\frac{d}{v_f} = \frac{(1-\epsilon_0)C_d}{v_f}$.*

Figure 30: All Possible Operating Scenarios

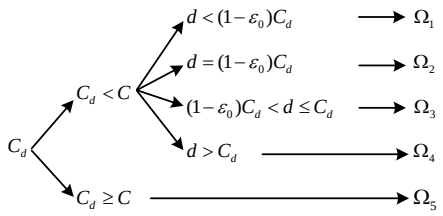

- $\forall \rho(0) \in (\frac{C_d}{v_f}, \rho^j - \frac{d}{w}]$, $\rho(t) = \rho(0), \forall t \geq 0$.
- $\forall \rho(0) \in (\rho^j - \frac{d}{w}, \rho^j]$, $\rho(t)$ *converges exponentially fast to* $\rho^j - \frac{d}{w} = \rho^j - \frac{(1-\epsilon_0)C_d}{w}$.

c) Let $I \in \Omega_3$. *Then*

- $\forall \rho(0) \in [0, \frac{C_d}{v_f}]$, $\rho(t)$ *converges exponentially fast to* $\frac{d}{v_f}$.
- $\forall \rho(0) \in (\frac{C_d}{v_f}, \rho^j]$, $\rho(t)$ *converges exponentially fast to* $\rho^j - \frac{(1-\epsilon_0)C_d}{w}$.

d) Let $I \in \Omega_4$. *Then* $\forall \rho(0) \in [0, \rho^j]$, $\rho(t)$ *converges exponentially fast to* $\rho^j - \frac{(1-\epsilon_0)C_d}{w}$.

e) Let $I \in \Omega_5$. *Then* $\forall \rho(0) \in [0, \rho^j]$, $\rho(t)$ *converges exponentially fast to* $\frac{\min\{d,C\}}{v_f}$.

Proof. a) When $I \in \Omega_1$, we plot the relationship of q_1, q_2 given by equation (33) in Fig. 31. From

Figure 31: Fundamental Diagram for $I \in \Omega_1$

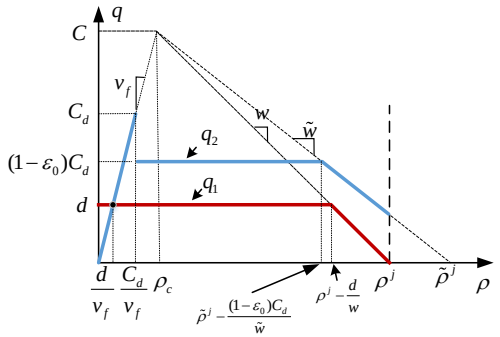

the density equation (32), the equilibrium points of the system are the values of ρ for which $\dot{\rho} = 0$, which happens when $q_1 = q_2$. It is clear from Fig. 31 that the only intersection of q_1 and q_2 is the point $\rho^e = \frac{d}{v_f}$, which implies that this is the only equilibrium of ρ in the region $[0, \rho^j]$ of feasible values of ρ. We define the Lyapunov function

$$V(\rho) = \frac{(\rho - d/v_f)^2}{2},$$

whose time derivative

$$\dot{V}(\rho) = (\rho - \frac{d}{v_f})\dot{\rho} = -(\rho - \frac{d}{v_f})(q_2 - q_1).$$

We show in Appendix A.1 that

$$\dot{V} \leq -\alpha(\rho - \frac{d}{v_f})^2,$$

where $\alpha = \min\{v_f, \frac{(1-\epsilon_0)C_d - d}{\rho^j - d/v_f}, \frac{(\tilde{w}-w)[\rho_c - (\rho^j - \frac{d}{w})]}{\rho^j - d/v_f}\} > 0$. Hence ρ converges exponentially fast to $\frac{d}{v_f}$ with a rate greater than or equal to α for all possible initial conditions in $[0, \rho^j]$ [81]. The rate of convergence is guaranteed to be greater than or equal to α as it is clear from the value of V and $\dot{V}$.

b) When $I \in \Omega_2$, the plot of q_1, q_2 generated from equation (33) is given in Fig. 32. In this case,

Figure 32: Fundamental Diagram for $I \in \Omega_2$

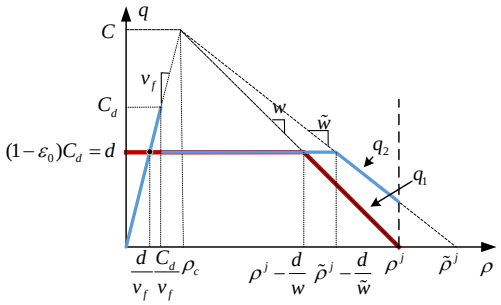

q_1 and q_2 intersect at one point $\rho = \frac{d}{v_f}$ and $q_1 = q_2$ for all $\rho \in (\frac{C_d}{v_f}, \rho^j - \frac{d}{w}]$. Therefore, we have one isolated equilibrium point $\rho_1^e = \frac{d}{v_f}$ and an equilibrium manifold which is the interval $(\frac{C_d}{v_f}, \rho^j - \frac{d}{w}]$.

From Fig. 32, we know that $\forall \rho \in [0, \frac{C_d}{v_f}],\ q_1 = (1-\epsilon_0)C_d = d$ and $q_2 = v_f\rho$ which gives

$$\dot{\rho} = -v_f\rho + d,\ \forall \rho(0) \in [0, \frac{C_d}{v_f}],$$

whose solution is

$$\rho(t) = \frac{d}{v_f} + (\rho(0) - \frac{d}{v_f})e^{-v_f t} \leq \frac{C_d}{v_f}.$$

Hence $\forall \rho(0) \in [0, \frac{C_d}{v_f}]$ we have $\rho(t) \in [0, \frac{C_d}{v_f}],\ \forall t \geq 0$ and according to the solution above, $\rho(t)$ converges exponentially fast to $\frac{d}{v_f} = \frac{(1-\epsilon_0)C_d}{v_f}$.

For $\rho(0) \in (\frac{C_d}{v_f}, \rho^j - \frac{d}{w}]$, we have $q_1 = q_2$, therefore $\dot{\rho} = 0$, which implies that $\rho(t) = \rho(0),\ \forall t \geq 0$, for all $\rho(0) \in (\frac{C_d}{v_f}, \rho^j - \frac{d}{w}]$.

If $\rho(0) \in (\rho^j - \frac{d}{w}, \rho^j]$, it is clear from Fig. 32 that $q_2 > q_1$ which implies that $\dot{\rho} < 0$ until $\rho(t) = \rho^j - \frac{d}{w}$ at which time $\dot{\rho} = 0$. This implies that for all $\rho(0) \in (\rho^j - \frac{d}{w}, \rho^j]$, $\rho(t)$ converges at least asymptotically with time to $\rho^j - \frac{d}{w}$. In Appendix A.2 we show that this rate of convergence is exponential, i.e.

$$|\rho(t) - (\rho^j - \frac{d}{w})| \leq c_0 e^{-\alpha t}, \forall \rho(0) \in (\rho^j - \frac{d}{w}, \rho^j],$$

where $c_0 > 0$ and $\alpha = \min\{w, w - \tilde{w}\} > 0$.
c) When $I \in \Omega_3$, q_1 and q_2 described by equation (33) are plotted in Fig. 33. From Fig. 33, it

Figure 33: Fundamental Diagram for $I \in \Omega_3$

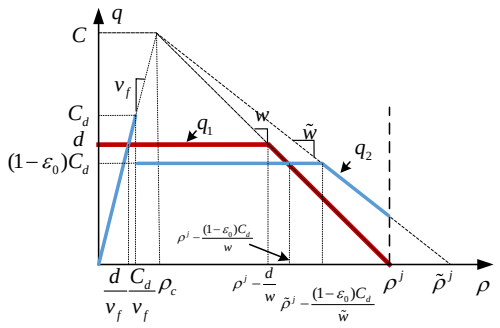

is clear that the only values of ρ for which $q_1 = q_2$ are $\frac{d}{v_f}$ and $\rho^j - \frac{(1-\epsilon_0)C_d}{w}$, which implies that the system has two isolated equilibrium points $\rho_1^e = \frac{d}{v_f}$ and $\rho_2^e = \rho^j - \frac{(1-\epsilon_0)C_d}{w}$ when $I \in \Omega_3$. We show below that $\rho_1^e = \frac{d}{v_f}$ is exponentially stable with a region of attraction $[0, \frac{C_d}{v_f}]$ and $\rho_2^e = \rho^j - \frac{(1-\epsilon_0)C_d}{w}$ is exponentially stable with a region of attraction $(\frac{C_d}{v_f}, \rho^j]$.
For $\rho(0) \in [0, \frac{C_d}{v_f}]$, we have $q_1 = d, q_2 = v_f\rho$, therefore $\dot{\rho} = -v_f\rho + d, \forall \rho(0) \in [0, \frac{C_d}{v_f}]$, whose solution is

$$\rho = e^{-v_f t}(\rho(0) - \frac{d}{v_f}) + \frac{d}{v_f},$$

which implies that $\rho(t) \in [0, \frac{C_d}{v_f}], \forall t \geq 0$ and $\rho(t)$ converges exponentially fast to $\rho_1^e = \frac{d}{v_f}$.
Consider the equilibrium point ρ_2^e and choose the Lyapunov function

$$V(\rho) = \frac{(\rho - \rho_2^e)^2}{2},$$

then $\dot{V} = -(\rho - \rho_2^e)(q_2 - q_1)$. We show in Appendix A.3 that

$$\dot{V} \leq -\alpha(\rho - \rho_2^e)^2,$$

where $\alpha = \min\{\frac{d-(1-\epsilon_0)C_d}{\rho_2^e - C_d/v_f}, w, (w - \tilde{w})\} > 0$, $\forall \rho(0) \in (\frac{C_d}{v_f}, \rho^j]$ which implies exponential

convergence to the equilibrium point $\rho_2^e = \rho^j - \frac{(1-\epsilon_0)C_d}{w}, \forall \rho(0) \in (\frac{C_d}{v_f}, \rho^j]$.
d) When $I \in \Omega_4$, q_1 and q_2 described by equation (33) are plotted in Fig. 34. From Fig. 34, it is

Figure 34: Fundamental Diagram for $I \in \Omega_4$

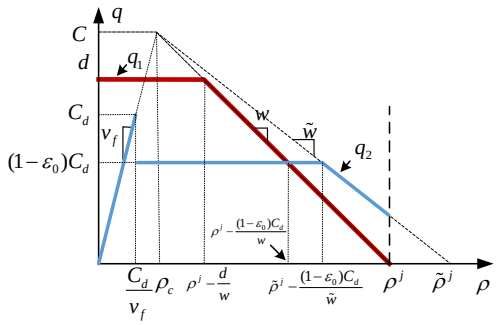

clear that $q_1 = q_2$ when $\rho = \rho^e = \rho^j - \frac{(1-\epsilon_0)C_d}{w}$, which is a unique equilibrium when $I \in \Omega_4$. Choose the Lyapunov function

$$V(\rho) = \frac{(\rho - \rho^e)^2}{2},$$

then $\dot{V} = -(\rho - \rho^e)(q_2 - q_1)$. We show in Appendix A.4 that

$$\dot{V} = -\alpha(\rho - \rho^e)^2,$$

where $\alpha = \min\{\frac{d-C_d}{\rho^e}, \frac{d-(1-\epsilon_0)C_d}{\rho^e - C_d/v_f}, w, (w - \tilde{w})\} > 0, \forall \rho \in [0, \rho^j]$, which implies exponential convergence to the equilibrium point $\rho^e = \rho^j - \frac{(1-\epsilon_0)C_d}{w}, \forall \rho(0) \in [0, \rho^j]$.
e) When $I \in \Omega_5$, q_1 and q_2 described by equation (33) are plotted in Fig. 35. In this case it is clear that there is only one equilibrium point $\rho^e = \frac{\min\{d,C\}}{v_f}$, depending whether the demand $d < C$ or $d \geq C$. We choose the Lyapunov function

$$V(\rho) = \frac{(\rho - \rho^e)^2}{2}$$

and show in Appendix A.5 that

$$\dot{V} = -\alpha(\rho - \rho^e)^2,$$

where $\alpha = \min\{v_f, \frac{(\tilde{w}-w)[\rho_c - (\rho^j - \frac{d}{w})]}{\rho^j - d/v_f}\} > 0$ if $d < C$ and $\alpha = \min\{v_f, (w - \tilde{w})\} > 0$ if $d \geq C$, $\forall \rho \in [0, \rho^j]$, which implies exponential convergence to the equilibrium point $\rho^e = \frac{\min\{d,C\}}{v_f}$, $\forall \rho(0) \in [0, \rho^j]$. □

Figure 35: Fundamental Diagram for $I \in \Omega_5$

(a) $d < C$ (b) $d \geq C$

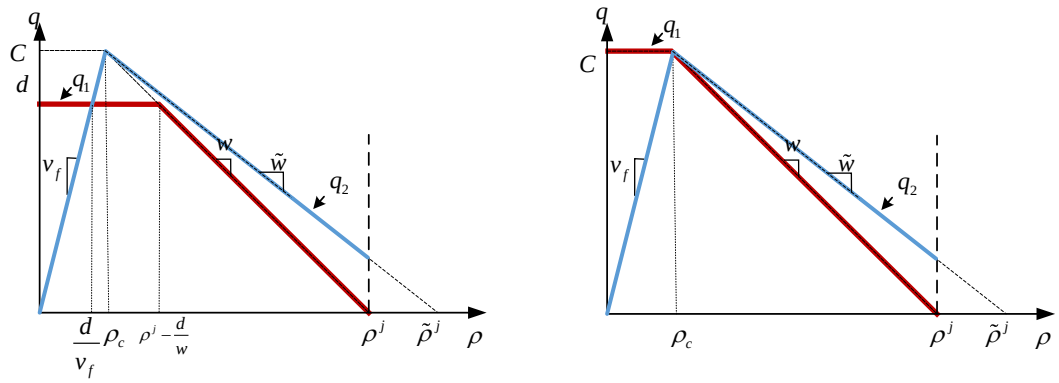

6.2. Stability of Traffic Flow in a Multi-Section Road Segment

The equilibrium points and their stability analysis of the single section CTM can be extended to the general N section case. Consider a road segment which is divided into N ($N \geq 2$) sections as in Fig. 36. Without loss of generality, we assume that the geometry of all sections is identical and each section has unit length. In the single section case, we assume the density ρ to be the same along the section. We extend this to the case of multiple sections 1 to N where each section has its own density. The capacity of all sections remains the same constant C and the capacity at the outlet is C_d whereas the demand d appears at the entrance of section 1 as shown in Fig. 36. It is well-known that the CTM in the multiple section case may include discontinuities in the values of densities when transitioning from one section to another. The control objective to be achieved via VSL, will require all section densities to converge to the same value in order to have smooth flow.

Figure 36: Multiple Section Road Network

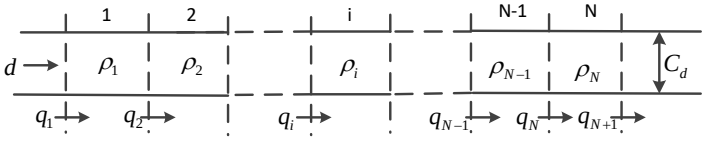

Let $\rho = [\rho_1, \rho_2, ..., \rho_N]^T$ be the state vector of the traffic flow system, where ρ_i represents the density in section i. Section i can absorb the flow $\min\{C, w(\rho^j - \rho_i)\}$ from upstream and can

generate the flow $\min\{v_f\rho_i, \tilde{w}(\tilde{\rho}^j - \rho_i)\}$ into the downstream section. Therefore, the dynamics of the vehicle densities in each section are formulated as:

$$\begin{aligned}
\dot{\rho}_i &= q_i - q_{i+1}, 0 \le \rho_i(0) \le \rho^j, \text{for } i = 1, 2, ..., N, \\
q_1 &= \min\{d, C, w(\rho^j - \rho_1)\}, \\
q_i &= \min\{v_f\rho_{i-1}, \tilde{w}(\tilde{\rho}^j - \rho_{i-1}), C, w(\rho^j - \rho_i)\}, i = 2, ..., N, \\
q_{N+1} &= \begin{cases} \min\{v_f\rho_N, \tilde{w}(\tilde{\rho}^j - \rho_N), (1 - \epsilon(\rho_N))C_d\} & \text{if } C_d < C \\ \min\{v_f\rho_N, \tilde{w}(\tilde{\rho}^j - \rho_N), C_d\} & \text{otherwise} \end{cases},
\end{aligned} \tag{34}$$

where

$$\epsilon(\rho_N) = \begin{cases} 0 & \text{if } 0 \le \rho_N \le \dfrac{C_d}{v_f} \\ \epsilon_0 & \text{otherwise} \end{cases}$$

and $0 < \epsilon_0 < 1$ denotes the level of capacity drop at the outlet of the Nth section. Since we assume that the capacities of all sections 1 to N have the same value C, the capacity drop can only happen at the outlet of section N, when $C_d < C$, which affects the value of q_{N+1}. We know that $\forall t \ge 0$, the density vector $\rho(t)$ belongs to the feasible set

$$S = \{\rho | 0 \le \rho_i \le \rho^j, \text{ for } i = 1, 2, ..., N\}.$$

Let $\rho^e = [\rho_1^e, \rho_2^e, ..., \rho_N^e]^T$ be the equilibrium vector of system (34), obtained by setting $\dot{\rho}_i = 0$, for $i = 1, 2, \cdots, N$. Let q_i^e denote the value of q_i when $\rho = \rho^e$, then the equilibrium condition of system (34) is given by

$$q_1^e = q_2^e = ... = q_{N+1}^e, \tag{35}$$

due to $\dot{\rho}_i = q_i - q_{i+1} = 0$, for $i = 1, 2, \cdots, N$.
Define the vector of initial condition $\rho(0) = [\rho_1(0), \rho_2(0), ..., \rho_N(0)]^T$ and the parameter vector $I = (C_d, C, d, \epsilon_0)$, whose partition sets are the same as in the case of a single section and are shown in Fig. 30. Then the equilibrium states of (34) for all possible I in the sets Ω_1 to Ω_5 and corresponding stability properties are given by the following theorem.

Theorem 6.2. *Let $\mathbf{1} = [1, 1, ..., 1]^T$ be a vector with N elements each equal to 1. For constant but otherwise arbitrary demand d, we have the following results:*

a) Let $I \in \Omega_1$. The equilibrium state of (34) is equal to $\rho^e = \frac{d}{v_f} \times \mathbf{1}$ and it is exponentially stable, i.e for all $\rho(0) \in S$, $\rho(t)$ converges exponentially fast to $\rho^e = \frac{d}{v_f} \times \mathbf{1}$.

b) Let $I \in \Omega_2$. System (34) has an isolated equilibrium state $\rho^e = \frac{d}{v_f} \times \mathbf{1}$, which is locally

exponentially stable, and an infinite number of equilibrium states defined by the set

$$S^e = \{(\rho^j - \frac{d}{w}) \times \mathbf{1}\} \cup \{\rho | \rho_i = \frac{d}{v_f}, i = 1, 2, ..., N-1, \frac{C_d}{v_f} < \rho_N < \rho^j - \frac{d}{w}\}$$
$$\cup [\bigcup_{i=1}^{N-1} \{\rho | \frac{d}{v_f} \leq \rho_i < \rho^j - \frac{d}{w}, \rho_k = \frac{d}{v_f}, 1 \leq k < i, \rho_r = \rho^j - \frac{d}{w}, i < r \leq N\}].$$

All equilibrium states $\rho^e \in S^e$ are stable in the sense that for any $\mu > 0, \exists \eta > 0$, such that $\forall \rho(0)$ that satisfy $\|\rho(0) - \rho^e\| < \eta$, $\rho(t)$ converges to a $\bar{\rho}^e \in S^e$ that satisfies $\|\bar{\rho}^e - \rho^e\| < \mu$. Furthermore, $\forall \rho(0) \in \{\rho | 0 \leq \rho_i \leq C_d/v_f, i = 1, 2, ..., N\}$, $\rho(t)$ converges to $\rho^e = \frac{d}{v_f} \times \mathbf{1}$ exponentially fast, and $\forall \rho(0) \notin \{\rho | 0 \leq \rho_i \leq C_d/v_f, i = 1, 2, ..., N\}$, $\exists \rho^e \in \{\frac{d}{v_f} \times \mathbf{1}\} \cup S^e$, such that $\rho(t)$ converges to ρ^e asymptotically with time.

c) *Let $I \in \Omega_3$. System (34) has two isolated equilibrium states $\rho^{e1} = \frac{d}{v_f} \times \mathbf{1}$ and $\rho^{e2} = (\rho^j - \frac{(1-\epsilon_0)C_d}{w}) \times \mathbf{1}$, which are both locally exponentially stable. Furthermore, $\forall \rho(0) \in \{\rho | 0 \leq \rho_i \leq C_d/v_f, i = 1, 2, ..., N\}$, $\rho(t)$ converges to ρ^{e1} exponentially fast and $\forall \rho(0) \notin \{\rho | 0 \leq \rho_i \leq C_d/v_f, i = 1, 2, ..., N\}$, $\rho(t)$ converges to either ρ^{e1} or ρ^{e2} exponentially fast.*

d) *Let $I \in \Omega_4$. The equilibrium state of (34) is equal to $\rho^e = (\rho^j - \frac{(1-\epsilon_0)C_d}{w}) \times \mathbf{1}$ and is exponentially stable, i.e for all $\rho(0) \in S$, $\rho(t)$ converges exponentially fast to $\rho^e = (\rho^j - \frac{(1-\epsilon_0)C_d}{w}) \times \mathbf{1}$.*

e) *Let $I \in \Omega_5$. The equilibrium state of (34) is equal to $\rho^e = \frac{\min\{d,C\}}{v_f} \times \mathbf{1}$ and is exponentially stable, i.e for all $\rho(0) \in S$, $\rho(t)$ converges exponentially fast to $\rho^e = \frac{\min\{d,C\}}{v_f} \times \mathbf{1}$.*

The proof of Theorem 6.2 is given in Appendix B.
The above stability properties show that depending on the situation classified by the operating scenarios Ω_1 to Ω_5 and initial density value in the section, the density will reach an equilibrium that is not always the one that corresponds to maximum flow rate. In fact when $I \in \Omega_2$ there are an infinite number of equilibrium points and when $I \in \Omega_3$, there are two equilibrium points. One in the free flow region and one in the congested region depending on the initial density condition. The objective of feedback is to close the loop so that the system converges to a single equilibrium point for the density which also corresponds to the maximum possible flow rate and speed. The feedback control variable is variable speed limit that provides speed commands to the upstream section in order to control the inflow to the section in a way that guarantees the maximum possible outflow from the downstream section. Such a design is presented in the next section.

7 VSL Control of the Cell Transmission Model under All Operating Conditions

7.1. Control of Traffic Flow: Single Section

The stability analysis of the flow in Section 6.1 shows that if $C_d \geq C$, i.e. the downstream capacity is higher than the capacity of the section, i.e. $I \in \Omega_5$ then the density $\rho(t)$ converges exponentially fast to a unique equilibrium point $\frac{\min\{d,C\}}{v_f}$, which corresponds to the maximum possible flow. The steady state speed of flow in the section is v_f and the steady state section flow will be at the maximum possible value $q = q_1 = q_2 = \min\{d, C\}$ according to the model (32)-(33). In this case no control action is needed. When $C_d < C$ and $d < (1-\epsilon_0)C_d$, i.e. $I \in \Omega_1$, the demand is lower than the dropped capacity of the downstream segment and therefore the density converges exponentially fast to $\frac{d}{v_f}$ and the steady state flow speed and flow rate in the section will be v_f and d respectively. In this case, no control action is needed as the section operates at the maximum possible flow rate level dictated by the demand d. The problem arises when $C_d < C$ and $d \geq (1-\epsilon_0)C_d$. where we have the following control problem cases:

(i) $(1-\epsilon_0)C_d = d < C_d < C$, i.e. $I \in \Omega_2$.

(ii) $(1-\epsilon_0)C_d < d \leq C_d < C$, i.e. $I \in \Omega_3$.

(iii) $C_d < d, C_d < C$, i.e. $I \in \Omega_4$.

In case (i) we showed in previous section that a maximum flow of $d = (1-\epsilon_0)C_d$ can be maintained at an infinite number of density equilibrium points specified by an isolated point and an equilibrium manifold, which include low and high density values with steady state speeds $v_{ss} \leq v_f$. In this case, the control objective is to maintain the maximum flow of $d = (1-\epsilon_0)C_d$ with a lowest possible density which in this case is $\frac{d}{v_f} = \frac{(1-\epsilon_0)C_d}{v_f}$ with free flow speed v_f.
In case (ii), we showed that we have two stable equilibrium points for density. One at low density which is equal to $\frac{d}{v_f}$ and one at high density equal to $\rho^j - \frac{(1-\epsilon_0)C_d}{v_f}$. In this case, maximum flow in the section corresponds to the density equilibrium point $\rho = \frac{d}{v_f}$ therefore the control objective is to choose the VSL in a way that the density converges to $\frac{d}{v_f}$ for all possible initial density conditions.
In case (iii), there is only one equilibrium point for density which is in the high density region and corresponds to the steady state flow of $(1-\epsilon_0)C_d$. In this case, the maximum possible flow is C_d and corresponds to the density of $\frac{C_d}{v_f}$. However, the convergence of ρ to $\frac{C_d}{v_f}$ does not guarantee that q_1 and q_2 converge to C_d due to the capacity drop. From equation (33) and Fig. 34, we know that q_2 is a function of ρ. For $\rho \in [0, \frac{C_d}{v_f}], q_2 = v_f\rho$, and for $\rho \in (\frac{C_d}{v_f}, \tilde{\rho}^j - \frac{(1-\epsilon_0)C_d}{\tilde{w}}], q_2 = (1-\epsilon_0)C_d$. Therefore we have

$$\lim_{\rho \to (\frac{C_d}{v_f})_-} q_2(\rho) = \lim_{\rho \to \frac{C_d}{v_f}} v_f\rho = C_d \text{ and } \lim_{\rho \to (\frac{C_d}{v_f})_+} q_2(\rho) = \lim_{\rho \to \frac{C_d}{v_f}} (1-\epsilon_0)C_d = (1-\epsilon_0)C_d,$$

i.e., if ρ converges to $\frac{C_d}{v_f}$ from the left side, then q_2 converges to the maximum value C_d. However, if ρ converges to $\frac{C_d}{v_f}$ from the right side, q_2 converges to $(1-\epsilon_0)C_d$. Therefore, the control

objective in this case is to choose the VSL so that $\rho(t)$ satisfies the following conditions: $\exists t_0 > 0$, such that $\forall t \geq t_0,\ \rho(t) \leq \frac{C_d}{v_f}$ and $\lim_{t\to\infty} \rho(t) = \frac{C_d}{v_f}$.
Therefore for all cases (i), (ii) and (iii), the control objective is to choose the VSL control so that $\rho(t)$ converges to the desired equilibrium point $\frac{\min\{d,C_d\}}{v_f}$, and the flow rate q_1 and q_2 converge to the maximum possible level which is equal to $\min\{d, C_d\}$.
A reasonable control action is to use VSL control to restrict the incoming flow q_1 to the level that is within the capacity constraints of the section at the bottleneck so that the density and flow rate converge to the desired possible values. As shown in Fig. 37, we apply the VSL command v in

Figure 37: Road Section with VSL Control

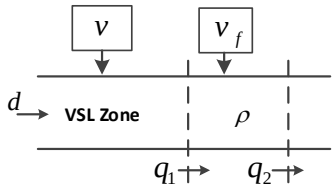

the upstream segment of the section under consideration, which is referred to as the VSL zone. All vehicles are asked to follow the speed limit v in the VSL zone and follow the free flow speed limit v_f inside the section. Decreasing the speed limit leads to lower flow q_1 from the VSL zone to the section as shown in Fig. 37. Fig. 38 shows how the changing of the speed limit v can control the flow rate q_1 entering the section through a nonlinear relationship. Suppose the VSL zone has similar characteristics as the road section under consideration. If the VSL command is set to $v < v_f$, the fundamental diagram of the VSL zone is distorted such that the parameters $\rho^j, w, \tilde{w}$ remain unchanged, while the maximum possible flow is decreased to $\frac{vw\rho^j}{v+w}$, as shown in Fig. 38, obtained by simple geometric considerations [26, 55, 56]. In Fig. 38, the red line s_v denotes the

Figure 38: Fundamental Diagram of the VSL Zone

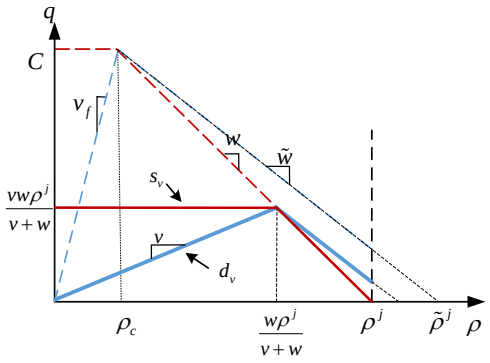

flow rate that the VSL zone can absorb from upstream under different densities in the VSL zone

and the blue line d_v denotes the flow rate that the VSL zone sends to the section under consideration. However, since the single section model does not include the density in the VSL zone, the flow into the road section from the VSL zone is assumed to be $\min\{d, \frac{vw\rho^j}{v+w}\}$, where $\frac{vw\rho^j}{v+w}$ is the maximum possible flow in the VSL zone under speed limit v. Then the density ρ in the section is given by the following equation:

$$\begin{aligned} \dot{\rho} &= q_1 - q_2,\ 0 \le \rho(0) \le \rho^j, \\ q_1 &= \min\{d, \frac{vw\rho^j}{v+w}, C, w(\rho^j - \rho)\}, \\ q_2 &= \min\{v_f\rho, \tilde{w}(\tilde{\rho}^j - \rho), (1-\epsilon(\rho))C_d\}. \end{aligned} \tag{36}$$

We design a VSL controller to overcome capacity drop and achieve the control objectives in all cases, by first considering the most complicated case $I \in \Omega_4$, in which $d > C_d$. Since in equation (36), $\frac{vw\rho^j}{v+w}$ is the only term in q_1 that depends on v, we derive the VSL controller using feedback linearization under the assumption that $q_1 = \frac{vw\rho^j}{v+w}$. Then we show in Theorem 7.1 that, for the general equation where $q_1 = \min\{d, \frac{vw\rho^j}{v+w}, C, w(\rho^j - \rho)\}$, the derived controller can still guarantee that ρ converges to $\frac{C_d}{v_f}$ and q_1, q_2 converge to the maximum value C_d. Furthermore, we also show in Theorem 7.1 below that, when $I \in \bigcup_{i=1}^{3} \Omega_i$, i.e. $d \le C_d$, the same controller guarantees the convergence of ρ to the desired equilibrium point $\frac{d}{v_f}$ and the convergence of q_1, q_2 to the maximum level d.

As discussed above, when $I \in \Omega_4$, the desired equilibrium point is $\rho^e = \frac{C_d}{v_f}$. Define the error state $x = \rho - \frac{C_d}{v_f}$ and recall that the control objective is to force ρ to converge to $\frac{C_d}{v_f}$, i.e. x converge to 0 from the left side ($\rho \le \frac{C_d}{v_f}$). If $x(0) \le 0$, that is $\rho(0) \le \frac{C_d}{v_f}$, we choose v so that

$$q_1 = q_2 - \lambda x, \tag{37}$$

where $\lambda > 0$ is a design constant to be selected. Thus we have

$$\dot{x} = \dot{\rho} = q_1 - q_2 = -\lambda x,$$

which implies that $\forall x(0) \le 0$ and $t \ge 0$, $x(t) \le 0$ and x converges to 0 exponentially fast. Since we assume that $q_1 = \frac{vw\rho^j}{v+w}$, solving equation (37) for v, we have,

$$v = \frac{w(q_2 - \lambda x)}{w\rho^j - (q_2 - \lambda x)}, \tag{38}$$

whose denominator is guaranteed to be greater than 0 as we show in detail in the proof of Theorem 7.1.

If $x(0) > 0$, i.e. $\rho(0) > \frac{C_d}{v_f}$ we choose v such that

$$q_1 = q_2 - \lambda(x + \delta_1), \tag{39}$$

where $\delta_1 > 0$ is a design constant. Then we have $\forall x(0) > 0$

$$\dot{x} = \dot{\rho} = q_1 - q_2 = -\lambda(x + \delta_1).$$

Thus x will decrease exponentially toward the value $-\delta_1 < 0$. At some finite time $t = t_0 > 0$, $x(t_0) = -\delta_2$, i.e. $\rho(t_0) = \frac{C_d}{v_f} - \delta_2$, where $0 < \delta_2 < \min\{\delta_1, \frac{C_d}{v_f}\}$, thus $\rho(t_0)$ is in the region of (37),(38). At the time instant $t = t_0$, we have $x(t) \leq 0$ and controller (38) is switched on which guarantees as shown above that $x(t)$ will converge to zero exponentially fast. Assuming that $q_1 = \frac{vw\rho^j}{v+w}$ and solving (39) for v, we have

$$v = \frac{w(q_2 - \lambda(x + \delta_1))}{w\rho^j - (q_2 - \lambda(x + \delta_1))}. \tag{40}$$

The use of the design constant δ_1 is to reduce the incoming flow via VSL so that the density of the section reduces to be within the set $[0, \frac{C_d}{v_f}]$, which guarantees convergence to the equilibrium point which corresponds to maximum flow and speed. The choice of δ_1 will depend on how aggressively we want the density to move to the "good" free speed region. Using the above VSL controller derivation and assuming that the speed is not allowed to go below zero or exceed the speed limit v_f, the following equations summarize the VSL controller for the section under the assumption that $q_1 = \frac{vw\rho^j}{v+w}$, which we will relax subsequently. When $I \in \bigcup_{i=1}^{4} \Omega_i$, the VSL control is generated as follows:

$$\begin{aligned}
\bar{v}_1 &= \frac{w[q_2 - \lambda(x + \delta_1)]}{w\rho^j - [q_2 - \lambda(x + \delta_1)]}, \\
\bar{v}_2 &= \frac{w(q_2 - \lambda x)}{w\rho^j - (q_2 - \lambda x)}, \\
v_i &= \text{med}\{0, \bar{v}_i, v_f\}, i = 1, 2, \\
v &= \begin{cases} v_1 & \text{if } \rho(0) > \dfrac{C_d}{v_f} \text{ and } \rho(t) > \dfrac{C_d}{v_f} - \delta_2 \\ v_2 & \text{if } \rho(0) > \dfrac{C_d}{v_f} \text{ and } \rho(t) = \dfrac{C_d}{v_f} - \delta_2 \\ v_2 & \text{if } \rho(0) \leq \dfrac{C_d}{v_f} \text{ and } \rho(t) \leq \dfrac{C_d}{v_f} \end{cases},
\end{aligned} \tag{41}$$

where $x = \rho - \frac{C_d}{v_f}$, and

$$\delta_1 > 0, 0 < \delta_2 < \min\{\delta_1, \frac{C_d}{v_f}\},\ 0 < \lambda < \frac{v_f w \rho^j}{C_d}$$

are design constants and med$\{\cdot\}$ denotes the median of the numbers, which indicates that the VSL command saturates at the upper bound v_f and the lower bound 0. The upper bound $\frac{v_f w \rho^j}{C_d}$ of λ guarantees that the denominator of v is not 0, which we will show in the proof of Theorem 7.1. The shape of the function v as it varies with ρ is shown in Fig. 39.

Figure 39: Switching Logic of VSL Controller

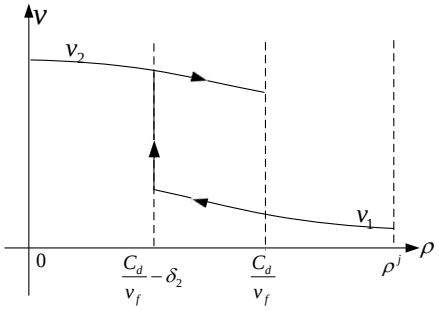

For $I \in \Omega_5$, the VSL control is

$$v = v_f. \tag{42}$$

In Theorem 7.1 below, we show that the above controller also works for any value of $q_1 = \min\{d, \frac{vw\rho^j}{v+w}, C, w(\rho^j - \rho)\}$, and guarantees the exponential convergence of the density to the desired equilibrium point and the exponential convergence of the flow rate to the maximum possible value of $q_1 = q_2 = C_d$. Furthermore, when $I \in \bigcup_{i=1}^{3} \Omega_i$, i.e. $d \leq C_d$, controller (41) guarantees the exponential convergence of ρ to the desired equilibrium point $\frac{d}{v_f}$ and the convergence of q_1, q_2 to the maximum level d.

Theorem 7.1. *For $q_1 = \min\{d, \frac{vw\rho^j}{v+w}, C, w(\rho^j - \rho)\}$, we have the following:*

a) Let $I \in \bigcup_{i=1}^{4} \Omega_i$, i.e. $C_d < C$, and consider the VSL controller (41). The closed-loop system (36), (41) has a unique equilibrium point $\rho^e = \frac{\min\{d, C_d\}}{v_f}$. In addition, $\forall \rho(0) \in [0, \frac{C_d}{v_f}]$, $\rho(t)$ converges to ρ^e exponentially fast and $\forall \rho(0) \in (\frac{C_d}{v_f}, \rho^j]$, $\rho(t)$ decreases to $\frac{C_d}{v_f} - \delta_2$ exponentially fast which brings it to the region where $\rho(t)$ converges to ρ^e exponentially fast. The flow rate and speed converge to the desired values of $\min\{d, C_d\}$ and v_f respectively with the same rate.

b) Let $I \in \Omega_5$, i.e. $C_d \geq C$, and consider the VSL controller (42). System (36),(42) has a unique equilibrium point $\rho^e = \frac{\min\{d,C\}}{v_f}$. In addition, $\forall \rho(0) \in [0, \rho^j]$, $\rho(t)$ converges to ρ^e exponentially fast. The flow rate and speed converge exponentially fast to the desired values of $\min\{d, C\}$ and v_f respectively.

The proof of Theorem 7.1 is given in Appendix C. Theorem 7.1 shows that the VSL controller (41), (42) guarantees that for all cases $I \in \bigcup_{i=1}^{5} \Omega_i$, the density, flow rate and flow speed converge exponentially fast to unique values that correspond to maximum possible flow through the section for all initial density conditions within the set $[0, \rho^j]$. Theorem 7.1 shows in an analytically rigorous manner that VSL control can stabilize the flow in the section and force it to converge to the maximum possible flow under any situation. This maximum flow depends on the characteristics and relationships between demand d and capacities C, C_d as well as capacity drop level ϵ_0. It is also clear from the analysis of the open-loop system that without the VSL control the flow can reach steady states that do not correspond to maximum possible flow.
From equation (41), we can see that the logic of the VSL controller is to deactivate the capacity drop with v_1 by suppressing the inflow sufficiently and then force the system state to converge to the desired equilibrium point with v_2. This logic and the feedback linearization technique can always be used to design a VSL controller if different capacity drop models such as those presented in [60] are included in the CTM.

7.2. N-section Road Segment with VSL Control

The analysis in Section 6.2 shows that the stability properties of the open-loop N-section system are similar to those of the single-section system. For the cases $I \in \Omega_1$ and $I \in \Omega_5$, $\rho(t)$ converges exponentially fast to the unique equilibrium state $\rho^e = \frac{d}{v_f} \times \mathbf{1}$ and $\rho^e = \frac{\min\{d,C\}}{v_f} \times \mathbf{1}$ respectively, which corresponds to the maximum possible flow rate. In these two cases no control action is needed.
When $I \in \Omega_2 \cup \Omega_3$, the control objective is to stabilize the system at the equilibrium state $\rho^e = \frac{d}{v_f} \times \mathbf{1}$, at which the maximum possible flow rate d is achieved and the densities in each section are stabilized at the lowest possible value whereas the speed of flow converges to the free flow speed v_f.
When $I \in \Omega_4$, the maximum possible flow rate is C_d, which corresponds to the equilibrium state $\rho^e = \frac{C_d}{v_f} \times \mathbf{1}$. From equation (34), we know that due to capacity drop

$$\lim_{\rho_N \to (\frac{C_d}{v_f})_-} q_{N+1}(\rho_N) = \lim_{\rho_N \to \frac{C_d}{v_f}} v_f \rho_N = C_d$$

and

$$\lim_{\rho_N \to (\frac{C_d}{v_f})_+} q_{N+1}(\rho_N) = \lim_{\rho_N \to \frac{C_d}{v_f}} (1-\epsilon_0) C_d = (1-\epsilon_0) C_d.$$

Therefore, in this case, in order to achieve the maximum possible flow rate C_d, we want to choose

the VSL control so that there exits $t_0 \geq 0$ such that $\forall t \geq t_0$, $\rho_N(t) \leq \frac{C_d}{v_f}$ and $\rho_i(t)$ converges to $\frac{C_d}{v_f}$, for $i = 1, 2, ..., N$. Furthermore we want to achieve a steady state flow speed v_f in all sections.
Similar to the single section case, the VSL controller is applied to the N-section road segment as shown in Fig. 40. All vehicles in the upstream segment of section 1 are asked to follow the VSL

Figure 40: VSL Controlled Road Segment

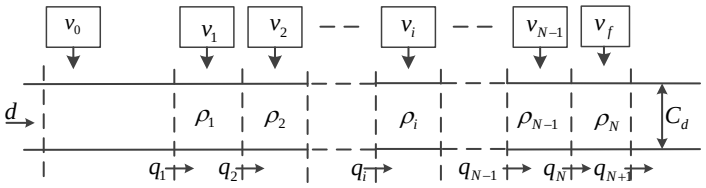

command v_0 and all vehicles in section i follow the VSL command v_i, for $i = 1, 2, ..., N-1$. The speed limit in section N is set to the constant free flow speed v_f.
If the speed limit of section i is set to be $v_i \leq v_f$, $i = 1, 2, ..., N-1$, then the fundamental diagram of section i is distorted as shown in Fig. 41. In Fig. 41, $s_i(\rho_i)$ denotes the ability of sec-

Figure 41: Fundamental Diagram of Section i

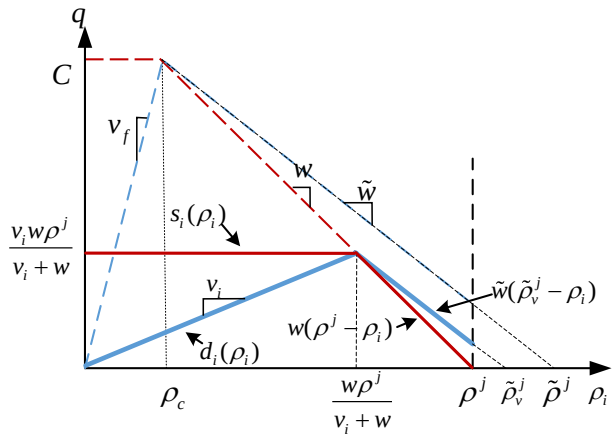

tion i to absorb traffic flow from section $i-1$. We have $s_i(\rho_i) = \min\{\frac{v_i w \rho^j}{v_i + w}, w(\rho^j - \rho_i)\}, i = 1, 2, ..., N-1$. $d_i(\rho_i)$ denotes the traffic flow generated by section i to go into section $i+1$. We have $d_i(\rho_i) = \min\{v_i \rho_i, \frac{v_i w \rho^j}{v_i + w}\}, i = 1, 2, ...N-1$. Therefore, in Fig. 40, we have

$$q_i = \min\{d_{i-1}(\rho_{i-1}), s_i(\rho_i)\} = \min\{v_{i-1}\rho_{i-1}, \frac{v_{i-1} w \rho^j}{v_{i-1} + w}, \frac{v_i w \rho^j}{v_i + w}, w(\rho^j - \rho_i)\}, i = 2, ..., N-1.$$

For the road segment upstream section 1, i.e. the segment with speed limit v_0, whose density is not included in system (34), we assume the flow rate generated by this segment to be $d_0 = \min\{d, \frac{v_0 w \rho^j}{v_0+w}\}$, which is independent of the density in the section with speed limit v_0, therefore

$$q_1 = \min\{d_0, s_1(\rho_1)\} = \min\{d, \frac{v_0 w \rho^j}{v_0 + w}, \frac{v_1 w \rho^j}{v_1 + w}, w(\rho^j - \rho_1)\}.$$

The speed limit in section N is constant v_f, therefore section N can absorb a flow of $s_N(\rho_N) = \min\{C, w(\rho^j - \rho_N)\}$, therefore

$$q_N = \min\{d_{N-1}(\rho_{N-1}), s_N(\rho_N)\} = \min\{v_{N-1}\rho_{N-1}, \frac{v_{N-1} w \rho^j}{v_{N-1} + w}, C, w(\rho^j - \rho_N)\}.$$

For the sake of simplicity, we omit the term $\tilde{w}(\tilde{\rho}_v^j - \rho_i)$ from $d_i(\rho_i)$, where $\tilde{\rho}_v^j$ is $\tilde{\rho}^j$ distorted by the VSL. As shown in Fig. 41, for $i = 1, ..., N-1$, if the outflow $q_{i+1} = \tilde{w}(\tilde{\rho}_v^j - \rho_i)$, then the inflow $q_i \leq s_i(\rho_i) = w(\rho^j - \rho_i) < q_{i+1}$ will force ρ_i to decrease until $q_{i+1} \neq \tilde{w}(\tilde{\rho}_v^j - \rho_i)$. Therefore, this simplification does not affect the results. The system model with VSL control inputs can be formulated as follows:

$$\begin{aligned}
\dot{\rho}_i &= q_i - q_{i+1}, 0 \leq \rho_i(0) \leq \rho^j, \text{for } i = 1, 2, ..., N, \\
q_1 &= \min\{d, \frac{v_0 w \rho^j}{v_0 + w}, \frac{v_1 w \rho^j}{v_1 + w}, w(\rho^j - \rho_1)\}, \\
q_i &= \min\{v_{i-1}\rho_{i-1}, \frac{v_{i-1} w \rho^j}{v_{i-1} + w}, \frac{v_i w \rho^j}{v_i + w}, w(\rho^j - \rho_i)\}, i = 2, 3, ..., N-1, \\
q_N &= \min\{v_{N-1}\rho_{N-1}, \frac{v_{N-1} w \rho^j}{v_{N-1} + w}, C, w(\rho^j - \rho_N)\}, \\
q_{N+1} &= \min\{v_f \rho_N, (1 - \epsilon(\rho_N))C_d, \tilde{w}(\tilde{\rho}^j - \rho_N)\}.
\end{aligned} \tag{43}$$

Similar to the single section system, the objective is to design a VSL controller that can overcome the capacity drop and achieve the control objectives in all cases. We derive the VSL controller using feedback linearization for the case of $I \in \Omega_4$ then show in Theorem 7.2 that the controller also works for all other scenarios.

When $I \in \Omega_4$, i.e. $d > C_d$, we need to decrease v_0 to suppress q_1 so that the flow from upstream can be handled by the downstream capacity C_d. We start by assuming that $q_1 = \frac{v_0 w \rho^j}{v_0+w}$, which is the only term in the equation of q_1 that depends on v_0 and then show that the VSL controller works for all values of q_1. Furthermore, in this case, the desired equilibrium density is $\rho_i^e = \frac{C_d}{v_f}$ for $i = 1, 2, ..., N$ and the equilibrium flow speed and flow rate are $v_i^e = v_f$ and $q_{i+1}^e = v_i^e \rho_i^e = C_d$ respectively for $i = 1, 2, ..., N-1$. Therefore, we initially assume that $q_i = v_{i-1}\rho_{i-1}$ for $i = 2, 3, ..., N$, which we relax in Theorem 7.2 below.

Let $x = [x_1, x_2, ..., x_N]^T$, where $x_i = \rho_i - \frac{C_d}{v_f}, i = 1, 2, ..., N$. If $x_N(0) \leq 0$, i.e. $\rho_N(0) \leq \frac{C_d}{v_f}$, we

choose $v = [v_0, v_1, ..., v_{N-1}]^T$, such that

$$q_i = q_{i+1} - \lambda_{i-1} x_i, i = 1, 2, .., N, \tag{44}$$

where $\lambda_i > 0, i = 0, 1, ..., N-1$ are design constants. Thus we have

$$\dot{x}_i = \dot{\rho}_i = q_i - q_{i+1} = -\lambda_{i-1} x_i, i = 1, 2, ..., N,$$

which implies that $x_i(t)$ converges to 0 exponentially fast and $x_N(0) \leq 0, \forall t \geq 0$. Since we assume that $q_1 = \frac{v_0 w \rho^j}{v_0 + w}$ and $q_i = v_{i-1}\rho_{i-1}$ for $i = 2, ..., N$, solving (44) for v gives

$$\begin{aligned} v_0 &= \frac{(q_2 - \lambda_0 x_1)w}{w\rho^j - q_2 + \lambda_0 x_1}, \\ v_i &= \frac{q_{i+2} - \lambda_i x_{i+1}}{\rho_i}, i = 1, 2, ..., N-1. \end{aligned} \tag{45}$$

If $x_N(0) > 0$, i.e. $\rho_N(0) > \frac{C_d}{v_f}$, we choose v such that

$$\begin{aligned} q_i &= q_{i+1} - \lambda_{i-1} x_i, i = 1, 2, .., N-1, \\ q_N &= q_{N+1} - \lambda_{N-1}(x_N + \delta_1), \end{aligned} \tag{46}$$

where $\delta_1 > 0$ is a design constant. Then we have

$$\begin{aligned} \dot{x}_i = \dot{\rho}_i &= q_i - q_{i+1} = -\lambda_{i-1} x_i, i = 1, 2, ..., N-1, \\ \dot{x}_N = \dot{\rho}_N &= q_N - q_{N+1} = -\lambda_{N-1}(x_N + \delta_1), \end{aligned}$$

which implies that $\forall x_N(0) > 0$, $x_N(t)$ will decrease exponentially toward $-\delta_1 < 0$. Therefore there exists $t_0 > 0$, such that $x_N(t_0) = -\delta_2$, i.e. $\rho_N(t_0) = \frac{C_d}{v_f} - \delta_2$, where $0 < \delta_2 < \min\{\delta_1, \frac{C_d}{v_f}\}$, which is in the region of (44), (45). At $t = t_0$, we have $x_N(0) < 0$ and the controller (45) is switched on, in which case $x(t)$ converges to 0 exponentially fast as shown above. Solving (46) for v, we have

$$\begin{aligned} v_0 &= \frac{(q_2 - \lambda_0 x_1)w}{w\rho^j - q_2 + \lambda_0 x_1}, \\ v_i &= \frac{q_{i+2} - \lambda_i x_{i+1}}{\rho_i}, i = 1, 2, ..., N-2, \\ v_{N-1} &= \frac{q_{N+1} - \lambda_{N-1}(x_N + \delta_1)}{\rho_{N-1}}. \end{aligned} \tag{47}$$

Using the above VSL controller and assuming that the speed is not allowed to go below zero or exceed the speed limit v_f, the following equations summarize the VSL controller for the N-section road system under the assumption that $q_1 = \frac{v_0 w \rho^j}{v_0 + w}$ and $q_i = v_{i-1}\rho_{i-1}, i = 2, 3, ..., N$, which we will relax subsequently. For all $I \in \bigcup_{i=1}^{4} \Omega_i$, the VSL commands are generated as fol-

lows:

$$
\begin{aligned}
\bar{v}_0 &= \frac{(q_2 - \lambda_0 x_1)w}{w\rho^j - q_2 + \lambda_0 x_1}, \\
\bar{v}_i &= \begin{cases} \dfrac{q_{i+2} - \lambda_i x_{i+1}}{\rho_i} & \rho_i > 0 \\ v_f & \rho_i = 0 \end{cases}, i = 1, 2, ..., N-2, \\
\bar{v}_{N-1,1} &= \frac{q_{N+1} - \lambda_{N-1}(x_N + \delta_1)}{\rho_{N-1}}, \\
\bar{v}_{N-1,2} &= \begin{cases} \dfrac{q_{N+1} - \lambda_{N-1} x_N}{\rho_{N-1}} & \rho_{N-1} > 0 \\ v_f & \rho_{N-1} = 0 \end{cases}, \\
\bar{v}_{N-1} &= \begin{cases} \bar{v}_{N-1,1} & \text{if } \rho_N(0) > \dfrac{C_d}{v_f} \text{ and } \rho_N(t) > \dfrac{C_d}{v_f} - \delta_2 \\ \bar{v}_{N-1,2} & \text{if } \rho_N(0) > \dfrac{C_d}{v_f} \text{ and } \rho_N(t) = \dfrac{C_d}{v_f} - \delta_2 \\ \bar{v}_{N-1,2} & \text{if } \rho_N(0) \le \dfrac{C_d}{v_f} \text{ and } \rho_N(t) \le \dfrac{C_d}{v_f} \end{cases}, \\
v_i &= \text{med}\{0, \bar{v}_i, v_f\}, i = 0, 1, ..., N-1,
\end{aligned}
\tag{48}
$$

where $\delta_1 > 0, 0 < \delta_2 < \min\{\delta_1, \frac{C_d}{v_f}\}$, $\lambda_i > v_f$, for $i = 1, 2..., N-1, 0 < \lambda_0 < \frac{v_f w \rho^j}{C_d}$. In controller (48), $\lambda_0 < \frac{v_f w \rho^j}{C_d}$ guarantees that the denominator of v_0 is always greater than 0. $\lambda_i > v_f$, for $i = 1, 2..., N-1$ guarantees the exponential convergence of the density states, which we will show in the proof of Theorem 7.2 below. The switching logic of v_{N-1} is similar to that of v shown in Fig.39 for the single section case. For $I \in \Omega_5$, the VSL command is

$$
v_i = v_f, i = 0, 1, ..., N-1. \tag{49}
$$

Similar to the single section case, we can show that v_0 is well-defined as its denominator is always greater than 0. For $i = 1, 2, ..., N-1$, v_i is also well-defined by setting $v_i = v_f$ when its denominator is equal to 0.

In Theorem 7.2, we show that the controller (48) also works for the general flow equations (43), and guarantees that $\rho_i(t)$ converges to $\frac{C_d}{v_f}$ exponentially fast, for $i = 1, 2, ..., N$ and the flow rates q_i converge exponentially fast to the maximum possible flow rate which in this case is equal to C_d, for $i = 1, 2, ..., N+1$. We also show in Theorem 7.2 that when $I \in \bigcup_{i=1}^{3} \Omega_i$, controller (48) guarantees that ρ_i converges to $\frac{d}{v_f}$ exponentially fast, for $i = 1, 2, ..., N$ and q_i converges to d, which is the maximum possible flow rate, for $i = 1, 2, ..., N+1$.

Theorem 7.2. *We consider the traffic flow model described by (43) with the VSL controller (48), (49):*

a) Let $I \in \bigcup_{i=1}^{4} \Omega_i$*, i.e.* $C_d < C$*. The closed-loop system (43), (48) has a unique equilibrium state* $\rho^e = \frac{\min\{d,C_d\}}{v_f} \times \mathbf{1}$*. In addition,* $\forall \rho(0) \in \{\rho | 0 \leq \rho_N \leq \frac{C_d}{v_f}\}$*, the density vector* $\rho(t)$ *converges to* ρ^e *exponentially fast and* $\forall \rho(0) \in \{\rho | \frac{C_d}{v_f}\} < \rho_N \leq \rho^j$*,* $\rho_N(t)$ *decreases to* $\frac{C_d}{v_f} - \delta_2$ *exponentially fast, which brings it to the region where the density vector* $\rho(t)$ *converges to* ρ^e *exponentially fast. Furthermore, the flow rates* $q_i, i = 1, 2, ..., N+1$ *and flow speeds* $v_i, i = 0, 1, ..., N-1$ *converge to* $\min\{d, C_d\}$ *and* v_f *respectively which is the state which corresponds to the maximum possible flow.*

b) Let $I \in \Omega_5$*, i.e.* $C_d \geq C$*. The closed-loop system (43), (49) has a unique equilibrium state* $\rho^e = \frac{\min\{d,C\}}{v_f} \times \mathbf{1}$*. In addition,* $\forall \rho(0) \in S$*, the density vector* ρ *converges exponentially fast to* ρ^e*. Furthermore, the flow rates and flow speeds converge exponentially fast to* $\min\{d, C\}$ *and* v_f *respectively, achieving the maximum possible flow at steady state.*

The proof of Theorem 7.2 is presented in Appendix D. Theorem 7.2 shows that the VSL controller (48)-(49) guarantees that for all cases $I \in \bigcup_{i=1}^{5} \Omega_i$, the steady state densities, flow rates and speeds of flow are stabilized at the desired values which correspond to the maximum flow rate through the road segment while achieving homogeneous density distribution.
We should note that in Theorem 7.2, the design of the VSL controller (48) and the stability analysis of the closed-loop system (43) are performed under the assumption that we have perfect knowledge of system parameters of the open-loop system (34) and accurate measurement of the density vector ρ. However when $I \in \Omega_4$, since the desired equilibrium point of the closed-loop system (43), i.e. $\rho^e = \frac{C_d}{v_f} \times \mathbf{1}$ lies exactly on the discontinuity plane of the fundamental diagram, which is $\{\rho | \rho_N = \frac{C_d}{v_f}\}$, when $\rho(t) = \frac{C_d}{v_f} \times \mathbf{1}$ at steady state, any disturbance in model parameters or measurement noise may push the density in section N to $\rho_N > \frac{C_d}{v_f}$, which may lead to temporary capacity drop which the controller tries to correct leading to a possible oscillation around the desired equilibrium point. Even though such oscillations may not have any significant impact in an actual traffic situation, the proposed controller can be easily modified to avoid such oscillatory response. This is achieved by setting the desired equilibrium point to be $\rho^e = (\frac{C_d}{v_f} - \sigma) \times \mathbf{1}$, where $\sigma > 0$, in order to provide a margin between ρ^e and the discontinuity at $\rho_N = \frac{C_d}{v_f}$. Thus in (48), $x_i = \rho_i - (\frac{C_d}{v_f} - \sigma)$. With sufficiently large feedback gains $\lambda_0, ..., \lambda_N$, controller (48) is able to stabilize the density state ρ at a point that is arbitrarily close to $\rho^e = (\frac{C_d}{v_f} - \sigma) \times \mathbf{1}$, therefore avoid the capacity drop. We will demonstrate this with numerical simulations in Section 7.3. Thus, although the controller (48) is designed for accurate system model, it can be robust with respect to system disturbance with simple modification. How to modify the controller of this paper to be robust with respect to a wide range of uncertainties is currently under investigation and it is outside the scope of this paper. However the ideal properties of the controller of this paper form the basis for comparison of any other controller under less ideal situations and for this reason it has its own merit.

7.3. Numerical Experiments

In this section, we use numerical simulations to demonstrate the analytical results of the previous sections, for both open-loop and closed-loop systems. The simulations are performed on a two-section road network, whose parameters are: $C = 6500$ veh/h, $w = 20$ mi/h, $\rho^j = 425$ veh/mi, $v_f = 65$ mi/h, $\tilde{w} = 10$ mi/h, $\tilde{\rho}^j = 750$ veh/mi, $\rho_c = 100$ veh/mi. When I belongs to Ω_1 to Ω_4, we set the downstream capacity $C_d = 5200$ veh/h, which is less than C, and $\epsilon_0 = 0.15$. When I belongs to Ω_5, we set $C_d = 7000$ veh/h, which is greater than C. The upstream demand d is set to be 4000 veh/h, 4420 veh/h, 5000 veh/h, 6000 veh/h and 6000 veh/h for the cases of I in Ω_1 to Ω_5 respectively. We apply controller (48),(49) to the two-section system with the following design constants: $\lambda_1 = \lambda_2 = 70$ mi/h, $\delta_1 = 20$ veh/mi, $\delta_2 = 5$ veh/mi. Among the abbreviated units we used above, "veh" stands for number of vehicles, "mi" stands for miles and "h" stands for hours.

Figure 42: Phase portrait when $I \in \Omega_1 (C_d < C, d < (1-\epsilon_0)C_d)$. Both the open-loop and closed-loop densities converge to the same low density equilibrium state. ● Single low density equilibrium state.

(a) Open-loop (b) Closed-loop

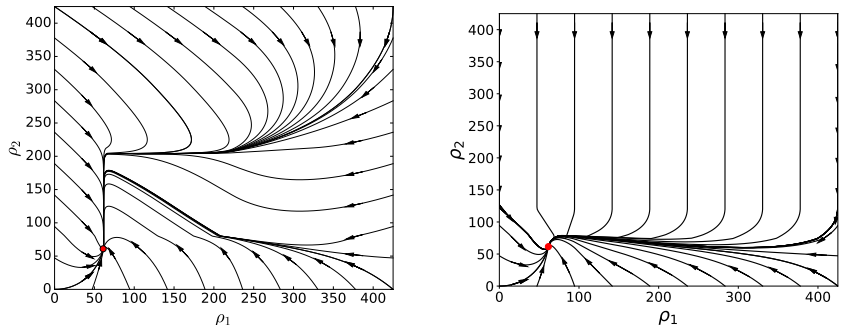

Fig. 42 - Fig. 46 show the phase portraits of the two-section open-loop and closed-loop systems when I belongs to Ω_1 to Ω_5. When $I \in \Omega_1$, all the density state trajectories of the open-loop system, shown in Fig. 42a, converge to the unique equilibrium state $\rho^e = (\frac{d}{v_f}, \frac{d}{v_f}) = (61.5, 61.5)$, indicated by the red dot. In Fig.42b, all density state trajectories of the closed-loop system converge to the same equilibrium state as in the open-loop case as expected from the analysis. When $I \in \Omega_2$, all density state trajectories of the open-loop system shown in Fig.43a converge to the isolated equilibrium state $\rho^e = (\frac{d}{v_f}, \frac{d}{v_f}) = (68, 68)$, indicated by the red dot in Fig. 43a, or to the equilibrium set

$$
\begin{aligned}
S^e =& \{\rho | \rho_1 = \frac{d}{v_f}, \frac{C_d}{v_f} < \rho_2 \leq \rho^j - \frac{d}{w}\} \cup \{\rho | \frac{d}{v_f} \leq \rho_1 \leq \rho^j - \frac{d}{w}, \rho_2 = \rho^j - \frac{d}{w}\} \\
=& \{\rho | \rho_1 = 68, 80 < \rho_2 \leq 204\} \cup \{\rho | 68 \leq \rho_1 \leq 204, \rho_2 = 204\},
\end{aligned}
$$

Figure 43: Phase portrait when $I \in \Omega_2(C_d < C, d = (1-\epsilon_0)C_d)$. The open-loop system has an infinite number of equilibrium density states which do not correspond to the maximum possible flow speed. Closed-loop system has a single low density equilibrium state. ● Equilibrium state; — Equilibrium manifold.

(a) Open-loop (b) Closed-loop

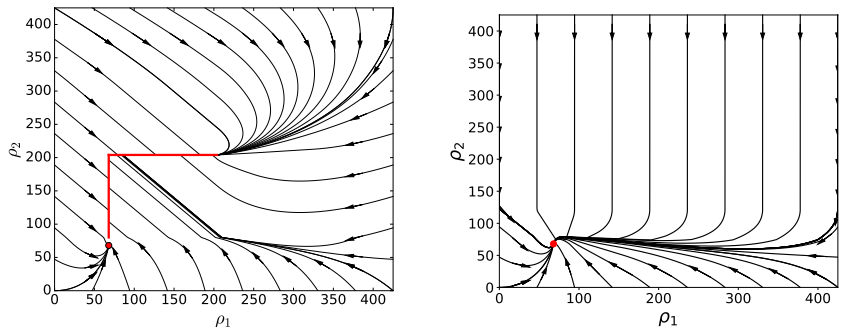

Figure 44: Phase portrait when $I \in \Omega_3$ $(C_d < C, (1-\epsilon_0)C_d < d \leq C_d)$. The open-loop system has two equilibrium density states one in the low density and the other in the high density region. The closed-loop system has a unique equilibrium state at low density. ● Low density equilibrium state; ★ High density equilibrium state.

(a) Open-loop (b) Closed-loop

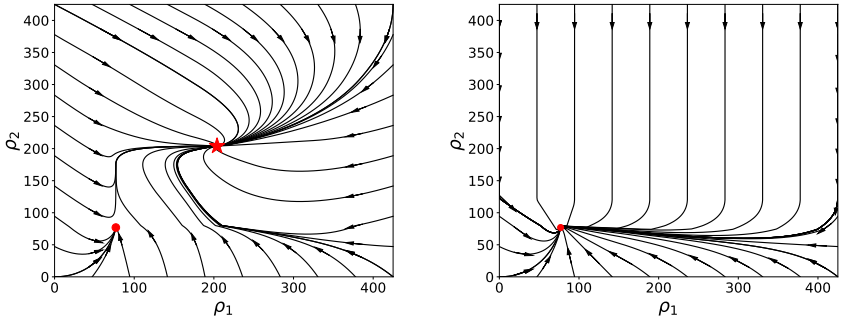

indicated by the red line in Fig. 43a. When the VSL control is applied, all the density state trajectories of the closed-loop system converge to the unique equilibrium state $\rho^e = (\frac{d}{v_f}, \frac{d}{v_f}) = (68, 68)$, as shown in Fig. 43b. When $I \in \Omega_3$, each density state trajectory of the open-loop system shown in Fig.44a converges to one of the two isolated equilibrium states, $\rho_1^e = (d/v_f, d/v_f) = (77, 77)$ and $\rho_2^e = (\rho^j - \frac{(1-\epsilon_0)C_d}{w}, \rho^j - \frac{(1-\epsilon_0)C_d}{w}) = (204, 204)$, indicated by the red dot and red star respectively. All closed-loop state trajectories shown in Fig.44b converge to the unique equilibrium state $\rho_1^e = (d/v_f, d/v_f) = (77, 77)$. Fig. 45a shows that when $I \in \Omega_4$, all the density state trajectories converge to the unique equilibrium state $\rho^e = (\rho^j - \frac{(1-\epsilon_0)C_d}{w}, \rho^j - \frac{(1-\epsilon_0)C_d}{w}) =$

Figure 45: Phase portrait when $I \in \Omega_4(C_d < C, d > C_d)$. The open-loop system has a unique equilibrium state in the high density region. The closed-loop system has a unique equilibrium state at low density. ● Low density equilibrium state; ★ High density equilibrium state.

(a) Open-loop (b) Closed-loop

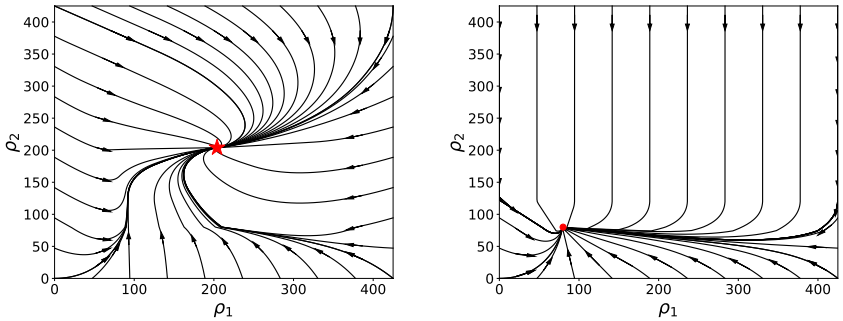

Figure 46: Phase portrait when $I \in \Omega_5(C_d \geq C)$. Same open-loop and closed-loop response. ● Single low density equilibrium state.

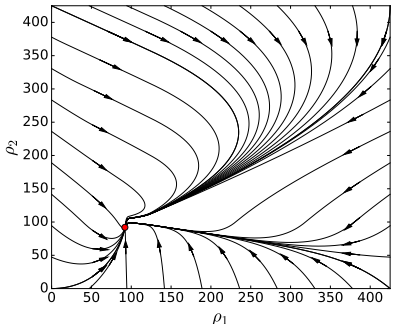

$(204, 204)$, indicated by the red dot. The phase portrait of the corresponding closed-loop system is plotted in Fig. 45b. As shown in Theorem 7.2, all density state trajectories converge to the desired equilibrium state $\rho^e = (C_d/v_f, C_d/v_f) = (80, 80)$, indicated by the red dot in Fig. 45b. Furthermore, ρ_2 converges to $\rho_2 = 80$ when the initial condition satisfies $\rho_2(0) \leq 80$. If $\rho_2(0) > 80$, $\rho_2(t)$ decreases to $\rho_2 = 75$ first, then increases and converges to 80, which guarantees the steady-state flow rate $C_d = 5200$ veh/h. When $I \in \Omega_5$, capacity drop will not occur since the downstream capacity is higher than the capacity of the road sections. All state trajectories in Fig. 46 converge to the unique equilibrium state $\rho^e = (\min\{d, C\}/v_f, \min\{d, C\}/v_f) = (92.3, 92.3)$. The open-loop and closed-loop behavior when $I \in \Omega_5$ are the same as expected.

Fig.47 shows the flow rate time responses of the open-loop and closed-loop systems when $I \in \Omega_4$ with initial condition $\rho = (110, 110)$. From Fig. 47a, we can see that at $t = 0$, $q_1(0) = d = 6000$ veh/h, $q_2(0) = v_f \rho_1(0) = 6500$ veh/h $< q_1(0)$ and decrease to the steady state value of

Figure 47: Flow rate when $I \in \Omega_4$

(a) Open-loop (b) Closed-loop

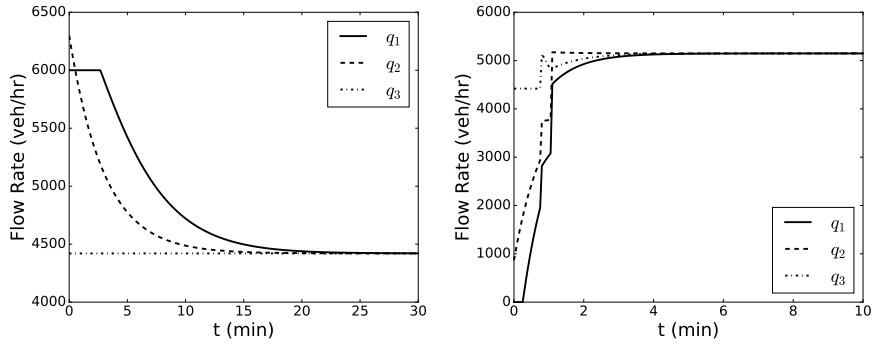

Figure 48: Flow rate with Perturbed v_f when $I \in \Omega_4$

(a) Original Controller (b) Modified Controller

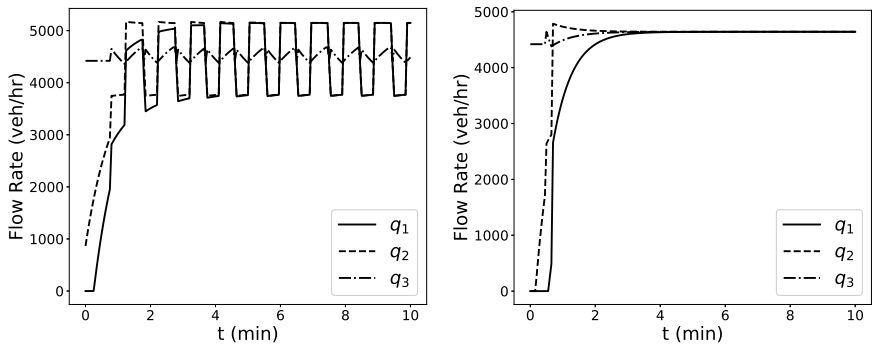

4420 veh/h. On the other hand, $q_3 = (1-\epsilon_0)C_d = 4420$ veh/h remains constant during the entire simulation time (30 min). In Fig. 47b, $q_3 = (1-\epsilon_0)C_d = 4420$ veh/h at the beginning of the simulation, then jumps to 5200 veh/h, then oscillates a little and converges to $C_d = 5200$ veh/h. The jump in the value of q_3 is due to the fact that ρ_2 decreases and crosses the value $\frac{C_d}{v_f}$, at which q_3 jumps from $(1-\epsilon_0)C_d$ to C_d. The values of q_1 and q_2 also have a jump between $t = 1$ min and $t = 2$ min. This jump is caused by the switching of the VSL control (48) which at this time does not affect q_3 since q_3 is only a function of ρ_2, and does not jump when the VSL switches.
Fig. 48 shows the performance of the closed-loop system in the same scenario as in Fig. 47, however with perturbed v_f. In this case, the actual free flow speed $v_f = 0.9v_{fn}$, where v_{fn} is the nominal value of v_f, based on which the controller (48) is designed. That is, the VSL controller is over-estimating the flow rate at the bottleneck, therefore sends more flow to section 2 than it can handle, which leads to temporary capacity drop, which the controller corrects creating an oscillation around an average that corresponds to the desired flow as shown in Fig. 48a. Our controller however can be easily modified to take care of the uncertainty without changing the fun-

damentals of the design and analysis. As shown in Fig. 48b, we modified the controller (48) as stated in Section 7.2 by setting $x_i = \rho_i - (\frac{C_d}{v_{fn}} - 5) = \rho_i - 75, i = 1, 2$ and increasing the feedback gains to be $\lambda_i = 100$ mi/h, $i = 0, 1$. The modified controller tries to stabilize the density vector at $\rho^e = (75, 75)$, which gives a margin between ρ^e and the boundary of capacity drop. The increased feedback gains are able to suppress the steady state error to make sure that the steady state value of ρ is close to ρ^e thus capacity drop does not occur. With the modified VSL controller, the steady state density is $\rho = (74.2, 78.44)$, and the steady state traffic flow is $q_1 = q_2 = q_3 = 4590$ veh/h, as shown in Fig. 48b. This a simple case how an uncertainty can be dealt with by the proposed controller. The robustness of the proposed controller with respect to a wide range of uncertainties is currently under investigation and it is outside the scope of this paper that focuses on the control design and analysis under ideal conditions. The results form the basis for comparison as uncertainties are included in the model.

8 Robust VSL Control of Cell Transmission Model with Disturbance

Section 7 shows the possibility of achieving the maximum possible flow rate at a bottleneck and avoiding capacity drop, under the assumption that we have perfect knowledge of model parameters of the CTM and accurate measurement of the vehicle densities. We have shown as well in section 7 that due to the discontinuous nature of the desired equilibrium point, any disturbance or measurement noise may lead to a oscillatory behavior of the closed-loop system. We also demonstrate with numerical simulations that with simple modification, the VSL controller can help the system avoid the oscillation and stabilize the density at an equilibrium point close to the desired one. In this section, we modify the VSL controller by adding the integral action in order to reject the constant disturbance which may be introduced by the ramp flows or biased measurement etc.

8.1. Robust Control of Traffic Flow in a Single-Section Road Segment

Consider a single road section of in Fig. 37, with a constant disturbance μ, which may be introduced by the ramp flows or biased measurement of the flow rate, the evolution of ρ with respect to time is given by the following differential equation:

$$\dot{\rho} = q_1 - q_2 + \mu, 0 \leq \rho(0) \leq \rho^j, \tag{50}$$

where

$$\begin{aligned} q_1 &= \min\{d, \frac{vw\rho^j}{v+w}, C, w(\rho^j - \rho)\}, \\ q_2 &= \min\{v_f\rho, \tilde{w}(\tilde{\rho}^j - \rho), (1-\epsilon(\rho))C_d\}., \\ v_f\rho_c &= w(\rho^j - \rho_c) = \tilde{w}(\tilde{\rho}^j - \rho_c) = C, \\ 0 &< \rho_c < \rho^j, 0 < \tilde{w} < w, v_f > 0, \\ \epsilon(\rho) &= \begin{cases} 0 & \text{if } 0 \le \rho \le \dfrac{C_d}{v_f} \\ \epsilon_0 & \text{otherwise} \end{cases}, \end{aligned} \tag{51}$$

We assume the constant disturbance μ satisfy that $|\mu| \le \mu_m \ll C_d$, that is, comparing to the bottleneck capacity, the magnitude of the disturbance is very small, which also guarantees that $0 \le \rho(t) \le \rho^j, \forall t \ge 0$.
We define constants $\mu_m < \rho^L \le \rho^\star < \rho^U < \frac{C_d}{v_f}$ as shown in Fig. 49 to help the design of the controller. In the equation of q_1, the only term that can be controlled by the VSL con-

Figure 49: Design Constants

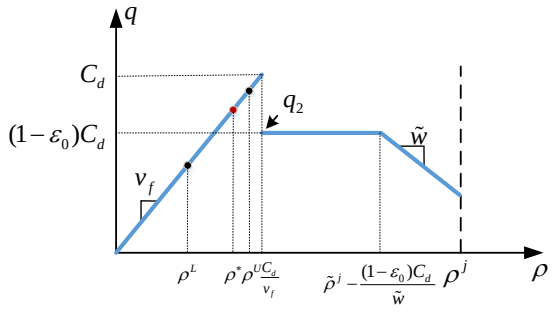

troller is $\frac{vw\rho^j}{v+w}$. Let $q_{1v} = \frac{vw\rho^j}{v+w}$ and assume $d < C$ without loss of generality. We have $q_1 = \min\{d, q_{1v}, w(\rho^j - \rho)\}$. Let $x_1 = \rho - \rho^\star$, system (50)-(51) can be rewritten as:

$$\dot{x}_1 = q_1 - q_2 + \mu, \ -\rho^\star \le x_1(0) \le \rho^j - \rho^\star \tag{52}$$

where

$$\begin{aligned} q_1 &= \min\{d, q_{1v}, w(\rho^j - \rho)\} \\ q_2 &= \min\{v_f\rho, \tilde{w}(\tilde{\rho}^j - \rho), (1-\epsilon(\rho))C_d\} \\ q_{1v} &= \text{median}\{0, \bar{q}_{1v}, C\}. \end{aligned} \tag{53}$$

In equation (53), the constraint $q_{1v} = \text{median}\{0, \bar{q}_{1v}, C\}$ is applied to guarantee that $0 \le v \le v_f$, where $\bar{q}_{1v}$ is the unconstrained control input to be designed. When the road section is congested,

i.e., x_1 is high, we try to decrease q_1 to bring x_1 back to the low region by letting

$$\bar{q}_{1v} = q_s \tag{54}$$

where $q_s < \min\{v_f\rho^L, (1-\epsilon_0)C_d, \tilde{w}(\tilde{\rho}^j - \rho^j)\}$ is a small constant flow which guarantees that $\forall \rho \geq \rho^L$, i.e. $\forall x_1 \geq \rho^L - \rho^\star$, $q_s < q_2$, which implies that $\dot{x}_1 < 0$. Thus, there exists a finite time instant $t_0 > 0$, at which $x_1(t_0) = \rho^L - \rho^\star$ and we set

$$\bar{q}_{1v} = q_2 - \lambda_1 x_1 - \lambda_2 \left(\int_{t_0}^{t} x_1 d\tau + c \right) \tag{55}$$

where $\lambda_2 > 0$ and $\lambda_1 > \max\{2\sqrt{\lambda_2}, v_f + \frac{\lambda_2}{v_f}\} > 0$. c is a constant we use to guarantee that ρ converges to $\rho^\star$ asymptotically, which we will show later. Controller (55) is a PI controller which tries to reject the disturbance μ and stabilize x_1 at $x_1 = 0$. Furthermore, once x_1 decreases to the uncongested region $x_1 \leq \frac{C_d}{v_f} - \rho^\star$, we do not want it to go back to the capacity drop region again. Therefore, if x_1 increases and reaches $\rho^U - \rho^\star$, we switch back to controller (54). To summarize, the controller with hysteresis characteristics can be formulated as below:

$$\begin{aligned} \bar{q}_{1v} &= k(t) \\ k(0) &= \begin{cases} k_1(0) & \text{if } x_1(0) \geq \rho^L - \rho^\star \\ k_2(0) & \text{otherwise} \end{cases} \\ k(t) &= \begin{cases} k_2(t) & \text{if } k(t^-) = k_1 \text{ and } x_1(t) = \rho^L - \rho^\star \\ k(t-) & \text{otherwise} \end{cases}, \forall t > 0 \end{aligned} \tag{56}$$

where

$$\begin{aligned} k_1(t) &= q_s \\ k_2(t) &= q_2 - \lambda_1 x_1 - \lambda_2 \left(\int_{t_0}^{t} x_1 d\tau - \frac{\lambda_1 x_1(t_0) - \mu_m}{\lambda_2} \right) \end{aligned} \tag{57}$$

Mapping the flow rate control input into the VSL command, we have

$$v = \frac{w\rho^j - q_{1v}}{wq_{1v}}$$

where $q_{1v} = \text{median}\{0, \bar{q}_{1v}, C\}$. In the equation of $k_2(t)$, if $k(0) = k_2(0)$ at $t = 0$, then $t_0 = 0$, and if $k(t)$ switches from $k_1(t)$ to $k_2(t)$ at $t = t_0$, then t_0 is the switching time instant. When $k(t) = k_2(t)$, we have that $x_1(t) \leq \rho^U - \rho^\star$, i.e. $\rho \leq \rho^U < \frac{C_d}{v_f}$, thus $q_2 = v_f\rho = v_f\rho^\star + v_f x_1$ and $q_1 = \text{median}\{0, d, \bar{q}_{1v}\}$, due to $d < C$. Let

$$x_2(t) = \int_{t_0}^{t} x_1(t) d\tau - \frac{\lambda_1 x_1(t_0) - \mu_m}{\lambda_2} - \frac{\mu}{\lambda_2}, t \geq t_0. \tag{58}$$

Then we have $\dot{x}_2 = x_1$. Since

$$x_2(t) = x_2(t_0) + \int_{t_0}^{t} \dot{x}_2 d\tau,\ t \geq t_0,$$

and substitute it into (58), we have

$$x_2(t_0) = -\frac{\lambda_1 x_1(t_0) - \mu_m + \mu}{\lambda_2}$$

Then with $k(t) = k_2(t)$, system (52) can be written as

$$\begin{aligned} \dot{x}_1 &= \text{median}\{0, d, \bar{q}_{1v}\} - (v_f\rho^\star + v_f x_1) + \mu \\ \dot{x}_2 &= x_1,\ \forall t \geq t_0 \\ x_1(t_0) &\leq \rho^L - \rho^\star, x_2(t_0) = -\frac{\lambda_1 x_1(t_0) - \mu_m + \mu}{\lambda_2} \end{aligned} \tag{59}$$

where

$$\bar{q}_{1v} = k_2(t) = (v_f\rho^\star + v_f x_1) - \lambda_1 x_1 - \lambda_2(x_2 + \frac{\mu}{\lambda_2}) \tag{60}$$

and $\lambda_2 > 0, \lambda_1 > \max\{2\sqrt{\lambda_2}, v_f + \frac{\lambda_2}{v_f}\} > 0$. Let $x = [x_1, x_2]^T$ be the state vector of system (59). We first ignore the capacity drop, i.e. assume that (59) holds for all $x_1 \in \Re$, and investigate the stability property of system (59) in the following lemma, which we will use to analyze the stability the system which takes the capacity drop into consideration.

Lemma 8.1. *Consider system (59), if $d + \mu \geq v_f\rho^\star$, we have the following results:*

1) System (59) has a unique equilibrium point $x^e = [0, 0]^T$.

2) $\forall x(t_0) \in \Re^2$, $x(t)$ converges to x^e asymptotically.

3) $\forall x(t_0) \in S = \{x | v_f\rho^\star - \mu - d \leq (\lambda_1 - v_f)x_1 + \lambda_2 x_2 \leq v_f\rho^\star - \mu\} \cap \{x | -\frac{v_f\rho^\star - \mu}{v_f} < x_1 < -\frac{v_f\rho^\star - \mu - d}{v_f}\}$, $x_1(t) \in S, \forall t \geq t_0$.

Proof. Consider the value of q_1, we have the following 3 cases:
1. When $0 \leq \bar{q}_{1v} \leq d$, i.e. $x \in S_1 = \{x | v_f\rho^\star - \mu - d \leq (\lambda_1 - v_f)x_1 + \lambda_2 x_2 \leq v_f\rho^\star - \mu\}$, we have $q_1 = \bar{q}_{1v}$, the dynamics of system (59) become:

$$\begin{aligned} \dot{x}_1 &= -\lambda_1 x_1 - \lambda_2 x_2 \\ \dot{x}_2 &= x_1 \end{aligned} \tag{61}$$

2. When $\bar{q}_{1v} < 0$, i.e. $x \in S_2 = \{x | (\lambda_1 - v_f)x_1 + \lambda_2 x_2 > v_f\rho^\star - \mu\}$, we have $q_1 = 0$, the dynamics of system (59) become:

$$\begin{aligned} \dot{x}_1 &= -v_f x_1 - v_f\rho^\star + \mu \\ \dot{x}_2 &= x_1 \end{aligned} \tag{62}$$

3. When $\bar{q}_{1v} > d$, i.e. $x \in S_3 = \{x|(\lambda_1 - v_f)x_1 + \lambda_2 x_2 < v_f\rho^\star - \mu - d\}$, we have $q_1 = d$, the dynamics of system (59) become:

$$\begin{aligned} \dot{x}_1 &= -v_f x_1 - v_f\rho^\star + \mu + d \\ \dot{x}_2 &= x_1 \end{aligned} \tag{63}$$

Therefore the state space is divided as shown in Figure 50.

Figure 50: State Space

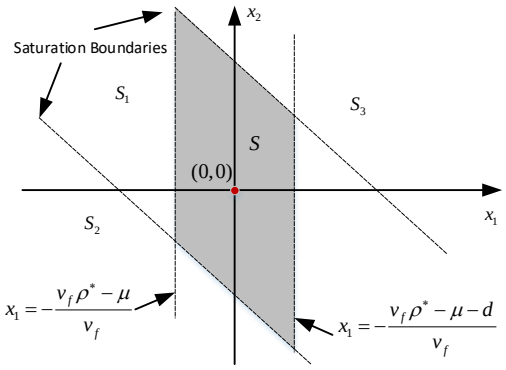

It is easy to show that system (62) and (63) have no equilibrium point. System (61) has a unique equilibrium point $x^e = [0,0]^T \in S_1$. Therefore the system (59) has a unique equilibrium point $x^e = [0,0]^T$. Consider the Lyapunov function

$$V(x) = x^T P x, \tag{64}$$

where

$$P = \begin{bmatrix} 2 & \lambda_1 \\ \lambda_1 & \lambda_1^2 + 2\lambda_2 \end{bmatrix}$$

It is easy to check that matrix P is symmetric and positive definite. Therefore $V(x)$ is positive definite. For all $x \in S_1$, we have

$$\dot{x} = Ax$$

where

$$A = \begin{bmatrix} -\lambda_1 & -\lambda_2 \\ 1 & 0 \end{bmatrix}$$

Therefore the derivative of the Lyapunov function is

$$\dot{V}(x) = x^T(A^T P + PA)x = -x^T Q x,$$

where

$$Q = \begin{bmatrix} 2\lambda_1 & \\ & 2\lambda_1\lambda_2 \end{bmatrix}.$$

Thus $\dot{V}(x) < 0$ for all $x \in S_1 \backslash \{0\}$.
Now we are going to show that if $\exists t_0 \geq 0$, such that $x(t_0) \in S_3$, then $\exists t_1 > t_0$, such that $x(t_1) \in S_1$. If $\exists t_0 \geq 0$, such that $x(t_0) \in S_3$, let $\alpha = v_f\rho^\star - \mu - d$, according to (63), we have that

$$\frac{dx_2}{dx_1} = \frac{x_1}{-v_f x_1 - \alpha} = -\frac{1}{v_f} + \frac{\alpha}{v_f^2 x_1 + v_f\alpha}$$
$$dx_2 = -\frac{1}{v_f}dx_1 + \frac{\alpha}{v_f^2 x_1 + v_f\alpha}dx_1$$

Take the integral of both sides, we have that

$$\begin{aligned} x_2(t) - x_2(t_0) &= -\frac{1}{v_f}(x_1(t) - x_1(t_0)) + \frac{\alpha}{v_f^2}\left[\ln(v_f^2 x_1(t) + v_f\alpha) - \ln(v_f^2 x_1(t_0) + v_f\alpha)\right] \\ x_2(t) &= -\frac{1}{v_f}x_1(t) + \frac{\alpha}{v_f^2}\ln(v_f^2 x_1(t) + v_f\alpha) + x_2(t_0) + \frac{1}{v_f}x_1(t_0) - \frac{\alpha}{v_f^2}\ln(v_f^2 x_1(t_0) + v_f\alpha) \end{aligned} \tag{65}$$

From (63), we know that $x_1(t)$ approaches $-\frac{\alpha}{v_f}$ when $x \in S_3$. According to (65), x_2 approaches infinite as $x_1(t)$ approaches $-\frac{\alpha}{v_f}$. Thus at some finite time instant t_1, $x_2(t_1)$ is large enough and $(\lambda_1 - v_f)x_1 + \lambda_2 x_2 = v_f\rho^\star - \mu - d$, i.e. $x \in S_1$.
Then we show that if $\exists t_0 \geq 0$, at which $x(t_0)$ lies on the boundary between S_1 and S_3, and $x(t)$ moves into S_3, then $\exists t_1 > t_0$, at which $x(t_0)$ lies on the boundary between S_1 and S_3, and $x(t)$ gets into S_1. Furthermore, $V(x(t_0)) > V(x(t_1))$.
The normal vector of the boundary line which points to S_3 is $n = [v_f - \lambda_1, -\lambda_2]^T$. If $\exists t_0 \geq 0$, at which $x(t_0)$ lies on the boundary between S_1 and S_3, and $x(t)$ moves into S_3, we have that

$$x(t_0) = [x_1(t_0), -\frac{\lambda_1 - v_f}{\lambda_2}x_1(t_0) + \frac{\alpha}{\lambda_2}]^T$$

and

$$\dot{x}(t_0) = [-v_f x_1(t_0) - \alpha, x_1(t_0)]^T$$

Since $\dot{x}(t_0)$ points to S_3, therefore $n^T\dot{x}(t_0) > 0$, that is

$$[v_f(\lambda_1 - v_f) - \lambda_2]x_1(t_0) - (v_f - \lambda_1)\alpha > 0$$

$$x_1(t_0) > \frac{(v_f - \lambda_1)\alpha}{v_f(\lambda_1 - v_f) - \lambda_2} > -\frac{\alpha}{v_f}$$

due to $\lambda_1 > v_f + \frac{\lambda_2}{v_f}$. According to (63), if $x(t_0) \in S_3$ and $x_1(t_0) > -\frac{\alpha}{v_f}$, then $x_1(t) > -\frac{\alpha}{v_f}$ and $\dot{x}_1(t) < 0, \forall t > t_0$, as long as $x(t)$ stays in S_3. Together with (65), we know that $\exists t_1 >$

t_0, at which $x(t)$ crosses the boundary and gets into S_1, and $x_1(t_1) > -\frac{\alpha}{v_f}$ and $x_1(t_1) < x_1(t_0)$.
For all points on the boundary between S_1 and S_3, the Lyapunov function is evaluated as

$$V(x) = 2x_1^2 + 2\lambda_1 x_1 x_2 + (\lambda_1^2 + 2\lambda_2)x_2^2,$$

whose partial derivative with respect to x_1 along the boundary line is

$$\frac{\partial V}{\partial x_1} = 4x_1 + 2\lambda_1 x_2 + 2\lambda_1 x_1 \frac{\partial x_2}{\partial x_1} + 2(\lambda_1^2 + 2\lambda_2)\frac{\partial x_2}{\partial x_1} \tag{66}$$

Since $x(t_0) = [x_1(t_0), -\frac{\lambda_1 - v_f}{\lambda_2}x_1(t_0) + \frac{\alpha}{\lambda_2}]^T$ on the boundary line, we have that

$$\frac{\partial x_2}{\partial x_1} = -\frac{\lambda_1 - v_f}{\lambda_2}.$$

Substituting into (66), we have

$$\frac{\partial V}{\partial x_1} = ax_1 + b$$

where

$$a = 4 - 4\lambda_1 \frac{\lambda_1 - v_f}{\lambda_2} + 2(\lambda_1^2 + 2\lambda_2)(\frac{\lambda_1 - v_f}{\lambda_2})^2$$

and

$$b = 2[\lambda_1 - (\lambda_1^2 + 2\lambda_2)]\frac{\alpha}{\lambda_2}.$$

Note that

$$a = 2[1, \frac{\lambda_1 - v_f}{\lambda_2}]^T P[1, \frac{\lambda_1 - v_f}{\lambda_2}] > 0$$

due to P is positive definite. And

$$a(-\frac{\alpha}{\lambda_2}) + b = -[2\lambda_1^2(\lambda_1 - v_f) + 2\lambda_1\lambda_2]\alpha > 0$$

due to $\alpha < 0$ and $\lambda_1 > v_f + \frac{\lambda_2}{v_f}$. Therefore, $\forall x_1 > -\frac{\alpha}{\lambda_2}$, $\frac{\partial V}{\partial x_1} = ax_1 + b > 0$. Therefore, $-\frac{\alpha}{\lambda_2} < x_1(t_1) < x_1(t_0)$ indicates that $V(x(t_0)) > V(x(t_1))$.
Similarly, we can show that if $\exists t_0 \geq 0$, such that $x(t_0) \in S_2$, then $\exists t_1 > t_0$, such that $x(t_1) \in S_1$. And if $\exists t_0 \geq 0$, at which $x(t_0)$ lies on the boundary between S_1 and S_2, and $x(t)$ gets into S_2, then $\exists t_1 > t_0$, at which $x(t_0)$ lies on the boundary between S_1 and S_2, and $x(t)$ gets into S_1. Furthermore, $V(x(t_0)) > V(x(t_1))$.
Summarizing the behavior of the Lyapunov function $V(x)$, we can conclude that $\forall x(t_0) \in \Re^2$, $x(t)$ converges to $x^e = [0, 0]^T$ asymptotically.
Since in (59),

$$-v_f x_1 - (v_f - \mu) \leq \dot{x}_1 \leq -v_f x_1 - (v_f - \mu - d),$$

thus for all $-\frac{v_f\rho^\star - \mu}{v_f} < x_1(t_0) < -\frac{v_f\rho^\star - \mu - d}{v_f}$, $-\frac{v_f\rho^\star - \mu}{v_f} < x_1(t) < -\frac{v_f\rho^\star - \mu - d}{v_f}$, $\forall t \geq t_0$. Also

we have shown that if $x(t) \in S_1 \cap \{x| -\frac{v_f\rho^\star-\mu}{v_f} < x_1 < -\frac{v_f\rho^\star-\mu-d}{v_f}\}$, $x(t)$ will not leave S_1. Therefore, $\forall x(t_0) \in S = \{x|v_f\rho^\star - \mu - d \leq (\lambda_1 - v_f)x_1 + \lambda_2(x_2) \leq v_f\rho^\star - \mu\} \cap \{x| -\frac{v_f\rho^\star-\mu}{v_f} < x_1 < -\frac{v_f\rho^\star-\mu-d}{v_f}\}$, $x_1(t) \in S, \forall t \geq t_0$. □

Lemma 8.1 shows that, if (59) holds for $\forall x_1 \in \Re$, then the unique equilibrium point $x^e = [0, 0]^T$ is globally asymptotically stable. However, the proof of Lemma 8.1 also shows that if $x(t_0) \in S_2$, it is possible that $x_1(t)$ approaches $-\frac{\alpha}{\lambda_2}$, which is already in the capacity drop region where (59) does not hold. Fortunately, in system (59), the initial conditions are set to be in a certain region. We only need to show that for some specific $x(t_0)$, (59) holds for all $t \geq t_0$ and $x_1(t)$ converges to 0.

Theorem 8.1. *Consider the system (52)(53) with controller (56), if* $d + \mu \geq v_f\rho^\star$, *then* $\forall x_1(0) \in [-\rho^\star, \rho^j - \rho^\star]$, $x_1(t)$ *converges to 0 asymptotically.*

Proof. $\forall x_1(0) < \rho^L - \rho^\star$, $k(0) = k_2(0)$. If $\forall t \geq 0$, $x_1(0) < \rho^U - \rho^\star$, then (59) holds for all $t \geq 0$, thus $x_1(t)$ converges to 0 asymptotically according to Lemma 8.1. If $\exists t > 0$, such that $x_1(t) = \rho^U - \rho^\star$, then $k(t)$ switches to $k_1(t)$, then for all $x_1(t) \geq \rho^L - \rho^\star$, $\dot{x}_1(t) = q_s - q_2 < 0$, thus $\exists t_0 > 0$, such that $x_1(t_0) = \rho^L - \rho^\star$ and $k(t_0) = k_2(t_0)$. Similarly, $\forall x_1(0) > \rho^L - \rho^\star$, $k(0) = k_1(0)$, then $\exists t_0 > 0$, such that $x_1(t_0) = \rho^L - \rho^\star$ and $k(t_0) = k_2(t_0)$. Therefore, we only need to consider the case that $x_1(t_0) = \rho^L - \rho^\star$ and $k(t_0) = k_2(t_0)$. As shown in (58) - (60), in this case, as long as $k(t) = k_2(t)$, the system (52)(53) can be written as

$$\begin{aligned}
&\dot{x}_1 = \text{median}\{0, d, \bar{q}_{1v}\} - (v_f\rho^\star + v_f x_1) + \mu \\
&\dot{x}_2 = x_1, \ \forall t \geq t_0 \\
&x_1(t_0) = \rho^L - \rho^\star, x_2(t_0) = -\frac{\lambda_1 x_1(t_0) - \mu_m + \mu}{\lambda_2}
\end{aligned}$$

Since $x_2(t_0) = -\frac{\lambda_1 x_1(t_0)-\mu_m+\mu}{\lambda_2}$, thus $\lambda_1 x_1(t_0) + \lambda_2 x_2(t_0) = \mu_m - \mu > 0$. And since $\mu_m \ll v_f\rho^\star$, we also have $\lambda_1 x_1(t_0) + \lambda_2 x_2(t_0) < v_f\rho^\star - \mu$. Furthermore, $x_1(t_0) = \rho^L - \rho^\star > -\frac{v_f\rho^\star-\mu_m}{v_f} > -\frac{v_f\rho^\star-\mu}{v_f}$. Similarly, $x_1(t_0) < -\frac{v_f\rho^\star-\mu-d}{v_f}$. Therefore $x(t_0) \in S$. According to Lemma 8.1, as long as $x_1(t) < \rho^U - \rho^\star$, then $x(t) \in S$, and (61) holds, i.e.

$$\dot{x} = Ax$$

$$x_1(t_0) = \rho^L - \rho^\star, x_2(t_0) = -\frac{\lambda_1 x_1(t_0)}{\lambda_2}$$

where

$$A = \begin{bmatrix} -\lambda_1 & -\lambda_2 \\ 1 & 0 \end{bmatrix}.$$

Therefore,

$$x(t) = e^{A(t-t_0)}x(t_0),$$

where $e^{At} = \mathcal{L}^{-1}[(sI - A)^{-1}]$ and $\mathcal{L}^{-1}[\cdot]$ is the inverse Laplace transform operator. We can show that

$$(sI - A)^{-1} = \begin{bmatrix} \frac{s}{s^2+\lambda_1 s+\lambda_2} & \frac{-\lambda_2}{s^2+\lambda_1 s+\lambda_2} \\ \frac{1}{s^2+\lambda_1 s+\lambda_2} & \frac{s+\lambda_1}{s^2+\lambda_1 s+\lambda_2} \end{bmatrix}$$

Since $\lambda_1 > 2\sqrt{\lambda_2}$, therefore $\lambda_1^2 - 4\lambda_2 > 0$, the equation $s^2 + \lambda_1 s + \lambda_2 = 0$ has 2 real negative roots, i.e.

$$p_1 = \frac{-\lambda_1 + \sqrt{\lambda_1^2 - 4\lambda_2}}{2},\ p_1 = \frac{-\lambda_1 - \sqrt{\lambda_1^2 - 4\lambda_2}}{2}$$

It is easy to check that $0 > p_1 > p_2$. We can calculate that

$$e^{At} = \mathcal{L}^{-1}[(sI - A)^{-1}] = \begin{bmatrix} a_{11}(t) & a_{12}(t) \\ a_{21}(t) & a_{22}(t) \end{bmatrix}$$

where

$$a_{11}(t) = \frac{1}{2}(e^{p_1 t} + e^{p_2 t}) - \frac{\lambda_1}{p_1 - p_2}(e^{p_1 t} - 2e^{p_2 t})$$

and

$$a_{12}(t) = -\frac{\lambda_2}{p_1 - p_2}(e^{p_1 t} - e^{p_2 t}).$$

Therefore

$$\begin{aligned} x(t) &= x_1(t_0)a_{11}(t - t_0) + x_2(t_0)a_{12}(t - t_0) \\ &= \frac{1}{2}x_1(t_0)(e^{p_1(t-t_0)} + e^{p_2(t-t_0)}) - \frac{\lambda_1 x_1(t_0) + \lambda_2 x_2(t_0)}{p_1 - p_2}(e^{p_1(t-t_0)} - e^{p_2(t-t_0)}) \end{aligned}$$

Since $p_1 > p_2, x_1(t_0) \leq 0$ and $\lambda_1 x_1(t_0) + \lambda_2 x_2(t_0) > 0$, we have that $x(t) < 0,\ \forall t \geq t_0$. Consequently, (63) holds for all $t > t_0$. According to Lemma 8.1, $x_1(t)$ converges to 0 asymptotically. □

Theorem 8.1 shows that if $d + \mu \geq v_f \rho^\star$, then controller (56) forces x_1 to converge to 0 asymptotically. In the case that $d + \mu < v_f \rho^\star$, the dynamics and the stability properties of the closed-loop system is shown in the following theorem.

Theorem 8.2. *Consider the system (52)(53) with controller (56), if $d + \mu < v_f \rho^\star$, then $\forall x_1(0) \in [-\rho^\star, \rho^j - \rho^\star]$, $x_1(t)$ converges to $\frac{d+\mu}{v_f} - \rho^\star$ asymptotically.*

Proof. Since $d + \mu < v_f \rho^\star$, then $\exists \eta > 0$, such that $d + \mu \leq v_f \rho^\star - \eta$. Similar to the case in Theorem 8.1, we only need to consider the case where $x_1(t_0) \leq \rho^L - \rho^\star$ and $k(t_0) = k_2(t_0)$. According to (52)(53), we have that

$$\dot{x}_1 \leq d - q_2 + \mu = d + \mu - (v_f \rho^\star + v_f x_1)$$

thus for all $x_1(t_0) \leq \rho^L - \rho^\star$, $x_1(t) \leq \frac{d+\mu}{v_f} - \rho^\star, \forall t \geq t_0$. Therefore

$$x_2(t) = x_2(t_0) + \int_{t_0}^{t} x_1(t)d\tau - \frac{\mu}{\lambda_2} \leq x_2(t_0) - \frac{\mu}{\lambda_2} - \eta(t - t_0), t \geq t_0$$

which decreases to negative infinity as t increases. Therefore q_1 saturates at d.

$$\dot{x}_1 = d + \mu - (v_f\rho^\star + v_f x_1)$$

Thus x_1 converges to $\frac{d+\mu}{v_f} - \rho^\star$. □

Therefore, with the controller (56), if the sum of the upstream demand d and the disturbance is greater than or equal to the predetermined equilibrium flow, the density in the section will converge to the equilibrium point $\rho^\star$. If the sum of the upstream demand d and the disturbance is less than the predetermined equilibrium flow, the density converges to $\frac{d+\mu}{v_f}$, at which the steady state flow is $d + \mu$, which is the maximum possible value. Note that the selection of ρ^L affects the distance from the switching point to the desired equilibrium point. According to the proof of Theorem 8.1, we can select $\rho^L = \rho^\star$ which minimizes the distance while still guarantees the convergence. In addition, since $\rho(t)$ always converges to $\rho^\star$ from the left side, $\rho^\star$ can be arbitrarily close to $\frac{C_d}{v_f}$.

8.2. Numerical Experiments

In this section, we use numerical simulations to demonstrate the analytical results of the previous sections. The simulations are performed on a single-section road network, whose parameters are: $C = 6500$ veh/h, $w = 20$ mi/h, $\rho^j = 425$ veh/mi, $v_f = 65$ mi/h, $\tilde{w} = 10$ mi/h, $\tilde{\rho}^j = 750$ veh/mi, $\rho_c = 100$ veh/mi, $d = 6000$ veh/h, $\mu = 300$ veh/h. We apply controller (56) to the perturbed single-section system with the following design constants: $\lambda_1 = 200, \lambda_2 = 900, \rho^\star = \rho^L = 75$ veh/mi, $\rho^U = 79$ veh/mi, $\mu_m = 350$ veh/h, $q_s = 3200$ veh/h. The initial condition $\rho(0) = 120$ veh/mi.

Figure 51 shows the behavior of the density, flow rate and the VSL commands respectively. We can see that the density converges asymptotically to the predetermined value $\rho^\star = 75$ veh/mi. There is a difference of 100 veh/h between the steady state values of q_1 and q_2, since in steady state $q_1 - q_2 + \mu = 0$. The outflow q_2 starts at the value of 3500 veh/h, which is the dropped capacity of the bottleneck. Then suddenly jump to 4250 veh/h since the density decreases and becomes lower than the critical density $C_d/v_f = 80$ veh/h, thus the capacity drop is removed. Then q_2 decreases as ρ keeps decreasing until $\rho = \rho^L$. Then the PI controller takes over, and q_2 increases and converges to the steady state value eventually.

Figure 51: System Behavior of the Perturbed Closed-loop System

(a) Density (b) Flow Rate (c) VSL

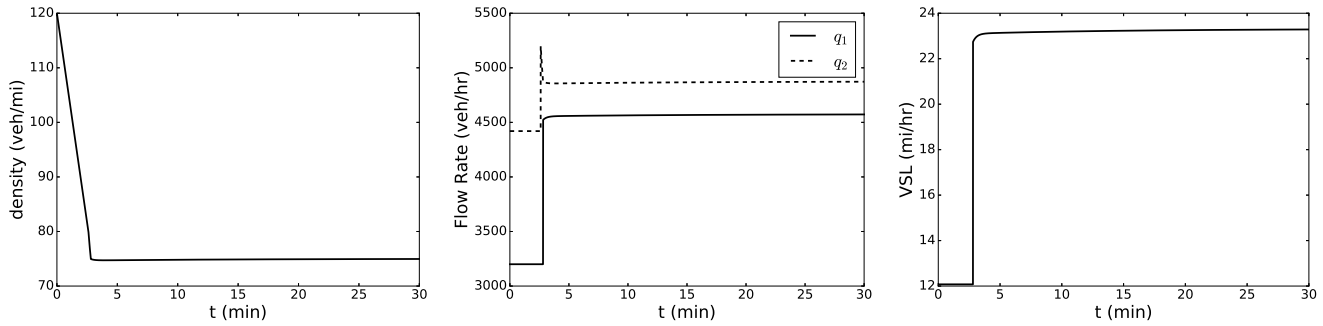

9 Conclusion

In this report, based on the first order cell transmission model, we conducted design, analyze and evaluate the performance of several integrated highway traffic flow control strategies in both macroscopic and microscopic simulations. We discovered that forced lane change at vicinity of the bottleneck is a major reason of the capacity drop phenomenon. We proposed a lane change controller which provides lane change recommendations to upstream vehicles in order to avoid the capacity drop. A feedback linearization variable speed limit controllers is designed to improve the mobility, safety and environmental impact at highway bottleneck together with the lane change controller. The combined LC and feedback linearization VSL controller can theoretically guarantee the global exponential convergence to the desired equilibrium point at which maximum possible flow rate is achieved. Furthermore, the combined LC and VSL controller is extended to coordinate with ramp metering controllers. The coordinated VSL, RM and LC controller is able to improve system performance, maintain the queue length on ramps and keep the fairness between mainline and on-ramp flows. Microscopic simulations show consistent improvement under different traffic demand and scenarios. The proposed controller is compared to the widely used MPC control strategy. Both macroscopic and microscopic simulations show that the performance and robustness with respect to model parameter errors and measurement noise of our controller is better than that of the MPC controller. The open-loop stability properties of the modified cell transmission traffic flow model (CTM) which takes the capacity drop phenomenon into consideration under all possible traffic flow scenarios are investigated, which motivates the design of a VSL controller which is able to avoid the capacity drop, stabilize the system and maximize the flow rate at the bottleneck. The VSL controller is extended with integral action in order to reject system disturbance.

References

[1] D. Schrank, B. Eisele, T. Lomax, and J. Bak, "2015 urban mobility scorecard," *Texas A&M Transportation Institute. The Texas A&M University System*, 2015.

[2] P. Marchesini and W. A. M. Weijermars, *The relationship between road safety and congestion on motorways*. SWOV Institute for Road Safety Research, 2010.

[3] A. Abadi, P. A. Ioannou, and M. M. Dessouky, "Multimodal dynamic freight load balancing," *IEEE Transactions on Intelligent Transportation Systems*, vol. 17, no. 2, pp. 356–366, 2016.

[4] V. A. Butakov and P. Ioannou, "Personalized driver/vehicle lane change models for adas," *IEEE Transactions on Vehicular Technology*, vol. 64, no. 10, pp. 4422–4431, 2015.

[5] Y. Zhang and P. A. Ioannou, "Combined variable speed limit and lane change control for highway traffic," *IEEE Transactions on Intelligent Transportation Systems*, vol. 18, no. 7, pp. 1812–1823, 2017.

[6] M. Papageorgiou, H. Hadj-Salem, and J.-M. Blosseville, "Alinea: A local feedback control law for on-ramp metering," *Transportation Research Record*, no. 1320, 1991.

[7] X.-Y. Lu, P. Varaiya, R. Horowitz, D. Su, and S. Shladover, "Novel freeway traffic control with variable speed limit and coordinated ramp metering," *Transportation Research Record: Journal of the Transportation Research Board*, no. 2229, pp. 55–65, 2011.

[8] E. Van den Hoogen and S. Smulders, "Control by variable speed signs: results of the dutch experiment," in *Road Traffic Monitoring and Control, 1994., Seventh International Conference on*. IET, 1994, pp. 145–149.

[9] Y. Wang and P. Ioannou, "Dynamic variable speed limit control: Design, analysis and benefits," Ph.D. dissertation, University of Southern California, 2011.

[10] X.-Y. Lu and S. E. Shladover, "Review of variable speed limits and advisories," *Transportation Research Record: Journal of the Transportation Research Board*, vol. 2423, no. 1, pp. 15–23, 2014.

[11] M. Hadiuzzaman, T. Z. Qiu, and X.-Y. Lu, "Variable speed limit control design for relieving congestion caused by active bottlenecks," *Journal of Transportation Engineering*, 2012.

[12] S. Baldi, I. Michailidis, E. Kosmatopoulos, A. Papachristodoulou, and P. Ioannou, "Convex design control for practical nonlinear systems," *IEEE Transactions on Automatic Control*, vol. 59, no. 7, pp. 1692–1705, July 2014.

[13] J. M. Torne Santos, D. Rosas, and F. Soriguera, "Evaluation of speed limit management on c-32 highway access to barcelona," in *Transportation Research Board 90th Annual Meeting*, no. 11-2397, 2011.

[14] K. Gao, "Multi-objective traffic management for livability," Ph.D. dissertation, MS thesis, TU Delft, Delft, The Netherlands, 2012.

[15] L. Kejun, Y. Meiping, Z. Jianlong, and Y. Xiaoguang, "Model predictive control for variable speed limit in freeway work zone," in *Control Conference, 2008. CCC 2008. 27th Chinese*. IEEE, 2008, pp. 488–493.

[16] P. Ioannou, Y. Wang, A. Abadi, and V. Butakov, "Dynamic variable speed limit control: Design, analysis and benefits," Tech. Rep., 2012.

[17] Y. Wang and P. Ioannou, "New model for variable speed limits," *Transportation Research Record: Journal of the Transportation Research Board*, no. 2249, pp. 38–43, 2011.

[18] S. Smulders, "Control of freeway traffic flow by variable speed signs," *Transportation Research Part B: Methodological*, vol. 24, no. 2, pp. 111–132, 1990.

[19] M. Papageorgiou, E. Kosmatopoulos, and I. Papamichail, "Effects of variable speed limits on motorway traffic flow," *Transportation Research Record: Journal of the Transportation Research Board*, no. 2047, pp. 37–48, 2008.

[20] A. Muralidharan and R. Horowitz, "Computationally efficient model predictive control of freeway networks," *Transportation Research Part C: Emerging Technologies*, vol. 58, pp. 532–553, 2015.

[21] J. R. D. Frejo, A. Núñez, B. De Schutter, and E. F. Camacho, "Hybrid model predictive control for freeway traffic using discrete speed limit signals," *Transportation Research Part C: Emerging Technologies*, vol. 46, pp. 309–325, 2014.

[22] B. Khondaker and L. Kattan, "Variable speed limit: A microscopic analysis in a connected vehicle environment," *Transportation Research Part C: Emerging Technologies*, vol. 58, pp. 146–159, 2015.

[23] R. C. Carlson, I. Papamichail, and M. Papageorgiou, "Comparison of local feedback controllers for the mainstream traffic flow on freeways using variable speed limits," *Journal of Intelligent Transportation Systems*, vol. 17, no. 4, pp. 268–281, 2013.

[24] G.-R. Iordanidou, C. Roncoli, I. Papamichail, and M. Papageorgiou, "Feedback-based mainstream traffic flow control for multiple bottlenecks on motorways," *Intelligent Transportation Systems, IEEE Transactions on*, vol. 16, no. 2, pp. 610–621, 2015.

[25] E. R. Müller, R. C. Carlson, W. Kraus, and M. Papageorgiou, "Microsimulation analysis of practical aspects of traffic control with variable speed limits," *IEEE Transactions on Intelligent Transportation Systems*, vol. 16, no. 1, pp. 512–523, 2015.

[26] H.-Y. Jin and W.-L. Jin, "Control of a lane-drop bottleneck through variable speed limits," *Transportation Research Part C: Emerging Technologies*, vol. 58, pp. 568–584, 2015.

[27] A. Hegyi, S. Hoogendoorn, M. Schreuder, H. Stoelhorst, and F. Viti, "Specialist: A dynamic speed limit control algorithm based on shock wave theory," in *Intelligent Transportation Systems, 2008. ITSC 2008. 11th International IEEE Conference on*. IEEE, 2008, pp. 827–832.

[28] J. Zhang, H. Chang, and P. A. Ioannou, "A simple roadway control system for freeway traffic," in *2006 American Control Conference*. IEEE, 2006, pp. 6–pp.

[29] H. Chang, Y. Wang, J. Zhang, and P. A. Ioannou, "An integrated roadway controller and its evaluation by microscopic simulator vissim," in *Control Conference (ECC), 2007 European*. IEEE, 2007, pp. 2436–2441.

[30] M. Abdel-Aty, J. Dilmore, and A. Dhindsa, "Evaluation of variable speed limits for real-time freeway safety improvement," *Accident analysis & prevention*, vol. 38, no. 2, pp. 335–345, 2006.

[31] Z. Li, P. Liu, W. Wang, and C. Xu, "Development of a control strategy of variable speed limits to reduce rear-end collision risks near freeway recurrent bottlenecks," *Intelligent Transportation Systems, IEEE Transactions on*, vol. 15, no. 2, pp. 866–877, 2014.

[32] Y. Zhang and P. A. Ioannou, "Environmental impact of combined variable speed limit and lane change control: A comparison of MOVES and CMEM model," *IFAC-PapersOnLine*, vol. 49, no. 3, pp. 323 – 328, 2016, 14th IFAC Symposium on Control in Transportation Systems CTS 2016, Istanbul, Turkey, 18-20 May 2016.

[33] ——, "Combined variable speed limit and lane change control for truck-dominant highway segment," in *2015 IEEE 18th International Conference on Intelligent Transportation Systems (ITSC)*. IEEE, 2015, pp. 1163–1168.

[34] S. K. Zegeye, B. De Schutter, H. Hellendoorn, and E. Breunesse, "Reduction of travel times and traffic emissions using model predictive control," in *American Control Conference, 2009. ACC'09.* IEEE, 2009, pp. 5392–5397.

[35] G. Horton, G. Hitchcock, C. Chiffi, A. Martino, C. Doll, V. Zeidler, H. Bruhova-Foltynova, Z. Sperat, R. Jordova, A. Roumboutsos, and I. Skinner, "Research Theme Analysis Report - Urban Mobility," European Union, Tech. Rep., 2016.

[36] Caltrans, "Ramp metering design manual," California Department of Transportation, Sacramento, United States, Tech. Rep., apr 2016.

[37] H.-U. Oh and V. P. Sisiopiku, "A modified alinea ramp metering model," in *Transportation Research Board 80th Annual Meeting*, 2001.

[38] E. Smaragdis and M. Papageorgiou, "Series of new local ramp metering strategies: Emmanouil smaragdis and markos papageorgiou," *Transportation Research Record: Journal of the Transportation Research Board*, no. 1856, pp. 74–86, 2003.

[39] M. Papageorgiou and A. Kotsialos, "Freeway ramp metering: an overview," *IEEE Transactions on Intelligent Transportation Systems*, vol. 3, no. 4, pp. 271–281, Dec 2002.

[40] Caltrans District 7, "Ramp Metering Annual Report," Los Angeles and Ventura Counties, Tech. Rep., 2006.

[41] X.-Y. Lu, T. Z. Qiu, P. Varaiya, R. Horowitz, and S. E. Shladover, "Combining variable speed limits with ramp metering for freeway traffic control," in *Proceedings of the 2010 American Control Conference*. IEEE, 2010, pp. 2266–2271.

[42] J. R. Scariza, "Evaluation of coordinated and local ramp metering algorithms using microscopic traffic simulation," Ph.D. dissertation, Massachusetts Institute of Technology, 2003.

[43] A. K. Rathi and Z. A. Nemeth, *FREESIM: A MICROSCOPIC SIMULATION MODEL OF FREEWAY LANE CLOSURES (ABRIDGMENT)*, 1986, no. 1091.

[44] H. S. Mahmassani and R. Jayakrishnan, "Dynamic analysis of lane closure strategies," *Journal of transportation engineering*, vol. 114, no. 4, pp. 476–496, 1988.

[45] L. Schaefer, J. Upchurch, and S. Ashur, "An evaluation of freeway lane control signing using computer simulation," *Mathematical and computer modelling*, vol. 27, no. 9, pp. 177–187, 1998.

[46] M. Jha, D. Cuneo, and M. Ben-Akiva, "Evaluation of freeway lane control for incident management," *Journal of transportation engineering*, vol. 125, no. 6, pp. 495–501, 1999.

[47] W.-L. Jin, "A multi-commodity lighthill–whitham–richards model of lane-changing traffic flow," *Transportation Research Part B: Methodological*, vol. 57, pp. 361–377, 2013.

[48] J. A. Laval and C. F. Daganzo, "Lane-changing in traffic streams," *Transportation Research Part B: Methodological*, vol. 40, no. 3, pp. 251–264, 2006.

[49] L. D. Baskar, B. De Schutter, and H. Hellendoorn, "Model-based predictive traffic control for intelligent vehicles: Dynamic speed limits and dynamic lane allocation," in *Intelligent Vehicles Symposium, 2008 IEEE*. IEEE, 2008, pp. 174–179.

[50] C. Roncoli, I. Papamichail, and M. Papageorgiou, "Model predictive control for multi-lane motorways in presence of VACS," in *2014 IEEE 17th International Conference on Intelligent Transportation Systems (ITSC)*, Oct 2014, pp. 501–507.

[51] A. Alessandri, A. Di Febbraro, A. Ferrara, and E. Punta, "Optimal control of freeways via speed signalling and ramp metering," *Control Engineering Practice*, vol. 6, no. 6, pp. 771–780, 1998.

[52] C. Caligaris, S. Sacone, and S. Siri, "Optimal ramp metering and variable speed signs for multiclass freeway traffic," in *2007 European Control Conference*. IEEE, 2007, pp. 1780–1785.

[53] A. Hegyi, B. De Schutter, and H. Hellendoorn, "Model predictive control for optimal coordination of ramp metering and variable speed limits," *Transportation Research Part C: Emerging Technologies*, vol. 13, no. 3, pp. 185–209, 2005.

[54] I. Papamichail, K. Kampitaki, M. Papageorgiou, and A. Messmer, "Integrated ramp metering and variable speed limit control of motorway traffic flow," *IFAC Proceedings Volumes*, vol. 41, no. 2, pp. 14 084–14 089, 2008.

[55] M. Hadiuzzaman and T. Z. Qiu, "Cell transmission model based variable speed limit control for freeways," *Canadian Journal of Civil Engineering*, vol. 40, no. 1, pp. 46–56, 2013.

[56] A. Csikós and B. Kulcsár, "Variable speed limit design based on mode dependent cell transmission model," *Transportation Research Part C: Emerging Technologies*, vol. 85, pp. 429–450, 2017.

[57] G. Gomes, R. Horowitz, A. A. Kurzhanskiy, P. Varaiya, and J. Kwon, "Behavior of the cell transmission model and effectiveness of ramp metering," *Transportation Research Part C: Emerging Technologies*, vol. 16, no. 4, pp. 485–513, 2008.

[58] E. Lovisari, G. Como, A. Rantzer, and K. Savla, "Stability analysis and control synthesis for dynamical transportation networks," *arXiv preprint arXiv:1410.5956*, 2014.

[59] A. Srivastava, W.-L. Jin, and J.-P. Lebacque, "A modified cell transmission model with realistic queue discharge features at signalized intersections," *Transportation Research Part B: Methodological*, vol. 81, pp. 302–315, 2015.

[60] M. Kontorinaki, A. Spiliopoulou, C. Roncoli, and M. Papageorgiou, "Capacity drop in first-order traffic flow models: Overview and real-data validation," in *Transportation Research Board 95th Annual Meeting*, no. 16-3541, 2016.

[61] S. Coogan and M. Arcak, "Stability of traffic flow networks with a polytree topology," *Automatica*, vol. 66, pp. 246–253, 2016.

[62] I. Karafyllis and M. Papageorgiou, "Global exponential stability for discrete-time networks with applications to traffic networks," *IEEE Transactions on Control of Network Systems*, vol. 2, no. 1, pp. 68–77, 2015.

[63] M. Kontorinaki, I. Karafyllis, and M. Papageorgiou, "Global exponential stabilisation of acyclic traffic networks," *International Journal of Control*, pp. 1–21, 2017.

[64] J. H. Banks, "The two-capacity phenomenon: some theoretical issues," *Transportation Research Record*, no. 1320, 1991.

[65] F. L. Hall and K. Agyemang-Duah, "Freeway capacity drop and the definition of capacity," *Transportation Research Record*, no. 1320, 1991.

[66] *VISSIM 5.30-04 User Manual*, PTV-Vision, Karlsruhe, Germany, feb 2011.

[67] H. K. Khalil and J. Grizzle, *Nonlinear systems*. Prentice hall New Jersey, 1996, vol. 3.

[68] X.-Y. Lu, P. Varaiya, R. Horowitz, D. Su, and S. E. Shladover, "A new approach for combined freeway variable speed limits and coordinated ramp metering," in *2010 13th International IEEE Conference on Intelligent Transportation Systems (ITSC)*. IEEE, 2010, pp. 491–498.

[69] R. C. Carlson, I. Papamichail, and M. Papageorgiou, "Local feedback-based mainstream traffic flow control on motorways using variable speed limits," *IEEE Transactions on Intelligent Transportation Systems*, vol. 12, no. 4, pp. 1261–1276, 2011.

[70] C. D. of Transportation. (2015) Caltrans performance measurement system (PeMS). [Online]. Available: http://pems.dot.ca.gov/

[71] M. Wright, G. Gomes, R. Horowitz, and A. A. Kurzhanskiy, "A new model for multi-commodity macroscopic modeling of complex traffic networks," *arXiv preprint arXiv:1509.04995*, 2015.

[72] EPA, "Motor vehicle emission simulator (moves) user guide," *US Environmental Protection Agency*, 2014.

[73] H. G. Bock and K.-J. Plitt, "A multiple shooting algorithm for direct solution of optimal control problems," in *Proceedings of the IFAC World Congress*, 1984.

[74] M. Diehl, H. G. Bock, H. Diedam, and P.-B. Wieber, "Fast direct multiple shooting algorithms for optimal robot control," in *Fast motions in biomechanics and robotics*. Springer, 2006, pp. 65–93.

[75] J. Andersson, "A General-Purpose Software Framework for Dynamic Optimization," PhD thesis, Arenberg Doctoral School, KU Leuven, Department of Electrical Engineering (ESAT/SCD) and Optimization in Engineering Center, Kasteelpark Arenberg 10, 3001-Heverlee, Belgium, October 2013.

[76] A. Wächter and L. T. Biegler, "On the implementation of an interior-point filter line-search algorithm for large-scale nonlinear programming," *Mathematical Programming*, vol. 106, no. 1, pp. 25–57, 2006.

[77] J. Lebacque, "Two-phase bounded-acceleration traffic flow model: analytical solutions and applications," *Transportation Research Record: Journal of the Transportation Research Board*, no. 1852, pp. 220–230, 2003.

[78] C. Roncoli, M. Papageorgiou, and I. Papamichail, "Traffic flow optimisation in presence of vehicle automation and communication systems–Part I: A first-order multi-lane model for motorway traffic," *Transportation Research Part C: Emerging Technologies*, vol. 57, pp. 241–259, 2015.

[79] A. Srivastava and W. Jin, "A lane changing cell transmission model for modeling capacity drop at lane drop bottlenecks," in *Transportation Research Board 95th Annual Meeting*. TRB, 2016, pp. 16–5452.

[80] C. F. Daganzo, "The cell transmission model: A dynamic representation of highway traffic consistent with the hydrodynamic theory," *Transportation Research Part B: Methodological*, vol. 28, no. 4, pp. 269–287, 1994.

[81] P. A. Ioannou and J. Sun, *Robust adaptive control*. Dover Publications, Mineola, New York, 2012.

Data Management Plan

The data management plan of this research includes the disclosure of raw simulation data of the combined variable speed limit and lane change control (Section 3) and the Coordinated Variable Speed Limit, Ramp Metering and Lane Change Controller (Section 4). The simulations are performend with PTV-VISSIM 5.30.
For the simulations in Section 3, data is generated under the following traffic demand levels, scenarios, control modes and data types:

- Demand levels:
    1. 6000 veh/hr
    2. 6500 veh/hr
- Scenarios:
    1. scenario 1: incident lasts for 30 minutes
    2. scenario 2: incident lasts for 10 minutes
    3. scenario 3: incident lasts for 60 minutes (cropped to the first 45 minutes of incidents for evaluation to demonstrate the case of long-term bottleneck).
- Control Modes:
    1. no control
    2. combined VSL and LC control.
- Data Types:
    1. vehicle densities
    2. flow rates
    3. VSL control commands

All data is generated from 10 rounds of Monte Carlo simulations, which are indexed from 0 to 9. For the simulations in Section 4, data is generated under one scenario and demand level which is described in Section 4.4, and different control modes and data types as listed below.

- Control Modes:
    1. RM control only
    2. Coordinated VSL, LC and RM control
- Data Types:
    1. vehicle densities
    2. flow rates
    3. VSL control commands
    4. RM control commands
    5. Ramp queue length

All data is generated from 10 rounds of Monte Carlo simulations, which are indexed from 0 to 9. The units of data in each data type is listed in Table 9.

Table 9: Data Units

Data Type	Units
Vehicle density	number of vehicles per mile
Flow rate	number of vehicles per 5 seconds
VSL control commands	miles per hour
RM control commands	number of vehicles per hr
Ramp queue length	number of vehicles

A Parts of Proof of Theorem 6.1

A.1. Case a), i.e. $I \in \Omega_1$

Consider the Lyapunov function

$$V(\rho) = \frac{(\rho - d/v_f)^2}{2},$$

then we have

$$\dot{V}(\rho) = (\rho - \frac{d}{v_f})\dot{\rho} = -(\rho - \frac{d}{v_f})(q_2 - q_1).$$

Using equation (33) and Fig. 31, we have that when $0 \leq \rho \leq \frac{C_d}{v_f}$, $q_1 = d$ and $q_2 = v_f\rho$. Thus

$$q_2 - q_1 = v_f(\rho - \frac{d}{v_f}) \tag{67}$$

therefore $\dot{V} = -v_f(\rho - \frac{d}{v_f})^2, \forall \rho \in [0, \frac{C_d}{v_f}]$. When $\frac{C_d}{v_f} < \rho \leq \tilde{\rho}^j - \frac{(1-\epsilon_0)C_d}{\tilde{w}}$, $\rho - \frac{d}{v_f} > 0$, $q_1 = d$ and $q_2 = (1-\epsilon_0)C_d$. Thus

$$q_2 - q_1 = (1-\epsilon_0)C_d - d \geq \frac{(1-\epsilon_0)C_d - d}{\rho^j - d/v_f}(\rho - d/v_f) \tag{68}$$

due to $(1-\epsilon_0)C_d - d > 0$ and $d/v_f < \rho \leq \rho^j, \forall \rho \in (\frac{C_d}{v_f}, \rho^j]$, which implies $0 < \frac{\rho - d/v_f}{\rho^j - d/v_f} \leq 1$. Therefore $\dot{V} \leq -\frac{(1-\epsilon_0)C_d - d}{\rho^j - d/v_f}(\rho - \frac{d}{v_f})^2, \forall \rho \in (\frac{C_d}{v_f}, \leq \tilde{\rho}^j - \frac{(1-\epsilon_0)C_d}{\tilde{w}}]$. When $\tilde{\rho}^j - \frac{(1-\epsilon_0)C_d}{\tilde{w}} < \rho \leq \rho^j - \frac{d}{w}$, $\rho - \frac{d}{v_f} > 0$, $q_1 = d$ and $q_2 = \tilde{w}(\tilde{\rho}^j - \rho)$. Thus

$$\begin{aligned} q_2 - q_1 &= \tilde{w}(\tilde{\rho}^j - \rho) - d \geq \tilde{w}[\tilde{\rho}^j - (\rho^j - \frac{d}{w})] - d = \tilde{w}[\tilde{\rho}^j - (\rho^j - \frac{d}{w})] - w[\rho^j - (\rho^j - \frac{d}{w})] \\ &= \tilde{w}(\tilde{\rho}^j - \rho_c) - w(\rho^j - \rho_c) + (\tilde{w} - w)[\rho_c - (\rho^j - \frac{d}{w})] \\ &= C - C + (\tilde{w} - w)[\rho_c - (\rho^j - \frac{d}{w})] \\ &\geq \frac{(\tilde{w} - w)[\rho_c - (\rho^j - \frac{d}{w})]}{\rho^j - d/v_f}(\rho - d/v_f), \end{aligned} \tag{69}$$

due to $0 < \frac{\rho - d/v_f}{\rho^j - d/v_f} \leq 1$, $\tilde{w} - w < 0$ and $\rho_c - (\rho^j - \frac{d}{w}) < 0$. Therefore, $\dot{V} \leq -\frac{(\tilde{w}-w)[\rho_c - (\rho^j - \frac{d}{w})]}{\rho^j - d/v_f}(\rho - d/v_f)^2, \forall \rho \in (\tilde{\rho}^j - \frac{(1-\epsilon_0)C_d}{\tilde{w}}, \rho^j - \frac{d}{w}]$. When $\rho^j - \frac{d}{w} < \rho \leq \rho^j$, $\rho - \frac{d}{v_f} > 0$, $q_1 = w(\rho^j - \rho)$ and $q_2 = \tilde{w}(\tilde{\rho}^j - \rho)$. Thus

$$\begin{aligned} q_2 - q_1 &= \tilde{w}(\tilde{\rho}^j - \rho) - w(\rho^j - \rho) \\ &= \tilde{w}(\tilde{\rho}^j - \rho_c) - w(\rho^j - \rho_c) + (\tilde{w} - w)(\rho_c - \rho) \\ &\geq (\tilde{w} - w)[\rho_c - (\rho^j - \frac{d}{w})] \\ &\geq \frac{(\tilde{w} - w)[\rho_c - (\rho^j - \frac{d}{w})]}{\rho^j - d/v_f}(\rho - d/v_f), \end{aligned} \tag{70}$$

since $0 < \frac{\rho - d/v_f}{\rho^j - d/v_f} \leq 1$, $\tilde{w} - w < 0$ and $\rho_c - (\rho^j - \frac{d}{w}) < 0$. Therefore $\dot{V} \leq -\frac{(\tilde{w}-w)[\rho_c - (\rho^j - \frac{d}{w})]}{\rho^j - d/v_f}(\rho - d/v_f)^2, \forall \rho \in (\rho^j - \frac{d}{w}, \rho^j]$. From (67) to (70), we can conclude that

$$\dot{V} \leq -\alpha(\rho - \frac{d}{v_f})^2, \ \forall \rho(0) \in [0, \rho^j] \tag{71}$$

where $\alpha = \min\{v_f, \frac{(1-\epsilon_0)C_d - d}{\rho^j - d/v_f}, \frac{(\tilde{w}-w)[\rho_c - (\rho^j - \frac{d}{w})]}{\rho^j - d/v_f}\} > 0$, $\forall \rho(0) \in [0, \rho^j]$, which implies exponential stability of the equilibrium point $\rho^e = \frac{d}{v_f}$ and exponential convergence of $\rho(t)$ to $\frac{d}{v_f}$, $\forall \rho(0) \in [0, \rho^j]$. The rate of convergence of ρ to the equilibrium $\frac{d}{v_f}$ is greater or equal to α and can be shown by substituting for $(\rho - \frac{d}{v_f})^2 = 2V$ in (71) and integrating both sides of the inequality.

A.2. Case b), i.e. $I \in \Omega_2$

From Fig. 32, the situation where $\rho(0) \in (\rho^j - \frac{d}{w}, \rho^j]$ is divided into two cases:

- Case I: $\rho(0) \in (\rho^j - \frac{d}{w}, \tilde{\rho}^j - \frac{d}{\tilde{w}}]$.
- Case II: $\rho(0) \in (\tilde{\rho}^j - \frac{d}{\tilde{w}}, \rho^j]$.

In case I, $q_1 = w(\rho^j - \rho)$ and $q_2 = d$ as long as $\rho \in (\rho^j - \frac{d}{w}, \tilde{\rho}^j - \frac{d}{\tilde{w}}]$, $\forall t \geq 0$, which we need to show. We have

$$\dot{\rho} = q_1 - q_2 = -w\rho + w\rho^j - d,$$

whose solution is

$$\rho(t) = (\rho^j - \frac{d}{w}) + [\rho(0) - (\rho^j - \frac{d}{w})]e^{-wt}.$$

Since $0 < \rho^j - \frac{d}{w} < \rho(0) \leq \tilde{\rho}^j - \frac{d}{\tilde{w}}$ and $w > 0$, it follows that $\rho \in (\rho^j - \frac{d}{w}, \tilde{\rho}^j - \frac{d}{\tilde{w}}]$, $\forall t \geq 0$ and $\rho(t)$ converges exponentially fast to $\rho^j - \frac{d}{w}$ according to the above equation.
In case II, when $\rho(0) \in (\tilde{\rho}^j - \frac{d}{\tilde{w}}, \rho^j]$, it follows from Fig. 32 that $q_1 = w(\rho^j - \rho)$, $q_2 = \tilde{w}(\tilde{\rho}^j - \rho)$ and

$$\dot{\rho} = -(w - \tilde{w})\rho + (w - \tilde{w})\rho_c,$$

as long as $\rho(t) \in (\tilde{\rho}^j - \frac{d}{\tilde{w}}, \rho^j]$, whose solution is

$$\rho(t) = \rho_c + (\rho(0) - \rho_c)e^{-w_0 t} \leq (\rho^j - \frac{d}{w}) + (\rho(0) - \rho_c)e^{-w_0 t},$$

where $w_0 = w - \tilde{w} > 0$ according to model (33). Since $\rho_c < \tilde{\rho}^j - \frac{d}{\tilde{w}}$, it follows that $\rho(t)$ will decrease exponentially to the value of $\tilde{\rho}^j - \frac{d}{\tilde{w}}$ at which instant $\dot{\rho}$ switches to case I which guarantees exponential convergence to $\rho^j - \frac{d}{w}$. The above equation implies that

$$|\rho(t) - (\rho^j - \frac{d}{w})| \leq c_0 e^{-\alpha t},$$

where $c_0 = \rho(0) - (\rho^j - \frac{d}{w})$ and $\alpha = \min\{w, w - \tilde{w}\}$.

A.3. Case c), i.e. $I \in \Omega_3$

Consider the Lyapunov function

$$V(\rho) = \frac{(\rho - \rho_2^e)^2}{2},$$

where $\rho_2^e = \rho^j - \frac{(1-\epsilon_0)C_d}{w}$. Then $\dot{V} = -(\rho - \rho_2^e)(q_2 - q_1)$. As shown before, when $\frac{C_d}{v_f} < \rho \leq \rho^j - \frac{d}{w}$, we have $\rho - \rho_2^e < 0$ and

$$q_2 - q_1 = (1-\epsilon_0)C_d - d \leq \frac{(1-\epsilon_0)C_d - d}{C_d/v_f - \rho_2^e}(\rho - \rho_2^e), \tag{72}$$

due to $0 < \frac{(\rho - \rho_2^e)}{C_d/v_f - \rho_2^e} < 1, \forall \rho \in (\frac{C_d}{v_f}, \rho^j - \frac{d}{w}]$ and $(1-\epsilon_0)C_d - d < 0$. Therefore $\dot{V} \leq -\frac{(1-\epsilon_0)C_d - d}{C_d/v_f - \rho_2^e}(\rho - \rho_2^e)^2$. When $\rho^j - \frac{d}{w} < \rho \leq \tilde{\rho}^j - \frac{(1-\epsilon_0)C_d}{\tilde{w}}$,

$$q_2 - q_1 = (1-\epsilon_0)C_d - w(\rho^j - \rho) = w[\rho - (\rho^j - \frac{(1-\epsilon_0)C_d}{w})] = w(\rho - \rho_2^e) \quad . \tag{73}$$

Therefore $\dot{V} = -w(\rho - \rho_2^e)^2$. When $\tilde{\rho}^j - \frac{(1-\epsilon_0)C_d}{\tilde{w}} < \rho \leq \rho^j$, we have $\rho - \rho_2^e > 0$ and

$$q_2 - q_1 = \tilde{w}(\tilde{\rho}^j - \rho) - w(\rho^j - \rho) = (w - \tilde{w})(\rho - \rho_c) \geq (w - \tilde{w})(\rho - \rho_2^e), \tag{74}$$

due to $w - \tilde{w} > 0$ and $\rho_2^e > \rho_c$. Therefore, $\dot{V} \leq -(w - \tilde{w})(\rho - \rho_2^e)^2$. From (72) to (74), we conclude that $\forall \rho \in (\frac{C_d}{v_f}, \rho^j]$,

$$\dot{V} \leq -\alpha(\rho - \rho_2^e)^2,$$

where $\alpha = \min\{\frac{d - (1-\epsilon_0)C_d}{\rho_2^e - C_d/v_f}, w, (w - \tilde{w})\} > 0$, $\forall \rho(0) \in (\frac{C_d}{v_f}, \rho^j]$ which implies exponential stability of the equilibrium point $\rho_2^e = \rho^j - \frac{(1-\epsilon_0)C_d}{w}$ and exponential convergence of $\rho(t)$ to ρ_2^e, $\forall \rho(0) \in (\frac{C_d}{v_f}, \rho^j]$.

A.4. Case d), i.e. $I \in \Omega_4$

Consider the Lyapunov function

$$V(\rho) = \frac{(\rho - \rho^e)^2}{2},$$

where $\rho^e = \rho^j - \frac{(1-\epsilon_0)C_d}{w}$. Thus

$$\dot{V} = -(\rho - \rho^e)(q_2 - q_1).$$

From Fig. 34, it is clear that $\forall \rho \in [0, \frac{C_d}{v_f}]$, $\rho - \rho^e < 0$ and

$$q_2 - q_1 \leq C_d - d \leq \frac{d - C_d}{\rho^e}(\rho - \rho^e),$$

therefore,

$$\dot{V} \leq -\frac{d - C_d}{\rho^e}(\rho - \rho^e)^2, \forall \rho \in [0, \frac{C_d}{v_f}].$$

Similar to the case $I \in \Omega_3$, we have $\forall \rho \in (\frac{C_d}{v_f}, \rho^j]$,

$$\dot{V} \leq -\min\{\frac{d - (1-\epsilon_0)C_d}{\rho^e - C_d/v_f}, w, (w - \tilde{w})\}(\rho - \rho^e)^2.$$

Therefore, $\forall \rho \in [0, \rho^j]$, the time derivative of the Lyapunov function satisfies

$$\dot{V} \leq -\alpha(\rho - \rho^e)^2,$$

where $\alpha = \min\{\frac{d-C_d}{\rho^e}, \frac{d-(1-\epsilon_0)C_d}{\rho^e - C_d/v_f}, w, (w - \tilde{w})\} > 0$, which implies exponential convergence to the equilibrium point $\rho^e, \forall \rho(0) \in [0, \rho^j]$.

A.5. Case e), i.e. $I \in \Omega_5$

Consider the Lyapunov function

$$V(\rho) = \frac{(\rho - \min\{d, C\}/v_f)^2}{2}.$$

Then if $d < C, \dot{V} = -(\rho - d/v_f)(q_2 - q_1)$. According to equation (33) and Fig. 35a, when $0 \leq \rho \leq \rho_c$, we have that $q_1 = d$, and $q_2 = v_f \rho$. Thus

$$q_2 - q_1 = v_f(\rho - d/v_f). \tag{75}$$

Therefore $\dot{V} = -v_f(\rho - d/v_f)^2$. When $\rho_c < \rho \leq \rho^j - \frac{d}{w}$, we have $\rho - d/v_f > 0$, $q_1 = d$ and $q_2 = \tilde{w}(\tilde{\rho}^j - \rho)$. Using equation (69), we have

$$q_2 - q_1 = \tilde{w}(\tilde{\rho}^j - \rho) - d \geq \tilde{w}[\tilde{\rho}^j - (\rho^j - \frac{d}{w})] - d \geq \frac{(\tilde{w} - w)[\rho_c - (\rho^j - \frac{d}{w})]}{\rho^j - d/v_f}(\rho - d/v_f). \tag{76}$$

Therefore $\dot{V} \leq -\frac{(\tilde{w}-w)[\rho_c-(\rho^j-\frac{d}{w})]}{\rho^j-d/v_f}(\rho-d/v_f)^2$. When $\rho^j-\frac{d}{w}<\rho\leq\rho^j$, we have $\rho-d/v_f>0$, $q_1=w(\rho^j-\rho)$ and $q_2=\tilde{w}(\tilde{\rho}^j-\rho)$, which together with equation (70) gives

$$q_2-q_1=\tilde{w}(\tilde{\rho}^j-\rho)-w(\rho^j-\rho)\geq\frac{(\tilde{w}-w)[\rho_c-(\rho^j-\frac{d}{w})]}{\rho^j-d/v_f}(\rho-d/v_f), \tag{77}$$

Therefore $\dot{V} \leq -\frac{(\tilde{w}-w)[\rho_c-(\rho^j-\frac{d}{w})]}{\rho^j-d/v_f}(\rho-d/v_f)^2$. From (75) - (77), we conclude that $\forall\rho\in[0,\rho^j]$,

$$\dot{V}\leq-\alpha(\rho-d/v_f)^2,$$

where $\alpha=\min\{v_f,\frac{(\tilde{w}-w)[\rho_c-(\rho^j-\frac{d}{w})]}{\rho^j-d/v_f}\}>0$, which guarantees exponential stability of the equilibrium point $\rho^e=d/v_f$ and exponential convergence of $\rho(t)$ to ρ^e, $\forall\rho(0)\in[0,\rho^j]$.
If $d\geq C$, $\forall\rho\in[0,\rho_c]$, $q_1=C$, $q_2=v_f\rho$, and $\forall\rho\in(\rho_c,\rho^j]$, $q_1=w(\rho^j-\rho)$, $q_2=\tilde{w}(\tilde{\rho}^j-\rho)$. Therefore

$$\dot{V}=\begin{cases}-v_f(\rho-\rho_c)^2, & \text{if } \rho\in[0,\rho_c]\\ -(w-\tilde{w})(\rho-\rho_c)^2, & \text{if } \rho\in(\rho_c,\rho^j]\end{cases},$$

which implies that $\dot{V}\leq-\min\{v_f,(w-\tilde{w})\}(\rho-\rho_c)^2$. The properties of V and $\dot{V}$ imply exponential stability of the equilibrium point $\rho^e=\rho_c=\frac{C}{v_f}$ and exponential convergence of $\rho(t)$ to ρ^e, $\forall\rho(0)\in[0,\rho^j]$, due to $w-\tilde{w}>0$. □

B Proof of Theorem 6.2

For the proof of Theorem 6.2, we use the following two lemmas: Lemma B.1 gives the region of ρ^e within the set S. For a set $A\subset\Re^N$ and a point $x_0\in\Re^N$, the distance between x_0 and A is defined as:

$$d(x_0,A)=\inf_{x\in A}\|x-x_0\|.$$

Then we have the following lemma.

Lemma B.1. *Let ρ^e be an equilibrium state of system (34), then we have the following results:*

a) If $C_d<C$, i.e. $I\in\bigcup_{i=1}^{4}\Omega_i$, then $\rho^e\in S^I$, where $S^I=\{\rho|\frac{\min\{d,C\}}{v_f}\leq\rho_i\leq\rho^j-\frac{(1-\epsilon_0)C_d}{w},i=1,2,...,N\}\subset S$. Furthermore, $\forall\rho(0)\in S$, $d(\rho(t),S^I)$ converges to 0 exponentially fast.

b) If $C_d\geq C$, i.e. $I\in\Omega_5$, then $\rho^e\in\bar{S}^I$, where $\bar{S}^I=\{\rho|\frac{\min\{d,C\}}{v_f}\leq\rho_i\leq\rho_c,i=1,2,...,N\}\subset S$. Furthermore, $\forall\rho(0)\in S$, $d(\rho(t),\bar{S}^I)$ converges to 0 exponentially fast.

Proof of Lemma B.1:

a) For $I \in \bigcup_{i=1}^{4} \Omega_i$, we first show that $\rho_i^e \geq \frac{\min\{d,C\}}{v_f}$, for $i = 1, 2, ..., N$. Assume that $0 \leq \rho_1^e < \frac{\min\{d,C\}}{v_f}$, then $w(\rho^j - \rho_1^e) \geq C$ due to $\rho_1^e < \frac{\min\{d,C\}}{v_f} \leq \rho_c$. Therefore the corresponding equilibrium flow rate

$$q_1^e = \min\{d, C, w(\rho^j - \rho_1^e)\} = \min\{d, C\},$$
$$q_2^e = \min\{v_f\rho_1^e, \tilde{w}(\tilde{\rho}^j - \rho_1^e), C, w(\rho^j - \rho_2^e)\} \leq v_f\rho_1^e,$$

which implies that

$$\dot{\rho}_1 = q_1^e - q_2^e \geq \min\{d, C\} - v_f\rho_1^e > 0, \text{ as } \rho_1^e < \frac{\min\{d, C\}}{v_f},$$

which violates the equilibrium condition (35), hence $\rho_1^e \geq \frac{\min\{d,C\}}{v_f}$. For any $i = 1, 2, .., N-1$, assume $\rho_i^e \geq \frac{\min\{d,C\}}{v_f}$ and check the property of ρ_{i+1}^e. If $0 \leq \rho_{i+1}^e < \frac{\min\{d,C\}}{v_f}$, we have $v_f\rho_{i+1}^e < \min\{d, C\} < C < w(\rho^j - \rho_{i+1}^e)$. Thus

$$q_{i+1}^e = \min\{v_f\rho_i^e, \tilde{w}(\tilde{\rho}^j - \rho_i^e), C, w(\rho^j - \rho_{i+1}^e)\} = \min\{v_f\rho_i^e, \tilde{w}(\tilde{\rho}^j - \rho_i^e)\},$$

$$q_{i+2}^e = \min\{v_f\rho_{i+1}^e, \tilde{w}(\tilde{\rho}^j - \rho_{i+1}^e), C, w(\rho^j - \rho_{i+2}^e)\} \leq v_f\rho_{i+1}^e < \min\{d, C\}.$$

If $q_{i+1}^e = \tilde{w}(\tilde{\rho}^j - \rho_i^e)$, then $\tilde{w}(\tilde{\rho}^j - \rho_i^e) \leq v_f\rho_i^e$, which implies $\rho_i^e \geq \rho_c$. Since ρ_i^e is the equilibrium density in section i, we have $q_i^e = q_{i+1}^e$, and

$$w(\rho^j - \rho_i^e) \geq q_i^e = q_{i+1}^e = \tilde{w}(\tilde{\rho}^j - \rho_i^e),$$

which implies $\rho_i^e \leq \rho_c$. Thus $\rho_i^e = \rho_c$ and $q_i^e = q_{i+1}^e = \tilde{w}(\tilde{\rho}^j - \rho_c) = C \geq \min\{d, C\} > q_{i+2}^e$. If $q_{i+1}^e = v_f\rho_i^e$, then $q_{i+1}^e \geq \min\{d, C\} > q_{i+2}^e$ due to $\rho_i^e \geq \frac{\min\{d,C\}}{v_f}$. Therefore, for all possible $q_{i+1} = \min\{v_f\rho_i^e, \tilde{w}(\tilde{\rho}^j - \rho_i^e)\}$, we have $q_{i+1}^e > q_{i+2}^e$, which violates the equilibrium condition (35). Therefore, the assumption $0 \leq \rho_{i+1}^e < \frac{\min\{d,C\}}{v_f}$ is invalid, which implies that $\rho_{i+1}^e \geq \frac{\min\{d,C\}}{v_f}$. By mathematical induction, we know that

$$\rho_i^e \geq \frac{\min\{d, C\}}{v_f}, i = 1, 2, ..., N. \tag{78}$$

Then we show that $\rho_i^e \leq \rho^j - \frac{(1-\epsilon_0)C_d}{w}$, for $i = 1, 2, ..., N$. Assume that $\rho^j - \frac{(1-\epsilon_0)C_d}{w} < \rho_N^e \leq \rho^j$, then

$$q_{N+1}^e = \min\{(1-\epsilon_0)C_d, \tilde{w}(\tilde{\rho}^j - \rho_N^e)\},$$
$$q_N^e = \min\{v_f\rho_{N-1}^e, \tilde{w}(\tilde{\rho}^j - \rho_{N-1}^e), C, w(\rho^j - \rho_N^e)\} \leq w(\rho^j - \rho_N^e).$$

Since $\rho_N^e > \rho^j - \frac{(1-\epsilon_0)C_d}{w} > \rho_c$, we have $w(\rho^j - \rho_N^e) < (1-\epsilon_0)C_d$ and $w(\rho^j - \rho_N^e) < \tilde{w}(\tilde{\rho}^j - \rho_N^e)$. Therefore $q_N^e \leq w(\rho^j - \rho_N^e) < q_{N+1}^e$, which contradicts the the equilibrium condition (35). Thus $\rho_N^e \leq \rho^j - \frac{(1-\epsilon_0)C_d}{w}$.

Assume $\rho_i^e \leq \rho^j - \frac{(1-\epsilon_0)C_d}{w}$, for any $i = 2, 3, ..., N$, we check the property of ρ_{i-1}^e. If $\rho^j - \frac{(1-\epsilon_0)C_d}{w} < \rho_{i-1}^e \leq \rho^j$, then $\tilde{w}(\tilde{\rho}^j - \rho_{i-1}^e) < C < v_f \rho_{i-1}^e$ as $\rho_{i-1}^e > \rho_c$. Therefore

$$q_i^e = \min\{v_f \rho_{i-1}^e, \tilde{w}(\tilde{\rho}^j - \rho_{i-1}^e), C, w(\rho^j - \rho_i^e)\} = \min\{\tilde{w}(\tilde{\rho}^j - \rho_{i-1}^e), w(\rho^j - \rho_i^e)\},$$
$$q_{i-1}^e = \min\{v_f \rho_{i-2}^e, \tilde{w}(\tilde{\rho}^j - \rho_{i-2}^e), C, w(\rho^j - \rho_{i-1}^e)\} \leq w(\rho^j - \rho_{i-1}^e).$$

Since $\rho_i^e \leq \rho^j - \frac{(1-\epsilon_0)C_d}{w} < \rho_{i-1}^e$, we have $w(\rho^j - \rho_{i-1}^e) < \tilde{w}(\tilde{\rho}^j - \rho_{i-1}^e)$ and $w(\rho^j - \rho_{i-1}^e) < (1-\epsilon_0)C_d \leq w(\rho^j - \rho_i^e)$. Thus $q_{i-1}^e < q_i^e$, which violates the equilibrium condition (35). Therefore $\rho_{i-1}^e \leq \rho^j - \frac{(1-\epsilon_0)C_d}{w}$. By mathematical induction, we have

$$\rho_i^e \leq \rho^j - \frac{(1-\epsilon_0)C_d}{w}, i = 1, 2, ..., N. \tag{79}$$

Combining the two inequalities (78) and (79), we can conclude

$$\frac{\min\{d, C\}}{v_f} \leq \rho_i^e \leq \rho^j - \frac{(1-\epsilon_0)C_d}{w}, i = 1, 2, ..., N.$$

To show that $d(\rho(t), S^I)$ converges to 0 exponentially fast $\forall \rho(0) \in S$, it is equivalent to show that $\forall \delta > 0, \exists T > 0$, such that $\forall t > T$

$$\frac{\min\{d, C\}}{v_f} - \delta < \rho_i(t) < \rho^j - \frac{(1-\epsilon_0)C_d}{w} + \delta, \ i = 1, 2, ..., N \tag{80}$$

and $d(\rho(t), S^I)$ is bounded from above by a decaying exponential function.
First we show the left half of inequality (80). Since $q_1 = \min\{d, C, w(\rho^j - \rho_1)\}$ and $q_2 \leq v_f \rho_1$, we have

$$\dot{\rho}_1 = q_1 - q_2 \geq \min\{d, C, w(\rho^j - \rho_1)\} - v_f \rho_1. \tag{81}$$

If $\exists t_0 \geq 0$, such that $\rho_1(t_0) \geq \frac{\min\{d,C\}}{v_f}$, then for all $t \geq t_0$ we have the following result: since $\rho_1(t)$ is uniformly continuous, if $\rho_1(t)$ keeps decreasing and $\rho_1(t_1) = \frac{\min\{d,C\}}{v_f}$ for some $t_1 \geq t_0$, then from (81) we have $\dot{\rho}_1(t_1) \geq 0$, which implies that $\rho_1(t)$ will no longer decrease and $\rho_1(t) \geq \frac{\min\{d,C\}}{v_f}, \forall t \geq t_0$. Therefore $\forall \delta_1 > 0$ and $\forall t \geq t_0$, $\rho_1(t) \geq \frac{\min\{d,C\}}{v_f} - \delta_1$.
If $\forall t \geq 0, \rho_1(t) < \frac{\min\{d,C\}}{v_f}$, then in the region $\rho_1(t) < \frac{\min\{d,C\}}{v_f}$, we have

$$\dot{\rho}_1(t) \geq \min\{d, C\} - v_f \rho_1 = -v_f(\rho_1 - \frac{\min\{d, C\}}{v_f}). \tag{82}$$

By Lemma 3.2.4 in [81], we have

$$\rho_1(t) \geq e^{-v_f t}[\rho_1(0) - \frac{\min\{d, C\}}{v_f}] + \frac{\min\{d, C\}}{v_f}, \forall t \geq 0. \tag{83}$$

The right side of (83) converges to $\frac{\min\{d,C\}}{v_f}$ exponentially fast, therefore $\forall \delta_1 > 0$, $\exists T_1 > 0$, such that $\forall t > T_1$, $\rho_1(t) \geq \frac{\min\{d,C\}}{v_f} - \delta_1$.
For $i = 1, 2, ..., N-1$, we assume $\rho_i \geq \frac{\min\{d,C\}}{v_f} - \delta_i, \forall t > 0$, where $\delta_i > 0$, then we examine the dynamics of ρ_{i+1}. We have

$$\dot{\rho}_{i+1} = q_{i+1} - q_{i+2} \geq \min\{v_f \rho_i, \tilde{w}(\tilde{\rho}^j - \rho_i), C, w(\rho^j - \rho^{i+1})\} - v_f \rho_{i+1}.$$

Since $\rho_i \geq \frac{\min\{d,C\}}{v_f} - \delta_i$, we have $v_f \rho_i \geq \min\{d, C\} - v_f \delta_i$, therefore

$$\dot{\rho}_{i+1} \geq \min\{\min\{d, C\} - v_f \delta_i, \tilde{w}(\tilde{\rho}^j - \rho_i), w(\rho^j - \rho^{i+1})\} - v_f \rho_{i+1}. \tag{84}$$

Similar to (81), we can show that if $\exists t_0 \geq 0$, such that $\rho_{i+1}(t) \geq \frac{\min\{d,C\}}{v_f} - \delta_i$, then $\rho_{i+1}(t) \geq \frac{\min\{d,C\}}{v_f} - \delta_i, \forall t \geq t_0$, that is, $\forall \delta_{i+1} > \delta_i$ and $\forall t \geq t_0$, $\rho_i(t) > \frac{\min\{d,C\}}{v_f} - \delta_{i+1}$.
If $\rho_{i+1}(t) < \frac{\min\{d,C\}}{v_f} - \delta_i, \forall t \geq 0$, then in the region $\rho_{i+1}(t) < \frac{\min\{d,C\}}{v_f} - \delta_i$, we have

$$\dot{\rho}_{i+1}(t) \geq \min\{d, C\} - v_f \delta_i - v_f \rho_{i+1} = -v_f(\rho_{i+1} - \frac{\min\{d, C\}}{v_f} + \delta_i).$$

By Lemma 3.2.4 in [81], we have

$$\rho_{i+1}(t) \geq e^{-v_f t}[\rho_{i+1}(0) - \frac{\min\{d, C\}}{v_f} + \delta_i] + \frac{\min\{d, C\}}{v_f} - \delta_i, \forall t \geq 0. \tag{85}$$

Similar to (83), the right hand side of equation (85) converges exponentially fast to $\frac{\min\{d,C\}}{v_f} - \delta_i$. Therefore, $\forall \delta_{i+1} > \delta_i$, $\exists T_{i+1} > 0$, such that $\forall t > T_{i+1}$, $\rho_i(t) > \frac{\min\{d,C\}}{v_f} - \delta_{i+1}$. By mathematical induction, we can conclude that for $i = 1, 2, ..., N$, $\forall \delta_i > 0$, $\exists T_i > 0$, such that $\forall t > \sum_{j=1}^{i} T_j$, $\rho_i(t) \geq \frac{\min\{d,C\}}{v_f} - \delta_i$. If we take $\delta_N < \delta$, $T_1 + T_2 + ... + T_N < T$, then the left side of inequality (80) holds.
Next we prove the right half of the inequality (80). Since $q_{N+1} = \min\{v_f \rho_N, \tilde{w}(\tilde{\rho}^j - \rho_N), (1 - \epsilon(\rho_N))C_d\}$ and $q_N < \min\{C, w(\rho^j - \rho_N)\}$, we have

$$\dot{\rho}_N = q_N - q_{N+1} \leq \min\{C, w(\rho^j - \rho_N)\} - \min\{v_f \rho_N, \tilde{w}(\tilde{\rho}^j - \rho_N), (1 - \epsilon(\rho_N))C_d\}.$$

Similar to (81), we can show that if $\exists t_0 \geq 0$, such that $\rho_N(t_0) \leq \rho^j - \frac{(1-\epsilon_0)C_d}{w}$, then $\rho_N(t_0) \leq \rho^j - \frac{(1-\epsilon_0)C_d}{w}, \forall t \geq t_0$, that is, $\forall 0 < \delta_N < \delta$, and $\forall t \geq 0$, $\rho_N(t) \leq \rho^j - \frac{(1-\epsilon_0)C_d}{w} + \delta_N$.
If $\rho_N(t) > \rho^j - \frac{(1-\epsilon_0)C_d}{w}, \forall t \geq 0$, then in the region $\rho_N > \rho^j - \frac{(1-\epsilon_0)C_d}{w}$, we have

$$\dot{\rho}_N \leq (\tilde{w} - w)(\rho_N - (\rho^j - \frac{(1-\epsilon_0)C_d}{w})).$$

By Lemma 3.2.4 in [81], we have

$$\rho_N(t) \leq e^{(\tilde{w}-w)t}[\rho_N(0) - (\rho^j - \frac{(1-\epsilon_0)C_d}{w})] + (\rho^j - \frac{(1-\epsilon_0)C_d}{w}), \forall t \geq 0. \tag{86}$$

Since $\tilde{w} - w < 0$, the right side of (86) converges to $\rho^j - \frac{(1-\epsilon_0)C_d}{w}$ exponentially fast. Therefore, $\forall 0 < \delta_N < \delta$, $\exists T_N > 0$, such that $\forall t > T_N$, $\rho_N(t) \leq \rho^j - \frac{(1-\epsilon_0)C_d}{w} + \delta_N$.
For $i = 1, ..., N-1$, we assume $\rho_{i+1} \leq \rho^j - \frac{(1-\epsilon_0)C_d}{w} + \delta_{i+1}, \forall t > 0$, where $\delta_{i+1} > 0$, then we check the dynamics of ρ_i. We have

$$\dot{\rho}_i = q_i - q_{i+1} \leq \min\{C, w(\rho^j - \rho_i)\} - \min\{v_f\rho_i, \tilde{w}(\tilde{\rho}^j - \rho_i), C, w(\rho^j - \rho_{i+1})\}.$$

Since $\rho_{i+1} \leq \rho^j - \frac{(1-\epsilon_0)C_d}{w} + \delta_{i+1}$, we have $w(\rho^j - \rho_{i+1}) \geq (1-\epsilon_0)C_d - w\delta_{i+1}$. Thus

$$\dot{\rho}_i \leq \min\{C, w(\rho^j - \rho_i)\} - \min\{v_f\rho_i, \tilde{w}(\tilde{\rho}^j - \rho_i), (1-\epsilon_0)C_d - w\delta_{i+1}\}.$$

Similar to (81), we can show that if $\exists t_0 \geq 0$, such that $\rho_i(t_0) \leq \rho^j - \frac{(1-\epsilon_0)C_d}{w} + \delta_{i+1}$, then $\rho_i(t_0) \leq \rho^j - \frac{(1-\epsilon_0)C_d}{w} + \delta_{i+1}, \forall t \geq t_0$, that is, $\forall \delta_i > \delta_{i+1}$, and $\forall t \geq 0$, $\rho_i(t) \leq \rho^j - \frac{(1-\epsilon_0)C_d}{w} + \delta_i$.
If $\rho_i(t_0) > \rho^j - \frac{(1-\epsilon_0)C_d}{w} + \delta_{i+1}, \forall t \geq 0$, then in the region $\rho_i > \rho^j - \frac{(1-\epsilon_0)C_d}{w} + \delta_{i+1}$, we have

$$\dot{\rho}_i \leq (\tilde{w} - w)(\rho_N - (\rho^j - \frac{(1-\epsilon_0)C_d}{w}) - \delta_{i+1}).$$

By Lemma 3.2.4 in [81], we have

$$\rho_i(t) \leq e^{(\tilde{w}-w)t}[\rho_i(0) - (\rho^j - \frac{(1-\epsilon_0)C_d}{w} + \delta_{i+1})] + (\rho^j - \frac{(1-\epsilon_0)C_d}{w} + \delta_{i+1}), \forall t \geq 0. \tag{87}$$

Similar to (86), the right hand side of equation (87) converges exponentially fast to $\rho^j - \frac{(1-\epsilon_0)C_d}{w} + \delta_{i+1}$. Therefore, $\forall \delta_i > \delta_{i+1}$, $\exists T_i > 0$, such that $\forall t > T_i$, $\rho_i(t) \leq \rho^j - \frac{(1-\epsilon_0)C_d}{w} + \delta_i$.
By mathematical induction, we can conclude that for $i = 1, 2, ..., N$, $\forall \delta_i > 0$, $\exists T_i > 0$, such that $\forall t > \sum_{j=1}^{i} T_j$, $\rho_i(t) \leq \rho^j - \frac{(1-\epsilon_0)C_d}{w} + \delta_i$. If we take $\delta_1 < \delta$, $T_1 + T_2 + ... + T_N < T$, then the right side of inequality (80) holds. Therefore, $d(\rho(t), S^I)$ converges to 0 exponentially fast for all $\rho(0)$ in the feasible set S.
b) Part b) of Lemma B.1 can be proved in a similar manner. □
Specifically, when $I \in \Omega_2$, the equilibrium points of system (34) satisfy the properties given by the following lemma.

Lemma B.2. *Let $I \in \Omega_2$. If ρ^e is an equilibrium state of system (34), then the corresponding equilibrium flow rate is $q_1^e = q_2^e = ... = q_{N+1}^e = d = (1-\epsilon_0)C_d$. Furthermore, ρ^e has the following properties:*

a) For $i = 1, 2, ..., N-1$, if $\frac{d}{v_f} < \rho_i^e \leq \rho^j - \frac{d}{w}$, then $\rho_k^e = \rho^j - \frac{d}{w}$, for all $i < k \leq N$.

b) For $i = 2, 3, ..., N$, if $\frac{d}{v_f} \leq \rho_i^e < \rho^j - \frac{d}{w}$, then $\rho_k^e = \frac{d}{v_f}$, for all $1 \leq k < i$.

Proof of Lemma B.2:
Assume ρ^e is an equilibrium state of system (34), then using Lemma B.1, we have $\frac{d}{v_f} \leq \rho_i^e \leq \rho^j - \frac{(1-\epsilon_0)C_d}{w} = \rho^j - \frac{d}{w}, i = 1, 2, ..., N$, therefore

$$q_1^e = \min\{d, C, w(\rho^j - \rho_1^e)\} \leq d,$$

$$q_{N+1}^e = \min\{v_f \rho_N^e, \tilde{w}(\tilde{\rho}^j - \rho_N^e), (1 - \epsilon(\rho_N^e))C_d\} \geq d.$$

Using the equilibrium condition (35), we have that the equilibrium flow $q_1^e = q_{N+1}^e = d$. Therefore $q_i^e = d$, for $i = 1, 2, ..., N+1$.
For any $i = 1, 2, ..., N-1$, if $\frac{d}{v_f} < \rho_i^e \leq \rho^j - \frac{d}{w}$, we have $v_f \rho_i^e > d$ and $\tilde{w}(\tilde{\rho}^j - \rho_i^e) \geq \tilde{w}[\tilde{\rho}^j - (\rho^j - d/w)] > w[\rho^j - (\rho^j - d/w)] = d$, therefore

$$d = q_{i+1}^e = \min\{v_f \rho_i^e, \tilde{w}(\tilde{\rho}^j - \rho_i^e), C, w(\rho^j - \rho_{i+1}^e)\} = w(\rho^j - \rho_{i+1}^e),$$

which gives that $\rho_{i+1}^e = \rho^j - d/w$. By mathematical induction, $\rho_k^e = \rho^j - \frac{d}{w}$, for all $i < k \leq N$.
For any $i = 2, 3, ..., N$, if $\frac{d}{v_f} \leq \rho_i^e < \rho^j - \frac{d}{w}$, we have that $w(\rho^j - \rho_i^e) > d$, therefore

$$d = q_i^e = \min\{v_f \rho_{i-1}^e, \tilde{w}(\tilde{\rho}^j - \rho_{i-1}^e), C, w(\rho^j - \rho_i^e)\} = \min\{v_f \rho_{i-1}^e, \tilde{w}(\tilde{\rho}^j - \rho_{i-1}^e)\}.$$

If $q_i^e = \tilde{w}(\tilde{\rho}^j - \rho_{i-1}^e) = d$, then $q_{i-1}^e \leq w(\rho^j - \rho_{i-1}^e) < \tilde{w}(\tilde{\rho}^j - \rho_{i-1}^e) < d$, which contradicts the fact that $q_{i-1}^e = d$, therefore $q_i^e = v_f \rho_{i-1}^e = d, \rho_{i-1}^e = \frac{d}{v_f}$. By mathematical induction, $\rho_k = \frac{d}{v_f}$, for all $1 \leq k < i$. □
Using the above two lemmas the proof of Theorem 6.2 is completed as follows:
Proof of Theorem 6.2:
From the part a) of Lemma B.1, we know that for $I \in \bigcup_{i=1}^{4} \Omega_i$ if ρ^e is an equilibrium state of system (34), then $\rho^e \in S^I$ and $d(\rho(t), S^I)$ converges to 0 exponentially fast, $\forall \rho(0) \in S$. Therefore, we only need to find all equilibrium states of system (34) in S^I and analyze the dynamics of $\rho(t)$ for all $\rho(0) \in S_\delta^I$, where

$$S_\delta^I = \{\rho | \frac{\min\{d, C\}}{v_f} - \delta \leq \rho_i \leq \rho^j - \frac{(1-\epsilon_0)C_d}{w} + \delta, i = 1, 2, ..., N\}$$

and $\delta > 0$ can be arbitrarily small.
From the part b) of Lemma B.1, we know that when $I \in \Omega_5$, we only need to find all equilibrium states of system (34) in the set $\bar{S}^I$ and analyze the dynamics of $\rho(t)$ for all $\rho(0)$ in the set $\bar{S}_\delta^I$, where

$$\bar{S}_\delta^I = \{\rho | \frac{\min\{d, C\}}{v_f} - \delta \leq \rho_i \leq \rho_c + \delta, i = 1, 2, ..., N\}.$$

Now we prove the statements of Theorem 6.2 from a) to e) respectively.
a) When $I \in \Omega_1, d < (1 - \epsilon_0)C_d$. By Lemma B.1, we have that $\frac{\min\{d,C\}}{v_f} \leq \rho_i^e \leq \rho^j - \frac{(1-\epsilon_0)C_d}{w}$,

therefore $w(\rho^j - \rho_i^e) \geq (1-\epsilon_0)C_d > d$, $i = 1, 2, ..., N$. Thus $q_1^e = \min\{d, C, w(\rho^j - \rho_1^e)\} = d$. Using the equilibrium condition (35), we have

$$q_i^e = d, \text{ for } i = 1, 2, ..., N+1$$

Now we show that $\rho_i^e = d/v_f$, for $i = 1, 2, ..., N$. For $i = 1, 2, ..., N-1$, $q_{i+1}^e = \min\{v_f\rho_i^e, \tilde{w}(\tilde{\rho}^j - \rho_i^e), C, w(\rho^j - \rho_{i+1}^e)\}$. If $\rho_c \leq \rho_i^e \leq \rho^j - \frac{(1-\epsilon_0)C_d}{w}$, we have

$$w(\rho^j - \rho_{i+1}^e) \geq (1-\epsilon_0)C_d > d,$$

$$v_f\rho_i^e \geq C \geq \tilde{w}(\tilde{\rho}^j - \rho_i^e) \geq w(\rho^j - \rho_i^e) > (1-\epsilon_0)C_d > d,$$

which implies that $q_{i+1}^e > d$, therefore the assumption $\rho_c \leq \rho_i^e \leq \rho^j - \frac{(1-\epsilon_0)C_d}{w}$ is invalid. Hence $d/v_f \leq \rho_i^e < \rho_c$, which gives that $\tilde{w}(\tilde{\rho}^j - \rho_i^e) > C > v_f\rho_i^e$, thus

$$q_{i+1}^e = \min\{v_f\rho_i^e, w(\rho^j - \rho_{i+1}^e)\}.$$

By Lemma B.1, we have $\rho_{i+1}^e \leq \rho^j - \frac{(1-\epsilon_0)C_d}{w}$, thus $w(\rho^j - \rho_{i+1}^e) \geq (1-\epsilon_0)C_d > d$. Solving the equation $q_{i+1}^e = d$ gives the unique equilibrium density $\rho_i^e = d/v_f$. Therefore, we have $\rho_i^e = d/v_f, i = 1, ..., N-1$. For $i = N$, we have $q_{N+1}^e = \min\{v_f\rho_N^e, \tilde{w}(\tilde{\rho}^j - \rho_N^e), (1-\epsilon(\rho_N^e))C_d\}$. If $C_d/v_f < \rho_N^e \leq \rho^j - \frac{(1-\epsilon_0)C_d}{w}$, we have $q_{N+1}^e = (1-\epsilon_0)C_d > d$, therefore the assumption $C_d/v_f < \rho_N^e \leq \rho^j - \frac{(1-\epsilon_0)C_d}{w}$ is invalid, which together with Lemma B.1 implies that $d/v_f \leq \rho_N^e \leq C_d/v_f$. Therefore $q_{N+1}^e = v_f\rho_N^e$. Solving the equation $q_{N+1}^e = d$ gives a unique solution $\rho_N^e = d/v_f$. Therefore, the point $\frac{d}{v_f} \times \mathbf{1}$ is the unique equilibrium state of system (34) when $I \in \Omega_1$.

Using Lemma B.1, we have that for all $\rho(0) \in S_\delta^I$, $d/v_f - \delta < \rho_i(t) < \rho^j - (1-\epsilon_0)C_d/w + \delta, \forall t \geq 0, \delta > 0$. Therefore

$$w(\rho^j - \rho_i) > w[\rho^j - (\rho^j - (1-\epsilon_0)C_d/w + \delta)] = (1-\epsilon_0)C_d - w\delta$$

and

$$\begin{aligned}\tilde{w}(\tilde{\rho}^j - \rho_i) &> \tilde{w}[\tilde{\rho}^j - (\rho^j - (1-\epsilon_0)C_d/w + \delta)] > w[\rho^j - (\rho^j - (1-\epsilon_0)C_d/w + \delta)] \\ &= (1-\epsilon_0)C_d - w\delta,\end{aligned}$$

for $i = 1, 2, ..., N$. Since $(1-\epsilon_0)C_d > d$, taking δ to be sufficiently small, we have $(1-\epsilon_0)C_d - w\delta > d$. Therefore $q_1 = \min\{d, C, w(\rho^j - \rho_1)\} = d$ and

$$\dot{\rho_1} = q_1 - q_2 = d - \min\{v_f\rho_1, \tilde{w}(\tilde{\rho}^j - \rho_1), C, w(\rho^j - \rho_2)\}. \tag{88}$$

Combine (34) and (88), we can show that

$$\dot{\rho}_1 \begin{cases} = -v_f(\rho_1 - \frac{d}{v_f}) & \text{if } \frac{d}{v_f} - \delta < \rho_1 < \frac{d}{v_f} \\ = 0 & \text{if } \rho_1 = \frac{d}{v_f} \\ \leq -\alpha(\rho_1 - \frac{d}{v_f}) & \text{if } \frac{d}{v_f} < \rho_1 < \rho^j - (1-\epsilon_0)C_d/w + \delta \end{cases},$$

where $\alpha = \min\{v_f, \frac{(1-\epsilon_0)C_d - w\delta - d}{\rho^j - d/v_f}\} > 0$, which implies that for all $\rho(0) \in S_\delta^I$, $\rho_1(t)$ converges to d/v_f exponentially fast.
Based on the convergence of ρ_1, we can show that ρ_2 also converges to d/v_f exponentially fast, followed by ρ_3 through ρ_N. Therefore, $\forall \rho(0) \in S$, $\rho(t)$ converges to $\frac{d}{v_f} \times \mathbf{1}$ exponentially fast.

b)When $I \in \Omega_2$, $d = (1-\epsilon_0)C_d$. Using Lemma B.2, we have that the equilibrium flow rate $q_i^e = d = (1-\epsilon_0)C_d$, for $i = 1, 2, ..., N+1$. If $0 \leq \rho_N^e \leq \frac{C_d}{v_f}$, then $q_{N+1}^e = d$ gives $\rho_N^e = \frac{d}{v_f}$. By part b) of Lemma B.2, we have $\rho_i^e = \frac{d}{v_f}$, $i = 1, 2, ..., N-1$. Therefore $\rho^e = d/v_f \times \mathbf{1}$ is a potential equilibrium point of system (34). Substituting $\rho^e = d/v_f \times \mathbf{1}$ into equation (34), we have $q_i^e = d$, for $i = 1, 2, ..., N+1$. Therefore, $\rho^e = d/v_f \times \mathbf{1}$ is the only equilibrium state in the region $0 \leq \rho_N^e \leq \frac{C_d}{v_f}$.
If $\rho_N^e \in (\frac{C_d}{v_f}, \rho^j - \frac{d}{w})$, according to Lemma B.2, we have that $\rho_1^e = ... = \rho_{N-1}^e = \frac{d}{v_f}$. Substituting any $\rho^e \in \{\rho | \rho_1 = ... = \rho_{N-1} = \frac{d}{v_f}, \frac{C_d}{v_f} < \rho_N < \rho^j - \frac{d}{w}\}$ into equation (34), we have $q_i^e = d$, for $i = 1, 2, ..., N+1$. Therefore all $\rho^e \in \{\rho | \rho_1 = ... = \rho_{N-1} = \frac{d}{v_f}, \frac{C_d}{v_f} < \rho_N < \rho^j - \frac{d}{w}\}$ are equilibrium states of system (34).
If $\rho_N^e = \rho^j - \frac{d}{w}$, we find all the equilibrium states of the system (34) by considering the following two cases:
Case I: for all $i = 1, 2, .., N-1$, $\rho_i^e = \rho^j - \frac{d}{w}$;
Case II: there exists $i \in \{1, 2, ..., N-1\}$, $d/v_f \leq \rho_i^e < \rho^j - \frac{d}{w}$ and $\rho_{i+1}^e = \rho^j - \frac{d}{w}$.
Case I contains only one point, that is, $\rho^e = (\rho^j - \frac{d}{w}) \times \mathbf{1}$. Substituting this density state into equation (34), we have $q_i^e = d$, for $i = 1, 2, ..., N+1$. Therefore $(\rho^j - \frac{d}{w}) \times \mathbf{1}$ is an equilibrium state of system (34).
For case II, it is clear from Lemma B.2 that $\rho_1^e = ...\rho_{i-1}^e = d/v_f, \rho_{i+1}^e = ... = \rho_N^e = \rho^j - \frac{d}{w}$. Taking $i = 1, 2, ..., N-1$, we have that all potential equilibrium points of system (34) in case II are in the set $\bigcup_{i=1}^{N-1} \{\rho | \frac{d}{v_f} \leq \rho_i < \rho^j - \frac{d}{w}, \rho_k = \frac{d}{v_f}, 1 \leq k < i, \rho_r = \rho^j - \frac{d}{w}, i < r \leq N\}$. Substituting any point in this set into equation (34), we have $q_i^e = d$, for $i = 1, 2, ..., N+1$. Therefore all $\rho^e \in \bigcup_{i=1}^{N-1} \{\rho | \frac{d}{v_f} \leq \rho_i < \rho^j - \frac{d}{w}, \rho_k = \frac{d}{v_f}, 1 \leq k < i, \rho_r = \rho^j - \frac{d}{w}, i < r \leq N\}$ are equilibrium states of system (34).
To summarize, when $I \in \Omega_2$, system (34) has an isolated equilibrium state $\frac{d}{v_f} \times \mathbf{1}$ and an equilib-

rium manifold

$$S^e = \{(\rho^j - \frac{d}{w}) \times \mathbf{1}\} \cup \{\rho | \rho_i = \frac{d}{v_f}, i = 1, 2, ..., N-1, \frac{C_d}{v_f} < \rho_N < \rho^j - \frac{d}{w}\}$$
$$\cup [\bigcup_{i=1}^{N-1} \{\rho | \frac{d}{v_f} \leq \rho_i < \rho^j - \frac{d}{w}, \rho_k = \frac{d}{v_f}, 1 \leq k < i, \rho_r = \rho^j - \frac{d}{w}, i < r \leq N\}].$$

We now prove the rest of part b) as follows: first we show that for all $\rho(0)$ in the feasible space S, $\rho(t)$ converges to one equilibrium state in $\bar{S}^e$, where $\bar{S}^e = S^e \cup \{\frac{d}{v_f} \times \mathbf{1}\}$. Then we show that $\frac{d}{v_f} \times \mathbf{1}$ is locally exponentially stable, and that every $\rho^e \in S^e$ is stable in the sense of Lyapunov, i.e. $\forall \mu > 0, \exists \eta > 0$, such that $\forall \rho(0)$ that satisfy $\|\rho(0) - \rho^e\| < \eta$, we have $\|\rho(t) - \rho^e\| \leq \mu, \forall t > 0$. Furthermore, $\rho(t)$ converges to some $\bar{\rho}^e \in S^e$ that satisfies $\|\bar{\rho}^e - \rho^e\| < \mu$.
For all $\rho(0) \in S^I$, by letting $\delta = 0$ in the proof of Lemma B.1, we can show $\rho(t) \in S^I, \forall t \geq 0$. From equation (34), we know that $\forall \rho \in S^I$, $q_1 = d$ and $q_i \geq d, i = 2, 3, ..., N$. Therefore,

$$\sum_{i=1}^{k} \dot{\rho}_i = q_1 - q_k \leq 0, k = 1, 2, ..., N.$$

Thus $\sum_{i=1}^{k} \rho_i$ is monotonically decreasing but bounded from below which implies that it converges to a limit. Therefore, we have $\rho = [\rho_1, \rho_2, ..., \rho_N]^T$ converges to a constant vector ρ^e. From equation (34) we know that $\dot{\rho}$ is a piecewise uniformly continuous function of ρ, therefore, as ρ converges to a constant ρ^e, $\dot{\rho}$ also converges to a constant, which has to be 0 (otherwise $\|\rho\|$ goes to infinity). Therefore ρ^e is a equilibrium point of system (34) by definition. Thus $\rho^e \in \bar{S}^e$. From part a) of Lemma B.1, for all $\rho(0) \in S$, $d(\rho(t), S^I)$ converges to 0 exponentially fast. Therefore $\forall \rho(0) \in S$, $\rho(t)$ converges to a equilibrium point $\rho^e \in \bar{S}^e$.
Next we show that the equilibrium state $\rho^e = \frac{d}{v_f} \times \mathbf{1}$ is exponentially stable, and that every $\rho^e \in S^e$ is stable in the sense of Lyapunov.
(1) When $\rho^e = \frac{d}{v_f} \times \mathbf{1}$, then for all $\rho(0) \in \{\rho | 0 \leq \rho_i \leq C_d/v_f, i = 1, 2, ..., N\}$, $q_i \leq C_d$ and $q_{i+1} = v_f \rho_i$, for $i = 1, 2, ..., N$. Thus $\dot{\rho}_i = q_i - q_{i+1} \leq C_d - v_f \rho_i$, which implies that $\rho_i(t) \leq C_d/v_f, \forall t \geq 0$. Therefore,

$$\dot{\rho}_1 = d - v_f \rho_1,$$
$$\dot{\rho}_i = v_f \rho_{i-1} - v_f \rho_i, i = 2, 3, ..., N,$$

which can be written in the compact form as

$$\dot{\rho} = A(\rho - \frac{d}{v_f} \times \mathbf{1})$$

where

$$A = \begin{bmatrix} -v_f & & & \\ v_f & -v_f & & \\ & \ddots & \ddots & \\ & & v_f & -v_f \end{bmatrix}.$$

Since $v_f > 0$, we have that A is Hurwitz. Therefore $\rho(t)$ converges to $\frac{d}{v_f} \times \mathbf{1}$ exponentially fast. ρ^e is in the interior of the set $\{\rho | 0 \leq \rho_i \leq C_d/v_f, i = 1, 2, ..., N\}$, thus we can always find a $\eta > 0$, such that $\{\rho \,|\|\rho - \rho^e\| < \eta\} \subset \{\rho | 0 \leq \rho_i \leq C_d/v_f, i = 1, 2, ..., N\}$. Therefore, $\forall \rho(0) \in \{\rho \,|\|\rho - \rho^e\| < \eta\}$, $\rho(t)$ converges to ρ^e exponentially fast, which implies that $\rho^e = \frac{d}{v_f} \times \mathbf{1}$ is exponentially stable.
(2) When $\rho^e = (\rho^j - \frac{d}{w}) \times \mathbf{1}$, $\forall \rho(0)$ that satisfy $\|\rho(0) - \rho^e\| < \eta$, with $\eta > 0$ sufficiently small, equation (34) gives the flow rates as follows: $q_1 = \min\{d, w(\rho^j - \rho_1)\}$, $q_i = w(\rho^j - \rho_i)$, for $i = 2, ..., N$, and $q_{N+1} = (1 - \epsilon_0)C_d = d$. Therefore,

$$\begin{aligned} \dot{\rho}_1 &= \min\{d, w(\rho^j - \rho_1)\} - w(\rho^j - \rho_2), \\ \dot{\rho}_i &= w(\rho^j - \rho_i) - w(\rho^j - \rho_{i+1}), i = 2, ..., N-1, \\ \dot{\rho}_N &= w(\rho^j - \rho_N) - d. \end{aligned}$$

Let $e_i = \rho_i - \rho_i^e$ and $\bar{e} = [e_2, e_3, ..., e_N]^T$, then we have $e = [e_1, \bar{e}^T]^T$, where

$$\dot{e}_1 = \begin{cases} we_2, & e_1 \leq 0 \\ -we_1 + we_2, & e_1 > 0 \end{cases} \tag{89}$$

and

$$\dot{\bar{e}} = \begin{bmatrix} -w & w & & \\ & -w & w & \\ & & \ddots & \ddots \\ & & & -w \end{bmatrix} \bar{e}.$$

Since $w > 0$, it follows that $\bar{e}$ converges to 0 exponentially fast, i.e. there exists constants $\alpha, \beta > 0$, such that

$$|e_i(t)| \leq |e_i(0)| \alpha \exp(-\beta t), i = 2, 3, ..., N. \tag{90}$$

From (89), we have that $\dot{e}_1 \leq -we_1 + we_2$, which together with the continuity of $\dot{e}_1$ implies that

$$e_1(t) \leq |e_1(0)| \exp(-wt) + |e_2(0)| \frac{\alpha w}{w - \beta_0} [\exp(-\beta_0 t) - \exp(-wt)], \tag{91}$$

where $0 < \beta_0 < \min\{w, \beta\}$. Therefore, e_1 is bounded from above by a function that decays exponentially fast to 0 with time. If $\forall t \geq 0, e_1(t) > 0$, then $e_1(t)$ converges exponentially fast to 0. Otherwise, if $\exists t_0 \geq 0$, such that $e_1(t_0) \leq 0$, then we have the following cases:

Case I: If $e_1(0) \leq 0$, then as long as $e_1(t) \leq 0$, we have

$$e_1(t) = e_1(0) + \int_0^t we_2(\tau)d\tau \geq -|e_1(0)| - \int_0^t w|e_2(\tau)|d\tau \geq -|e_1(0)| - \frac{\alpha w}{\beta}|e_2(0)|\exp(-\beta t),$$

which together with (91) implies that for any given $\epsilon > 0$, there exists a finite time T such that

$$-|e_1(0)| - \epsilon \leq e_1(t) \leq \epsilon, \forall t \geq T,$$

which implies that the equilibrium $e_1 = 0$ is stable in the sense of Lyapunov.
Case II: If $e_1(0) > 0$, note that $e_1(t_0) \leq 0$, then due to the uniform continuity of e_1, we have that $\exists t_1 \in (0, t_0]$, such that $e_1(t_1) = 0$. Then $\forall t \geq t_1$, as long as $e_1(t) \leq 0$, we have

$$\begin{aligned} e_1(t) &= \int_{t_1}^t we_2(\tau)d\tau \geq -\int_{t_1}^t w|e_2(\tau)|d\tau \geq -\frac{\alpha w}{\beta}|e_2(0)|\exp(-\beta t_1)[1-\exp(-\beta(t-t_1))] \\ &\geq -\frac{\alpha w}{\beta}|e_2(0)|\exp(-\beta t_1), \end{aligned}$$

which together with (91) implies that for any given $\epsilon > 0$, there exists a finite time $T \geq t_1$ such that

$$-\frac{\alpha w}{\beta}|e_2(0)|\exp(-\beta t_1) \leq e_1(t) \leq \epsilon, \forall t \geq T,$$

which implies that the equilibrium $e_1 = 0$ is stable in the sense of Lyapunov.
To summarize the above analysis, we have that the equilibrium state $\rho^e = (\rho^j - \frac{d}{w}) \times \mathbf{1}$ is stable in the sense of Lyapunov.
(3) When $\rho^e \in \{\rho | \frac{d}{v_f} \leq \rho_i < \rho^j - \frac{d}{w}, \rho_k = \frac{d}{v_f}, 1 \leq k < i, \rho_r = \rho^j - \frac{d}{w}, i < r \leq N\}$, $i = 1, 2, ..., N-1$, $\forall \rho(0)$ that satisfy $\|\rho(0) - \rho^e\| < \eta$, if η is sufficiently small, we can get the flow rates from equation (34) as follows: $q_1 = d$, $q_k = v_f\rho_{k-1}, k = 2, ..., i$, $q_r = w(\rho^j - \rho_r), r = i+1, ..., N$, and $q_{N+1} = (1-\epsilon_0)C_d = d$. Therefore, we have

$$\begin{aligned} \dot{\rho}_1 &= d - v_f\rho_1, \\ \dot{\rho}_k &= v_f\rho_{k-1} - v_f\rho_k, k = 2, ..., i-1, \\ \dot{\rho}_i &= v_f\rho_{i-1} - w(\rho^j - \rho_{i+1}), \\ \dot{\rho}_r &= w(\rho^j - \rho_r) - w(\rho^j - \rho_{r+1}), r = i+1, ..., N-1, \\ \dot{\rho}_N &= w(\rho^j - \rho_N) - d. \end{aligned}$$

Let $e_i = \rho_i - \rho_i^e$ and $e = [e_1, e_2, ..., e_N]^T$, the dynamics of e can be presented in the compact form as follows:

$$\dot{e} = Ae,$$

where

$$A = \begin{bmatrix} -v_f & 0 & & & & & \\ v_f & -v_f & 0 & & & & \\ & \ddots & \ddots & \ddots & & & \\ & & v_f & 0 & w & & \\ & & & 0 & -w & w & \\ & & & & \ddots & \ddots & \ddots \\ & & & & & 0 & -w \end{bmatrix},$$

Let $\bar{e} = [e_1, e_2, ..., e_{i-1}]^T$ and $\underline{e} = [e_{i+1}, ..., e_N]^T$, then

$$\dot{\bar{e}} = \begin{bmatrix} -v_f & & & \\ v_f & -v_f & & \\ & \ddots & \ddots & \\ & & v_f & -v_f \end{bmatrix} \bar{e}$$

and

$$\dot{\underline{e}} = \begin{bmatrix} -w & w & & \\ & \ddots & \ddots & \\ & & -w & w \\ & & & -w \end{bmatrix} \underline{e}.$$

The above two subsystems are both linear and exponentially stable. Thus $\bar{e}$ and $\underline{e}$ both converge to 0 exponentially fast. $\dot{e}_i = v_f e_{i-1} + w e_{i+1}$, therefore

$$e_i(t) = e_i(0) + v_f \int_0^t e_{i-1}(\tau)d\tau + w \int_0^t e_{i+1}(\tau)d\tau.$$

Since

$$\|e_{i-1}\| \leq \|\bar{e}\| \leq \|\bar{e}(0)\|\alpha_1 \exp(-\beta_1 t),$$
$$\|e_{i+1}\| \leq \|\underline{e}\| \leq \|\underline{e}(0)\|\alpha_2 \exp(-\beta_2 t),$$

where $\alpha_1, \alpha_2, \beta_1, \beta_2 > 0$, thus

$$\begin{aligned} e_i &= e_i(0) + \int_0^t (v_f e_{i-1} + w e_{i+1})d\tau, \\ \|e_i\| &\leq \|e_i(0)\| + \int_0^t (v_f \|e_{i-1}\| + w\|e_{i+1}\|)d\tau \\ &\leq \|e_i(0)\| + v_f \int_0^t \|\bar{e}(0)\|\alpha_1 \exp(-\beta_1 t)d\tau + w \int_0^t \|\underline{e}(0)\|\alpha_2 \exp(-\beta_2 t)d\tau \\ &= \|e_i(0)\| + \|\bar{e}(0)\|\frac{v_f \alpha_1}{\beta_1}(1 - \exp(-\beta_1 t)) + \|\underline{e}(0)\|\frac{w\alpha_2}{\beta_2}(1 - \exp(-\beta_2 t)). \end{aligned}$$

Since we have shown before that $\forall \rho(0) \in S, \rho(t)$ converges to a constant, i.e. the limit $\lim_{t\to\infty} \rho(t)$ exists, which implies that the limit $\lim_{t\to\infty} \|e_i\|$ also exists. Therefore,

$$\lim_{t\to\infty} \|e_i\| \leq \|e_i(0)\| + \|\bar{e}(0)\| \frac{v_f \alpha_1}{\beta_1} + \|\underline{e}(0)\| \frac{w\alpha_2}{\beta_2}.$$

For all $\mu > 0$, by selecting $\rho(0)$ sufficiently close to ρ^e, we have $\|\rho(t) - \rho^e\| \leq \mu, \forall t \geq 0$, i.e. all equilibrium points $\rho^e \in \{\rho | \frac{d}{v_f} \leq \rho_i < \rho^j - \frac{d}{w}, \rho_k = \frac{d}{v_f}, 1 \leq k < i, \rho_r = \rho^j - \frac{d}{w}, i < r \leq N\}$, $i = 1, 2, ..., N-1$ are stable in the sense of Lyapunov.
(4) When $\rho^e \in \{\rho | \rho_i = d/v_f, i = 1, 2, ..., N-1, \frac{C_d}{v_f} < \rho_N < \rho^j - \frac{d}{w}\}$, $\forall \rho(0)$ that satisfy $\|\rho(0) - \rho^e\| < \eta$, if η is sufficiently small, we get the flow rates from equation (34) as: $q_1 = d$, $q_i = v_f \rho_{i-1}, i = 2, 3, ..., N$, and $q_{N+1} = (1 - \epsilon_0) C_d = d$. Therefore we have that

$$\begin{aligned}
\dot{\rho}_1 &= d - v_f \rho_1, \\
\dot{\rho}_i &= v_f \rho_{i-1} - v_f \rho_i, i = 2, ..., N-1, \\
\dot{\rho}_N &= v_f \rho_{N-1} - d.
\end{aligned}$$

Let $e_i = \rho_i - \rho_i^e$ and $e = [e_1, e_2, ..., e_N]^T$, the dynamics of e can be expressed in the compact form as follows:

$$\dot{e} = Ae,$$

where

$$A = \begin{bmatrix} -v_f & & & & \\ v_f & -v_f & & & \\ & \ddots & \ddots & & \\ & & v_f & -v_f & \\ & & & v_f & 0 \end{bmatrix}.$$

The stability of ρ^e can be shown by following a similar analysis as in previous case.
Therefore, all $\rho^e \in S^e$ are stable in the sense of Lyapunov. Recall that $\forall \rho(0) \in S, \rho(t)$ converges to an equilibrium state in S^e, thus $\forall \mu > 0, \exists \eta > 0$, such that $\forall \rho(0)$ that satisfy $\|\rho(0) - \rho^e\| < \eta$, $\rho(t)$ converges to some $\bar{\rho}^e \in S^e$ that satisfies $\|\bar{\rho}^e - \rho^e\| < \mu$.

c) For the case $I \in \Omega_3$, from part a) of Lemma B.1, we know $\frac{d}{v_f} \leq \rho_i^e \leq \rho^j - \frac{(1-\epsilon_0)C_d}{w}, i = 1, 2, ..., N$. If $\frac{d}{v_f} \leq \rho_1^e \leq \rho^j - \frac{d}{w}$, then $w(\rho^j - \rho_1^e) \geq d$, thus $q_1^e = \min\{d, C, w(\rho^j - \rho_1^e)\} = d$ and $q_i^e = q_1^e = d, i = 2, 3, ..., N+1$, according to the equilibrium condition (35). Solving the equation $q_{N+1}^e = d$ gives only one solution $\rho_N^e = d/v_f$. For $i = 1, 2, ..., N-1$, given $\rho_{i+1}^e = d/v_f, q_i^e = q_{i+1}^e = d$, we have $d = q_i^e \leq w(\rho^j - \rho_i^e)$, thus $\rho_i^e \leq \rho^j - d/w$. Since

$$q_{i+1}^e = \min\{v_f \rho_i^e, \tilde{w}(\tilde{\rho}^j - \rho_i^e), C, w(\rho^j - \rho_{i+1}^e)\}$$

and

$$w(\rho^j - \rho_{i+1}^e) > C > d, \text{ as } \rho_{i+1}^e = d/v_f < \rho_c,$$

$$\tilde{w}(\tilde{\rho}^j - \rho_i^e) \geq \tilde{w}[\tilde{\rho}^j - (\rho^j - d/w)] > w[\rho^j - (\rho^j - d/w)] = d.$$

The equation $q_{i+1}^e = d$ gives only one solution, that is $v_f \rho_i^e = d$,

$$\rho_i^e = d/v_f.$$

By mathematical induction, we have that $\rho_i^e = d/v_f, i = 1, 2, ..., N$. Therefore in the region $\frac{d}{v_f} \leq \rho_1^e \leq \rho^j - \frac{d}{w}$, system (34) has only one equilibrium state $\frac{d}{v_f} \times \mathbf{1}$.
If $\rho^j - \frac{d}{w} < \rho_1^e \leq \rho^j - \frac{(1-\epsilon_0)C_d}{w}$, we have $w(\rho^j - \rho_1^e) < d < C$, thus

$$q_1^e = \min\{d, C, w(\rho^j - \rho_1^e)\} = w(\rho^j - \rho_1^e) < d.$$

For $i = 2, 3, ..., N$, given $\rho^j - \frac{d}{w} < \rho_{i-1}^e \leq \rho^j - \frac{(1-\epsilon_0)C_d}{w}$ and $q_{i-1}^e = q_i^e = q_1^e = w(\rho^j - \rho_1^e)$, then we have

$$q_i^e = \min\{v_f \rho_{i-1}^e, \tilde{w}(\tilde{\rho}^j - \rho_{i-1}^e), C, w(\rho^j - \rho_i^e)\} = w(\rho^j - \rho_1^e).$$

Since $v_f \rho_{i-1}^e > C > d$ as $\rho_{i-1}^e > \rho_c$, $v_f \rho_{i-1}^e \neq w(\rho^j - \rho_1^e)$. If $\tilde{w}(\tilde{\rho}^j - \rho_{i-1}^e) = w(\rho^j - \rho_1^e)$, then

$$q_{i-1}^e \leq w(\rho^j - \rho_{i-1}^e) < \tilde{w}(\tilde{\rho}^j - \rho_{i-1}^e) = w(\rho^j - \rho_1^e),$$

which contradicts the fact that $q_{i-1}^e = w(\rho^j - \rho_1^e)$, therefore $\tilde{w}(\tilde{\rho}^j - \rho_{i-1}^e) \neq w(\rho^j - \rho_1^e)$. Thus we have

$$q_i^e = w(\rho^j - \rho_i^e) = w(\rho^j - \rho_1^e) \text{ and } \rho_i^e = \rho_1^e,\ i = 2, 3, ..., N.$$

Therefore $\rho^j - \frac{d}{w} < \rho_N^e \leq \rho^j - \frac{(1-\epsilon_0)C_d}{w}$, equation (34) gives that $q_{N+1}^e = (1 - \epsilon_0)C_d$. Using the equilibrium condition (35), we have $q_i^e = w(\rho^j - \rho_i^e) = (1-\epsilon_0)C_d$ for $i = 1, 2, ..., N$, which gives only one solution, that is, $(\rho^j - \frac{(1-\epsilon_0)C_d}{w}) \times \mathbf{1}$ is the only equilibrium state of system (34) in the region $\rho^j - \frac{d}{w} < \rho_1^e \leq \rho^j - \frac{(1-\epsilon_0)C_d}{w}$. To summarize, $\rho^{e1} = \frac{d}{v_f} \times \mathbf{1}$ and $\rho^{e2} = (\rho^j - \frac{(1-\epsilon_0)C_d}{w}) \times \mathbf{1}$ are 2 isolated equilibrium states of system (34) when $I \in \Omega_3$.
Now we are going to show that for all $0 \leq \rho(0) \leq \rho^j$, $\rho(t)$ converges to either ρ^{e1} or ρ^{e2}. According to part a) of Lemma B.1, we have that $\forall \delta > 0, \exists T > 0$, such that $d/v_f - \delta < \rho_i < \rho^j - (1 - \epsilon_0)C_d + \delta, i = 1, 2, ..., N$. Without loss of generality, let $T = 0$.
If $\forall t \geq 0$, $\rho_N(t) \leq \frac{C_d}{v_f}$, then $w(\rho^j - \rho_N) > C$, due to $\frac{C_d}{v_f} < \rho_c$. We have

$$q_N = \min\{v_f \rho_{N-1}, \tilde{w}(\tilde{\rho}^j - \rho_{N-1})\},$$

$$q_{N-1} = \min\{v_f \rho_{N-2}, \tilde{w}(\tilde{\rho}^j - \rho_{N-2}), C, w(\rho^j - \rho_{N-1})\} \leq w(\rho^j - \rho_{N-1}).$$

Therefore, $\forall \rho_{N-1} > \rho_c$, $\dot{\rho}_{N-1} = q_{N-1} - q_N \leq w(\rho^j - \rho_{N-1}) - \tilde{w}(\tilde{\rho}^j - \rho_{N-1}) < 0$, thus $\limsup_{t\to\infty} \rho_{N-1} \leq \rho_c$. Consequently, we have that $\limsup_{t\to\infty} \rho_i \leq \rho_c, i - 1, 2, ..., N - 1$. When $\rho_i^e \leq \rho_c, i = 1, 2, ..., N - 1$, $\rho_N \leq C_d/v_f$, equation (34) gives that $q_1 = d, q_i = v_f \rho_{i-1}, i = 2, 3, ..., N + 1$, therefore,

$$\dot{\rho}_1 = d - v_f \rho_1,$$
$$\dot{\rho}_i = v_f \rho_{i-1} - v_f \rho_i, i = 2, 3, ..., N.$$

which can be written in the compact form as

$$\dot{\rho} = A(\rho - \frac{d}{v_f} \times \mathbf{1})$$

where

$$A = \begin{bmatrix} -v_f & & & \\ v_f & -v_f & & \\ & \ddots & \ddots & \\ & & v_f & -v_f \end{bmatrix}.$$

Since $v_f > 0$, we have that A is Hurwitz. Therefore $\rho(t)$ converges to $\rho^{e1} = \frac{d}{v_f} \times \mathbf{1}$ exponentially fast.
If there exists $t_0 \geq 0$, $\rho_N(t_0) > \frac{C_d}{v_f}$, then $q_{N+1}(t_0) = (1-\epsilon_0)C_d$, due to $\frac{C_d}{v_f} < \rho_N(t_0) < \rho^j - (1-\epsilon_0)C_d + \delta$. Recall that

$$q_N = \min\{v_f\rho_{N-1}, \tilde{w}(\tilde{\rho}^j - \rho_{N-1}), C, w(\rho^j - \rho_N)\}.$$

and $d/v_f - \delta < \rho_{N-1} < \rho^j - (1-\epsilon_0)C_d + \delta$, we have that

$$\begin{aligned} v_f\rho_{N-1} &> d - v_f\delta, \\ \tilde{w}(\tilde{\rho}^j - \rho_{N-1}) &> \tilde{w}(\tilde{\rho}^j - (\rho^j - (1-\epsilon_0)C_d + \delta)) \\ &= (w - \tilde{w})(\rho^j - (1-\epsilon_0)C_d - \rho_c) + (1-\epsilon_0)C_d - \tilde{w}\delta. \end{aligned}$$

therefore

$$\dot{\rho}_N = q_N - q_{N+1} \begin{cases} > -\alpha_1[\rho_N - (\rho^j - \frac{(1-\epsilon_0)C_d}{w})] > 0, & \text{if } \rho_N < \rho^j - \frac{(1-\epsilon_0)C_d}{w} \\ = 0, & \text{if } \rho_N = \rho^j - \frac{(1-\epsilon_0)C_d}{w} \\ < -\alpha_2[\rho_N - (\rho^j - \frac{(1-\epsilon_0)C_d}{w})] < 0, & \text{if } \rho_N > \rho^j - \frac{(1-\epsilon_0)C_d}{w} \end{cases}, \tag{92}$$

where

$$\alpha_1 = \min\{\frac{d - v_f\delta - (1-\epsilon_0)C_d}{\rho^j - (1-\epsilon_0)C_d/w}, \frac{(w-\tilde{w})(\rho^j - (1-\epsilon_0)C_d - \rho_c) - \tilde{w}\delta}{\rho^j - (1-\epsilon_0)C_d/w}, w\}$$

and

$$\alpha_2 = \min\{\frac{d - v_f\delta - (1-\epsilon_0)C_d}{(1-\epsilon_0)C_d/w}, \frac{(w-\tilde{w})(\rho^j - (1-\epsilon_0)C_d - \rho_c) - \tilde{w}\delta}{(1-\epsilon_0)C_d/w}, w\}.$$

When δ is sufficiently small, α_1 and α_2 are both positive. Therefore $\rho_N(t) > \frac{C_d}{v_f}, \forall t \geq t_0$ and $\rho_N(t)$ converges to $\rho^j - \frac{(1-\epsilon_0)}{w}$ exponentially fast. Consequently, $\rho_i(t)$ also converges exponen-

tially fast to $\rho^j - \frac{(1-\epsilon_0)}{w}$ for $i = 1, 2, ..., N-1$, that is, $\rho(t)$ converges exponentially fast to ρ^{e2}. Therefore, for all initial condition $\rho(0) \in S$, $\rho(t)$ converges to one of the two equilibrium states exponentially fast.
From the analysis above, we have that $\forall \rho(0) \in \{\rho | \frac{d}{v_f} - \delta \leq \rho_i \leq \rho^j - \frac{(1-\epsilon_0)C_d}{w} + \delta, i = 1, 2, ..., N-1, \frac{C_d}{v_f} < \rho_N \leq \rho^j - \frac{(1-\epsilon_0)C_d}{w} + \delta\}$, $\rho(t)$ converges to the equilibrium state ρ^{e2} exponentially fast. Therefore this equilibrium state is locally exponentially stable.
Similar to the case $I \in \Omega_2$, we can show that for all $\rho(0) \in \{\rho | 0 \leq \rho_i \leq C_d/v_f, i = 1, 2, ..., N\}$, $\rho(t)$ converges to the point ρ^{e1} exponentially fast. Therefore this equilibrium state is exponentially stable.

d) When $I \in \Omega_4$, $d > C_b$. If ρ^e is an equilibrium state of system (34), then we have $\frac{\min\{d,C\}}{v_f} \leq \rho_i^e \leq \rho^j - \frac{(1-\epsilon_0)C_d}{w}, i = 1, 2, ..., N$ by using Lemma B.1, in this region

$$q_{N+1}^e = \min\{v_f \rho_N^e, \tilde{w}(\tilde{\rho}^j - \rho_N^e), (1 - \epsilon(\rho_N^e))C_d\} = (1-\epsilon_0)C_d,$$

From the equilibrium condition (35), we have that $q_i^e = (1-\epsilon_0)C_d, i = 1, 2, ..., N$. Recall that

$$q_1^e = \min\{d, C, w(\rho^j - \rho_1^e)\}.$$

Since $d > (1-\epsilon_0)C_d$ and $C > (1-\epsilon_0)C_d$, $q_1^e = (1-\epsilon_0)C_d$ gives only one solution $\rho_1^e = \rho^j - \frac{(1-\epsilon_0)C_d}{w}$. For $i = 2, 3, ..., N$, given $\rho_{i-1}^e = \rho^j - \frac{(1-\epsilon_0)C_d}{w}$, we check the value of ρ_i^e. Recall that

$$q_i^e = \min\{v_f \rho_{i-1}^e, \tilde{w}(\tilde{\rho}^j - \rho_{i-1}^e), C, w(\rho^j - \rho_i^e)\}.$$

Since $v_f \rho_{i-1}^e > C > (1-\epsilon_0)C_d$ and $\tilde{w}(\tilde{\rho}^j - \rho_{i-1}^e) > w(\rho^j - \rho_{i-1}^e) = (1-\epsilon_0)C_d$ as $\rho_{i-1}^e > \rho_c$, thus $q_i^e = (1-\epsilon_0)C_d$ gives $w(\rho^j - \rho_i^e) = (1-\epsilon_0)C_d$, i.e., $\rho_i^e = \rho^j - \frac{(1-\epsilon_0)C_d}{w}$. Therefore the point $(\rho^j - \frac{(1-\epsilon_0)C_d}{w}) \times \mathbf{1}$ is the unique equilibrium state of system (34) when $I \in \Omega_4$.
For all $\rho(0) \in S_\delta^I$, we have $v_f \rho_N > d - v_f \delta$ and $\tilde{w}(\tilde{\rho}^j - \rho_N) > \tilde{w}(\tilde{\rho}^j - \rho^j + \frac{(1-\epsilon_0)C_d}{w} - \delta)$ by using Lemma B.1. Take δ to be sufficiently small, we have $v_f \rho_N > C_d$ and $\tilde{w}(\tilde{\rho}^j - \rho_N) > (1-\epsilon_0)C_d$. Thus

$$q_{N+1} = \min\{v_f \rho_N, \tilde{w}(\tilde{\rho}^j - \rho_N), (1 - \epsilon(\rho_N))C_d\} = (1-\epsilon_0)C_d,$$

then

$$\dot{\rho_N} = q_N - q_{N+1} = \min\{v_f \rho_{N-1}, \tilde{w}(\tilde{\rho}^j - \rho_{N-1}), C, w(\rho^j - \rho_N)\} - (1-\epsilon_0)C_d. \tag{93}$$

Similar to equation (92), we have

$$\dot{\rho}_N \begin{cases} > -\alpha_1[\rho_N - (\rho^j - \frac{(1-\epsilon_0)C_d}{w})] > 0, & \text{if } \rho_N < \rho^j - \frac{(1-\epsilon_0)C_d}{w} \\ = 0, & \text{if } \rho_N = \rho^j - \frac{(1-\epsilon_0)C_d}{w} \\ < -\alpha_2[\rho_N - (\rho^j - \frac{(1-\epsilon_0)C_d}{w})] < 0, & \text{if } \rho_N > \rho^j - \frac{(1-\epsilon_0)C_d}{w} \end{cases},$$

where

$$\alpha_1 = \min\{\frac{d - v_f\delta - (1-\epsilon_0)C_d}{\rho^j - (1-\epsilon_0)C_d/w}, \frac{(w-\tilde{w})(\rho^j - (1-\epsilon_0)C_d - \rho_c) - \tilde{w}\delta}{\rho^j - (1-\epsilon_0)C_d/w}, w\}$$

and

$$\alpha_2 = \min\{\frac{d - v_f\delta - (1-\epsilon_0)C_d}{(1-\epsilon_0)C_d/w}, \frac{(w-\tilde{w})(\rho^j - (1-\epsilon_0)C_d - \rho_c) - \tilde{w}\delta}{(1-\epsilon_0)C_d/w}, w\}.$$

When δ is sufficiently small, α_1 and α_2 are both positive. Therefore ρ_N converges to $\rho^j - \frac{(1-\epsilon_0)C_d}{w}$ exponentially fast.
Based on the converges of ρ_N, we can show that ρ_{N-1} also convergences to $\rho^j - \frac{(1-\epsilon_0)C_d}{w}$, followed by ρ_{N-2} through ρ_1. Therefore, $\forall\rho(0) \in S$, $\rho(t)$ converges to $(\rho^j - \frac{(1-\epsilon_0)C_d}{w}) \times \mathbf{1}$ exponentially fast.

e) For the case $I \in \Omega_5$ The proof of this part can be demonstrated by following the same routine of the case of $I \in \Omega_1$ based on part b) of Lemma B.1. For the sake of briefness, we omit the detailed proof here. □

C Proof of Theorem 7.1

a) If $I \in \bigcup_{i=1}^{4} \Omega_i$, the VSL controller (41) is applied. First we show that the controller v is well-defined $\forall\rho \in [0, \rho^j]$. According to (41), $\bar{v}_1$ is defined in the region $\frac{C_d}{v_f} - \delta_2 \le \rho \le \rho^j$, in which $q_2 \le C_d$ and $x + \delta_1 > 0$. Therefore the denominator of $\bar{v}_1$

$$w\rho^j - q_2 + \lambda(x + \delta_1) \ge w\rho^j - C_d > w(\rho^j - \rho_c) - C_d = C - C_d > 0.$$

Hence $v_1 = \text{med}\{0, \bar{v}_1, v_f\}$ is well-defined in the region $\frac{C_d}{v_f} - \delta_2 \le \rho \le \rho^j$. $\bar{v}_2$ is defined in the region $0 \le \rho \le \frac{C_d}{v_f}$, in which $q_2 = v_f\rho = C_d + v_f x$. Since $0 < \lambda < \frac{v_f w\rho^j}{C_d}$ and $-\frac{C_d}{v_f} \le x \le 0$, we have that

$$q_2 - \lambda x = C_d + v_f x - \lambda x > C_d + v_f x \ge 0$$

and

$$w\rho^j - (q_2 - \lambda x) > w\rho^j - C_d - (v_f - \frac{v_f w\rho^j}{C_d})x \ge w\rho^j - C_d - (v_f - \frac{v_f w\rho^j}{C_d})(-\frac{C_d}{v_f}) = 0$$

due to $v_f - \frac{v_f w\rho^j}{C_d} < 0$. Therefore, the denominator of $\bar{v}_2$ is greater than 0, $v_2 = \text{med}\{0, \bar{v}_2, v_f\}$ is well-defined, and $\bar{v}_2 = \frac{w(q_2 - \lambda x)}{w\rho^j - (q_2 - \lambda x)} > 0$.
Now we find the equilibrium point of system (36),(41) and analyze its stability properties. We have that $\forall\rho(0) \in (C_d/v_f, \rho^j], v = v_1$. If $v_1 = 0$, i.e. $\bar{v}_1 \le 0$, we have $q_1 = \frac{v_1 w\rho^j}{v_1 + w} = 0$. In the

region $\frac{C_d}{v_f} - \delta_2 \leq \rho \leq \rho^j$, we have

$$\begin{aligned}
&v_f\rho \geq C_d - v_f\delta_2 > 0, \text{ as } \delta_2 < \frac{C_d}{v_f},\\
&\tilde{w}(\tilde{\rho}^j - \rho) \geq \tilde{w}(\tilde{\rho}^j - \rho^j) > 0, \text{ as } \tilde{\rho}^j > \rho^j \geq \rho,\\
&(1-\epsilon(\rho))C_d \geq (1-\epsilon_0)C_d > 0, \text{ as } \epsilon_0 < 1.
\end{aligned}$$

Therefore,

$$\begin{aligned}
q_2 &= \min\{v_f\rho, \tilde{w}(\tilde{\rho}^j - \rho), (1-\epsilon(\rho))C_d\} \geq \min\{C_d - v_f\delta_2, \tilde{w}(\tilde{\rho}^j - \rho^j), (1-\epsilon_0)C_d\}\\
&\geq \frac{\min\{C_d - v_f\delta_2, \tilde{w}(\tilde{\rho}^j - \rho^j), (1-\epsilon_0)C_d\}}{\rho^j - C_d/v_f + \delta_1}(\rho - \frac{C_d}{v_f} + \delta_1)
\end{aligned}$$

due to $\frac{C_d}{v_f} - \delta_2 \leq \rho \leq \rho^j$, which implies $0 < \frac{\rho - C_d/v_f + \delta_1}{\rho^j - C_d/v_f + \delta_1} \leq 1$, since $\delta_2 < \delta_1$. Thus we have

$$\dot{\rho} = q_1 - q_2 \leq -\frac{\min\{C_d - v_f\delta_2, \tilde{w}(\tilde{\rho}^j - \rho^j), (1-\epsilon_0)C_d\}}{\rho^j - C_d/v_f + \delta_1}(\rho - \frac{C_d}{v_f} + \delta_1) \tag{94}$$

If $v_1 > 0$, i.e., $\bar{v}_1 > 0$, $v_1 = \min\{\bar{v}_1, v_f\} \leq \bar{v}_1$ and

$$\frac{v_1 w\rho^j}{v_1 + w} - \frac{\bar{v}_1 w\rho^j}{\bar{v}_1 + w} = w\rho^j \frac{(v_1 - \bar{v}_1)w}{(v_1 + w)(\bar{v}_1 + w)} \leq 0,$$

which implies $\frac{v_1 w\rho^j}{v_1+w} \leq \frac{\bar{v}_1 w\rho^j}{\bar{v}_1+w}$. Hence,

$$q_1 = \min\{d, \frac{v_1 w\rho^j}{v_1 + w}, C, w(\rho^j - \rho)\} \leq \frac{v_1 w\rho^j}{v_1 + w} \leq \frac{\bar{v}_1 w\rho^j}{\bar{v}_1 + w} = q_2 - \lambda(x + \delta_1)$$

and

$$\dot{\rho} = q_1 - q_2 \leq -\lambda(\rho - \frac{C_d}{v_f} + \delta_1) < 0. \tag{95}$$

According to equation (94) and (95),

$$\dot{\rho} \leq -\alpha(\rho - \frac{C_d}{v_f} + \delta_1),$$

where $\alpha = \min\{\lambda, \frac{\min\{C_d - v_f\delta_2, \tilde{w}(\tilde{\rho}^j - \rho^j), (1-\epsilon_0)C_d\}}{\rho^j - C_d/v_f + \delta_1}\} > 0$. Using Lemma 3.2.4 in [81], we have

$$\rho(t) \leq \frac{C_d}{v_f} - \delta_1 + [\rho(0) - \frac{C_d}{v_f} + \delta_1]e^{-\alpha t}.$$

Since $C_d/v_f - \delta_1 < C_d/v_f - \delta_2 < C_d/v_f < \rho(0)$, $\rho(t)$ will decrease exponentially to the value $\rho(t_0) = C_d/v_f - \delta_2$ at some finite time t_0, at which v switches to v_2, in which case the dynamics

of $\rho(t)$ are analyzed below.
Either the initial condition $0 \leq \rho(0) \leq \frac{C_d}{v_f}$ or v switches to v_2 from v_1, there exists a $t_0 \geq 0$, at which $0 \leq \rho(t_0) \leq \frac{C_d}{v_f}$ and $v = v_2$. Since $\bar{v}_2 > 0$, we have $v_2 = \min\{\bar{v}_2, v_f\} \leq v_f$ and

$$\frac{v_2 w \rho^j}{v_2 + w} \leq \frac{v_f w \rho^j}{v_f + w} = C < w(\rho^j - \rho) \text{ as } \rho \leq C_d/v_f < \rho_c.$$

Therefore,

$$\begin{aligned} q_1 &= \min\{d, \frac{v_2 w \rho^j}{v_2 + w}, C, w(\rho^j - \rho)\} = \min\{d, \frac{v_2 w \rho^j}{v_2 + w}\} = \min\{d, \frac{v_f w \rho^j}{v_f + w}, \frac{\bar{v}_2 w \rho^j}{\bar{v}_2 + w}\} \\ &= \min\{d, \frac{\bar{v}_2 w \rho^j}{\bar{v}_2 + w}\} = \min\{d, q_2 - \lambda x\} \end{aligned}$$

and $q_2 = C_d + v_f x$. Consequently,

$$\dot{\rho} = q_1 - q_2 = \min\{d - v_f \rho, -\lambda(\rho - \frac{C_d}{v_f})\}. \tag{96}$$

In the case $d > C_d$, we have $\dot{\rho} \geq -\min\{v_f, \lambda\}(\rho - \frac{C_d}{v_f})$, $\forall \rho \in [0, C_d/v_f]$ and $\dot{\rho} = 0$ at $\rho = C_d/v_f$, which implies that $\rho(t)$ converges exponentially fast to $\rho = \frac{C_d}{v_f}$, and $\forall t \geq t_0, \rho \leq \frac{C_d}{v_f}$, therefore the flow at the exit of the section $q_2 = v_f \rho$ converges to C_d. In the case $d \leq C_d$,

$$\dot{\rho} = \min\{d - v_f \rho, -\lambda(\rho - \frac{C_d}{v_f})\} \begin{cases} \geq -\min\{v_f, \lambda\}(\rho - \frac{d}{v_f}) & \text{if } \rho \in [0, \frac{d}{v_f}) \\ = 0 & \text{if } \rho = \frac{d}{v_f} \\ \leq -v_f(\rho - \frac{d}{v_f}) & \text{if } \rho \in (\frac{d}{v_f}, \frac{C_d}{v_f}] \end{cases}. \tag{97}$$

Therefore, $\rho(t)$ converges to $\frac{d}{v_f}$ exponentially fast, and $q_2 = v_f \rho$ converges to d with the same rate. In summary, the closed-loop system (36) - (41) has a unique equilibrium point $\rho^e = \frac{\min\{d, C_d\}}{v_f}$. In addition, $\forall \rho(0) \in [0, \frac{C_d}{v_f}]$, $\rho(t)$ converges to ρ^e exponentially fast and $\forall \rho(0) \in (\frac{C_d}{v_f}, \rho^j]$, $\rho(t)$ decreases to $\frac{C_d}{v_f} - \delta_2$ exponentially fast and then converges to ρ^e exponentially fast. The flow rate at the exit of the section converges to the maximum possible value $\min\{d, C_d\}$ exponentially fast while the speed of flow converges with the same rate to v_f.
b) Part b) of Theorem 7.1 can be derived directly from part e) of Theorem 6.1. □

D Proof of Theorem 7.2

a) In controller (48), v_1 through v_{N-1} is well-defined by letting $v_i = v_f$ when $\rho_i = 0$, for $i = 1, 2, ..., N-1$. Since $0 < \lambda_0 \leq \frac{v_f w \rho^j}{C_d}$, we can show that v_0 is also well-defined in a similar manner to the single section case in Theorem 7.1.
For all $\rho_N(0) \in (\frac{C_d}{v_f}, \rho^j], \bar{v}_{N-1} = \bar{v}_{N-1,1}$. If $v_{N-1} = 0$, i.e. $\bar{v}_{N-1,1} \leq 0$, we have $q_N = 0$, thus in the region $\frac{C_d}{v_f} - \delta_2 \leq \rho_N(t) \leq \rho^j$, we have

$$\begin{aligned}\dot{\rho}_N &= -q_{N+1} = -\min\{v_f \rho_N, (1-\epsilon(\rho_N))C_d, \tilde{w}(\tilde{\rho}^j - \rho_N)\} \\ &\leq -\frac{\min\{C_d - v_f\delta_2, \tilde{w}(\tilde{\rho}^j - \rho^j), (1-\epsilon_0)C_d\}}{\rho^j - C_d/v_f + \delta_1}(\rho_N - \frac{C_d}{v_f} + \delta_1).\end{aligned}$$

If $v_{N-1} > 0$, i.e. $\bar{v}_{N-1} > 0$, then $q_N \leq v_{N-1}\rho_{N-1} \leq \bar{v}_{N-1}\rho_{N-1}$,

$$\dot{\rho}_N \leq \bar{v}_{N-1}\rho_{N-1} - q_{N+1} = -\lambda_{N-1}(\rho_N - \frac{C_d}{v_f} + \delta_1).$$

Therefore, $\forall \rho_N(0) \in (\frac{C_d}{v_f}, \rho^j]$, we have

$$\dot{\rho}_N \leq -\alpha(\rho_N - \frac{C_d}{v_f} + \delta_1),$$

where $\alpha = \min\{\lambda_{N-1}, \frac{\min\{C_d - v_f\delta_2, \tilde{w}(\tilde{\rho}^j - \rho^j), (1-\epsilon_0)C_d\}}{\rho^j - C_d/v_f + \delta_1}\} > 0$. Since $\alpha > 0$ and $\frac{C_d}{v_f} - \delta_1 < \frac{C_d}{v_f} - \delta_2 < \frac{C_d}{v_f} < \rho_N(0)$, and $\frac{C_d}{v_f} - \delta_2 > 0$, $\rho_N(t)$ will decrease exponentially fast to the value $\frac{C_d}{v_f} - \delta_2$ at some finite time t_0, at which $\bar{v}_{N-1}$ switches to $\bar{v}_{N-1,2}$, in which case $\rho(t)$ evolves as analyzed below. Either the initial condition $\rho_N(0) \in [0, \frac{C_d}{v_f}]$ or $\bar{v}_{N-1}$ switches to $\bar{v}_{N-1,2}$ from $\bar{v}_{N-1,1}$ at $\rho_N = \frac{C_d}{v_f} - \delta_2$, there exists $t_0 \geq 0$, at which time instant $\rho_N(t_0) \leq \frac{C_d}{v_f}$ and $\bar{v}_{N-1} = \bar{v}_{N-1,2}$. Since $\rho_N \leq \frac{C_d}{v_f}, q_{N+1} \geq 0$, and $\rho_{N-1} \geq 0$, we have $\bar{v}_{N-1,2} \geq 0$ from equation (48), thus $v_{N-1} = \min\{v_f, \bar{v}_{N-1,2}\}$. Therefore

$$\dot{\rho}_N \leq \bar{v}_{N-1,2}\rho_{N-1} - q_2 = -\lambda_{N-1}(\rho_N - \frac{C_d}{v_f}).$$

Without loss of generality, let $t_0 = 0$, then we have

$$\rho_N(t) \leq \frac{C_d}{v_f} + (\rho_N(0) - \frac{C_d}{v_f})e^{-\lambda_{N-1}t},$$

which implies that $\forall t \geq 0, \rho_N(t) \leq \frac{C_d}{v_f}, \bar{v}_{N-1} = \bar{v}_{N-1,2}$. Then we examine the dynamics of ρ_{N-1}.

If $v_{N-2}=0$, i.e. $\bar{v}_{N-2}\le 0$, $q_{N-1}=0$, we have

$$\dot{\rho}_{N-1}=-q_N=-\min\{v_{N-1}\rho_{N-1},\frac{v_{N-1}w\rho^j}{v_{N-1}+w},C,w(\rho^j-\rho_N)\}.$$

Since $\rho_N\le\frac{C_d}{v_f}<\rho_c,\ w(\rho^j-\rho_N)>C$ and $v_{N-1}=\min\{v_f,\bar{v}_{N-1,2}\}$, we have

$$\dot{\rho}_{N-1}=-\min\{\bar{v}_{N-1,2}\rho_{N-1},v_f\rho_{N-1},\frac{\bar{v}_{N-1,2}w\rho^j}{\bar{v}_{N-1,2}+w},\frac{v_fw\rho^j}{v_f+w},C\}.$$

Since $0\le\rho_N\le\frac{C_d}{v_f},\lambda_{N-1}>v_f$ and $\rho_{N-1}\le\rho^j$, we have

$$\begin{aligned}
\bar{v}_{N-1,2}\rho_{N-1}&=C_d+(v_f-\lambda_{N-1})(\rho_N-\frac{C_d}{v_f})\ge C_d\ge\frac{C_d}{\rho^j-\frac{C_d}{v_f}}(\rho_{N-1}-\frac{C_d}{v_f}),\\
v_f\rho_{N-1}&\ge v_f(\rho_{N-1}-\frac{C_d}{v_f}),\\
\frac{\bar{v}_{N-1,2}w\rho^j}{\bar{v}_{N-1,2}+w}&=w\rho^j\frac{C_d+(v_f-\lambda_{N-1})x_N}{C_d+(v_f-\lambda_{N-1})x_N+w\rho_{N-1}}\ge\frac{w\rho^jv_fC_d}{v_fw\rho^j+\lambda_{N-1}C_d}\\
&\ge\frac{w\rho^jv_fC_d}{(v_fw\rho^j+\lambda_{N-1}C_d)(\rho^j-\frac{C_d}{v_f})}(\rho_{N-1}-\frac{C_d}{v_f}),\\
\frac{v_fw\rho^j}{v_f+w}&=C\ge\frac{C}{\rho^j-\frac{C_d}{v_f}}(\rho_{N-1}-\frac{C_d}{v_f}).
\end{aligned}$$

Thus $\dot{\rho}_{N-1}\le-\min\{\frac{C_d}{\rho^j-\frac{C_d}{v_f}},v_f,\frac{w\rho^jv_fC_d}{(v_fw\rho^j+\lambda_{N-1}C_d)(\rho^j-\frac{C_d}{v_f})},\frac{C}{\rho^j-\frac{C_d}{v_f}}\}(\rho_{N-1}-\frac{C_d}{v_f})$. If $v_{N-2}>0$, i.e. $\bar{v}_{N-2}>0$,

$$\dot{\rho}_{N-1}\le\bar{v}_{N-2}\rho_{N-2}-q_N=-\lambda_{N-2}(\rho_{N-1}-\frac{C_d}{v_f}).$$

To conclude,

$$\dot{\rho}_{N-1}\le-\alpha(\rho_{N-1}-\frac{C_d}{v_f}),$$

where

$$\alpha=\min\{\frac{C_d}{\rho^j-\frac{C_d}{v_f}},v_f,\frac{w\rho^jv_fC_d}{(v_fw\rho^j+\lambda_{N-1}C_d)(\rho^j-\frac{C_d}{v_f})},\frac{C}{\rho^j-\frac{C_d}{v_f}},\lambda_{N-2}\}>0.$$

Therefore $\limsup_{t\to\infty}\rho_{N-1}(t)\le C_d/v_f$ and $\liminf_{t\to\infty}\bar{v}_{N-1,2}\ge v_f$ due to $\bar{v}_{N-1,2}=\frac{C_d+(v_f-\lambda_{N-1})x_N}{C_d/v_f+x_{N-1}}\ge\frac{C_d}{\rho_{N-1}}$, which implies $\lim_{t\to\infty}v_{N-1}=v_f$.
Similarly, we can show that $\limsup_{t\to\infty}\rho_i(t)\le C_d/v_f$ and $\lim_{t\to\infty}v_i=v_f$ for $i=1,2,...,N-1$.

Then the dynamics of $\rho(t)$ become

$$\dot{\rho}_1 = \min\{d, \frac{\bar{v}_0 w \rho^j}{\bar{v}_0 + w}, \frac{v_f w \rho^j}{v_f + w}\} - v_f \rho_1 = \min\{d - v_f \rho_1, C - v_f \rho_1, -\lambda_0(\rho_1 - C_d/v_f)\},$$
$$\dot{\rho}_i = v_f \rho_{i-1} - v_f \rho_i, i = 2, ..., N.$$

Note that the first differential equation is the same as equation (96) in the single-section case. Therefore we can directly take the analysis result of equation (96), which shows that ρ_1 converges to $\rho_1 = \frac{\min\{d, C_d\}}{v_f}$ exponentially fast. Consequently, ρ_i converges exponentially fast to $\rho_i = \frac{\min\{d, C_d\}}{v_f}$, for $i = 1, 2, ..., N$. Recall that $\rho_N(t) \leq \frac{C_d}{v_f}, \forall t \geq t_0$, thus q_{N+1} converges to C_d exponentially fast. Consequently, q_i converge to C_d exponentially fast for $i = 1, 2, ..., N$.
b) This part can be shown directly with part e) of Theorem 6.2. □